



TEL AVIV UNIVERSITY
THE IBY AND ALADAR FLEISCHMAN FACULTY OF ENGINEERING
The Zandman-Slaner Graduate School of Engineering

**SELECTED TOPICS IN DIRECT GEOLOCATION
OF RADIO TRANSMITTERS & PASSIVE TARGETS**

By

Ofer Bar-Shalom

DISSERTATION SUBMITTED TO THE SENATE OF TEL-AVIV
UNIVERSITY

in partial fulfillment of the requirements for the degree of
"DOCTOR OF PHILOSOPHY"

October 2015

THE IBY AND ALADAR FLEISCHMAN FACULTY OF ENGINEERING
The Zandman-Slaner Graduate School of Engineering

**Selected Topics in Direct Geolocation of Radio
Transmitters & Passive Targets**

By

Ofer Bar-Shalom

DISSERTATION SUBMITTED TO THE SENATE OF TEL-AVIV
UNIVERSITY
in partial fulfillment of the requirements for the degree of
“DOCTOR OF PHILOSOPHY”

Under The Supervision of Professor Anthony J. Weiss
October 2015

This work was carried out under the supervision of
Professor Anthony J. Weiss

Acknowledgements

I have been very fortunate to work under the supervision of Professor Anthony Weiss. I thank him for his valuable guidance during my research, for his patience and his help, for his prompt responses to any of my questions, and for letting me explore topics of my choice.

A special thanks goes to my family, first and foremost, to my wife Galya, for her constant support and encouragement.

I dedicate this dissertation to my father Baruch (Borka) R.I.P., who taught me that the sky is the limit....



Abstract

This dissertation is dedicated to the exploration of various *direct positioning* algorithms for radio transmitters and passive target geolocation. Contrary to the traditional “two-step” approach, the “direct positioning” approach states that the radio transmitter’s position can be extracted directly from the raw samples of the radio transmitter signals collected by the system sensors, without explicitly going through an estimation of position-related parameters such as time-delay, angular or amplitude information. In this work, the concept of direct positioning is applied to various models and consistently outperforms the traditional two-step position estimators, while tightly attaining the theoretical performance bounds.

In the sequel, we explore 3 models for radio transmitters and passive target geolocation. The first model discussed in chapter 3, harnesses the transmit signal diversity of MIMO Radar systems to enhance passive-target position estimation via direct estimation algorithms. The algorithms are developed for both known and unknown transmitted signal waveforms. The known transmitted waveform is applicable to the classical radar model, while the unknown waveform assumption is applicable to passive MIMO radars utilizing “signals of opportunity” for target localization.

The second model addressed in chapter 4, explores the performance of radio transmitter geolocation using a so-called “single platform geolocation” (SPG). The geolocation system in this case consists of only a single sensor (or a single array of sensors). The transmitter localization is accomplished using “in-band aiding” enabled by passive signal reflectors or transponders that are placed at known locations. Algorithms that enable direct geolocation of radio transmitters emitting waveforms, which are either known or unknown to the receiver, are derived and analyzed.

The third model, described in chapter 5, addresses the problem of emitter geolocation in the presence of local scattering. In contrast to the first two models, which rely on the classical assumption of the emitting source being a point in the 3-D space, this model assumes that the emitting source is surrounded by a large number of closely-spaced local scatterers. The local-

scattering assumption which often characterizes geolocation of radio transmitters in indoor, urban or suburban scenarios, imposes certain challenges on the geolocation task. The geolocation system in this model consists of multiple receiving sensor-arrays deployed in various geographical locations. The emitter signals impinging upon the arrays are associated with random angular information that is distributed according to some known statistical distribution. The angular distribution model known as the Gaussian angle of arrival (GAA) is employed. Following the GAA assumption, a spatio-temporal model is developed and various algorithms for direct geolocation under local scattering are derived and analyzed. For all the models outlined, theoretical analyzes, as well as simulated data are provided.

Contents

1	Introduction	1
1.1	Overview of Geolocation Problems	1
1.2	The Radio Channel in Geolocation	5
2	Literature Survey & Dissertation Contributions	9
2.1	Literature Survey of Geolocation	10
2.2	Dissertation Contributions	13
3	Direct Positioning of Stationary Targets Using MIMO Radar	15
3.1	Introduction	15
3.2	Problem Formulation	17
3.3	Algorithms for Direct Target Positioning	20
	3.3.1 Known Signals	21
	3.3.2 Unknown Signals	23
3.4	Numerical Examples	32
3.5	Discussion	40
3.6	Summary	41
4	Emitter Geolocation using Single Moving Receiver	43
4.1	Introduction	43
4.2	Problem Formulation	46
4.3	Positioning Algorithms	50
	4.3.1 Known Signal Waveform	50
	4.3.2 Unknown Signal Waveform	52
	4.3.3 Computational Complexity Analysis	63
4.4	Numerical Examples	64
4.5	Summary	70
5	Direct Emitter Geolocation under Local Scattering	73
5.1	Introduction	73
5.2	Problem Formulation	75

5.2.1	Spatial Model	75
5.2.2	Temporal Model	80
5.3	Positioning Algorithms	83
5.3.1	Maximum Likelihood Estimation	83
5.3.2	Sub-Optimal Estimators	87
5.4	Numerical Examples	92
5.5	Computational Complexity Analysis	98
5.6	Summary	100
6	Conclusions	103
6.1	Directions for Future Work	104
APPENDICES		107
A	Appendix Related to Chapter 3	109
A.1	Derivation of Cramér Rao Lower Bound	109
A.1.1	Known Signals	110
A.1.2	Random Gaussian Signals	116
B	Appendix Related to Chapter 4	119
B.1	Derivation of Cramér Rao Lower Bound for Wideband SPG	119
B.2	Derivation of Multiple-Receivers DPD	129
B.2.1	Unknown Signals	131
B.2.2	Known Signals	133
B.3	SPG for Deterministic, Unknown Signal Waveform	133
C	Appendix Related to Chapter 5	137
C.1	Derivation of Cramér Rao Lower Bound for Geolocation in Rayleigh Fading Channels	137
C.1.1	Derivatives w.r.t. Emitter Coordinates	138
C.1.2	Derivatives w.r.t. Position Spread $\sigma_{\mathbf{p}}$	141
C.1.3	Derivatives w.r.t. Transmit Time t_0	142
BIBLIOGRAPHY		143

List of Notations

In this document, scalars are denoted by Latin and Greek regular fonts, vectors by bold lower-case fonts and matrices by bold upper-case fonts.

$\mathbf{1}_N$	Vector of ones with N entries
$\mathbf{1}_{N \times M}$	A $N \times M$ matrix of ones
$\mathbf{0}_N$	Vector of zeros with N entries
\mathbf{I}_N	Identity matrix with dimension N
x	Scalar
\mathbf{x}	Column vector
\mathbf{X}	Matrix
$\{\mathbf{x}\}_k$	The k -th entry of a vector \mathbf{X}
$\{\mathbf{X}\}_{k,\ell}$	The (k, ℓ) -th entry of the matrix \mathbf{X}
$\text{vec}\{\mathbf{X}\}$	Vectorization (converts matrices into vectors)
$\text{diag}\{\mathbf{X}\}$	Vector formed from the diagonal of \mathbf{X}
$\text{diag}\{\mathbf{x}\}$	Diagonal matrix formed from the vector \mathbf{x}
\odot	Schür-Hadamard element-wise matrix product, $(\mathbf{A} \odot \mathbf{B})_{ij} \triangleq \mathbf{A}_{ij}\mathbf{B}_{ij}$.
\otimes	Kronecker product
i, j	Imaginary unit, $i, j = \sqrt{-1}$
\Re	Real part
\Im	Imaginary part
$\{\cdot\}^T$	Transpose
$\{\cdot\}^H$	Hermitian transpose
$\{\cdot\}^*$	Complex conjugate
$ x $	Absolute value of the scalar x
$\text{Tr}\{\mathbf{X}\}$	The trace of the matrix \mathbf{X}
$ \mathbf{X} $	The determinant of the matrix \mathbf{X}
$\ \mathbf{x}\ ^2$	The squared Euclidean norm of the vector \mathbf{x} i.e., $\sum_i \mathbf{x}_i ^2$
$\ \mathbf{X}\ ^2, \ \mathbf{X}\ _F^2$	The Frobenius norm of the matrix \mathbf{X} i.e., $\sum_i \sum_j \mathbf{X}_{i,j} ^2$
$\text{sgn}\{x\}$	The sign of x
$\lfloor x \rfloor$	Floor function: the largest integer less than or equal to x
$\lceil x \rceil$	Ceiling function: the smallest integer greater than or equal to x
$O(N)$	“Big O” notation when the function argument tends towards N .

$E\{\cdot\}$	Expected value
$\mathcal{N}(\mu, \sigma)$	Normal distribution with mean μ and standard deviation σ
$\mathcal{CN}(\mu, \sigma)$	Complex-Normal distribution with mean μ and standard deviation σ

List of Abbreviations

AOA, DOA, DF	Angle of Arrival, Direction of Arrival, Direction Finding
AWGN	Additive White Gaussian Noise
CPU	Central Processing Unit
CRLB	Cramér Rao Lower Bound
DPD	Direct Position Determination
FDOA, DDOP	Frequency Difference of Arrival, Differential Doppler
FIM	Fisher Information Matrix
FLOPS, flops	Floating point Operations
GHz	Gigahertz
GNSS	Global Navigation Satellite System
GPS	Global Positioning System
LoS, NLoS	Line-of-Sight, Non-Line-of-Sight
LS, LSE	Least Squares (Estimator)
MAP	Maximum <i>a Posteriori</i>
MFP	Matched-Field Processing
MHz	Megahertz
MIMO	Multiple Input Multiple Output
ML, MLE	Maximum Likelihood (Estimator)
MUSIC	Multiple Signal Classification
OFDM	Orthogonal Frequency Division Multiplexing
PCL	Passive Coherent Location
RF	Radio-Frequency
RMSE	Root Mean Square Error
RSS	Received Signal Strength
RX	Receive
SNR	Signal to Noise Ratio
SVD	Singular Value Decomposition
SPG	Single Platform Geolocation
TDOA, DTOA	Time Difference of Arrival, Difference of TOA
TOA	Time of Arrival
TX	Transmit

List of Figures

1.1	Google N-gram Results for Positioning-Related English Phrases	2
3.1	System Architecture for Direct Positioning using MIMO Radar	17
3.2	DPD Estimation Scatter Plot	33
3.3	Unknown Deterministic Signals: AOA+TOA vs. DPD	35
3.4	DPD using Known and Unknown Deterministic Signals vs. CRLB	36
3.5	Stochastic DPD Performance	37
3.6	Location Error Probability for Unknown Signals	38
3.7	Effect of TX Diversity on the "Whiteness" of the Channel	39
4.1	SPG Geometry with Moving Receiver & Static Transponders	46
4.2	System Layout	64
4.3	RMSE $T = 166.7\mu s$, Bandwidth = 300[KHz], $V=100\frac{m}{s}$	66
4.4	RMSE $T = 50\mu s$, Bandwidth = 1[MHz], $V=5\frac{m}{s}$	67
4.5	RMSE $T = 50\mu s$, Bandwidth = 1[MHz], $V=100\frac{m}{s}$	67
4.6	Known Signal CRLB for 2 Transponders and a receiver moving at $V = 100\frac{m}{s}$, SNR = 25[dB]	69
4.7	Known Signal CRLB for 4 Transponders and a receiver moving at $V = 100\frac{m}{s}$, SNR = 25[dB]	70
4.8	Empirical CDF for 2 Transponders	71
4.9	Empirical CDF for 4 Transponders	72
5.1	Emitter Geolocation in Presence of Local Scattering - Problem Definition	75
5.2	Geolocation of Emitter under Local Scattering - System Layout	92
5.3	RMSE Performance for Quasi-Static Channel ($N_s = 4$), $L = 3$ and $\sigma_p = 50m$	93
5.4	1-Step vs. 2-Step Position Estimation with $L = 3$ Base-Station.	94
5.5	CRLB for Quasi-Static Fading Channel $N_s = 4$, $K = 100$, $L = 3$ @ SNR = 10[dB]	96

5.6 CRLB for Fast-Fading Channel $N_s = 1, K = 100, L = 3$ @ SNR
= 10[dB] 97

List of Algorithms

1	DPD Algorithm for Known MIMO Radar Signals	23
2	DPD Algorithm for Unknown MIMO Radar Signals	26
3	DPD Algorithm for Stochastic Signals	31
4	Direct SPG Algorithm for Known Emitter Signal and Unknown Transmission Time	53
5	Direct SPG Algorithm for Unknown Emitter Signal using a Mov- ing Receiver	57
6	Direct SPG Algorithm for Unknown, Arbitrary Emitter Signal and Slowly Moving Receiver	61
7	Pilot-Aided Direct SPG Algorithm for Unknown Emitter Signal using a Moving Receiver	62
8	Direct SPG Algorithm for Unknown, Arbitrary Emitter Signal . .	136

List of Tables

4.1	Computational Complexity of SPG using Moving Receiver . . .	63
5.1	Computational Complexity of DPD under Local Scattering . . .	100

Chapter 1

Introduction

1.1 Overview of Geolocation Problems

We address the problem of the “geolocation” of mobile radio-transmitters and passive targets; namely, the geographical location of passive targets or devices that transmit radio-signals, is of interest and has to be estimated. Over recent decades, this problem has attracted increasing research attention. An interesting graphical illustration for this increased attention is provided in Fig. 1.1. This figure depicts the normalized recurrence of English language phrases related to the topic of geolocation and positioning in literature published between 1970-2008¹.

The geolocation system typically consists of sensors or arrays of sensors distributed over a large geographical area at known locations. Each sensor intercepts signals arriving from the mobile devices (or reflected back from passive targets).

The geolocation problem consists of optimally exploiting the location dependent information embedded in the signals received by the sensors, in order to retrieve the locations of the mobile devices. The common approach employed in many geolocation problems states that the location estimation is split into two phases: first, the collected signals are processed to obtain loca-

¹This recurrence can be measured using an online tool called “Google Books N-gram viewer” provided by Google: <https://books.google.com/ngrams>

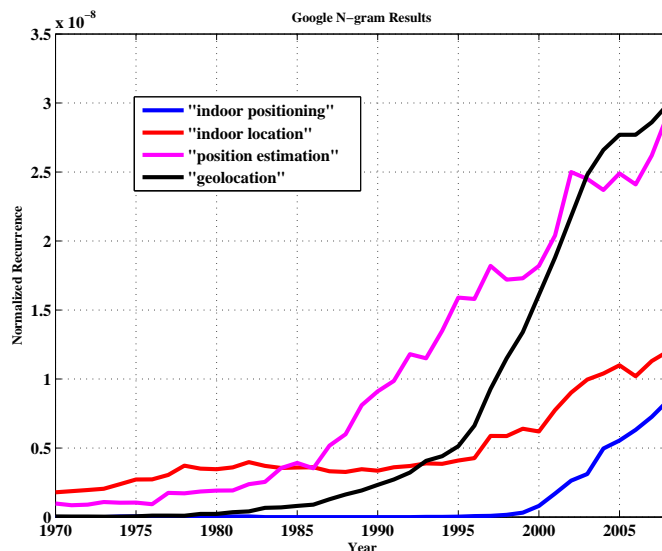


Figure 1.1: Google N-gram Results for Positioning-Related English Phrases

tion dependent information, such as time-of-arrival (TOA) of signals at a given sensor, time-difference-of-arrival (TDOA) of signals between pairs of sensors, angle-of-arrival (AOA), received signal strength (RSS), and Doppler data. The location-dependent information extracted by each sensor defines a geographical line of position (LOP), on which the transmitter (or the target) might lie. In the second step, the system applies procedures known as triangulation (in the case of AOA), trilateration (in case of TOA/RSS), or multilateration (in case of TDOA), in order to calculate the intersection points between the LOPs and estimate the geographical location of the transmitter/target. This procedure is commonly referred to as the “two-step” approach.

This dissertation is dedicated to exploring the performance of direct positioning, that is: the position of the transmitter or the passive target is estimated directly from the raw samples of the signals received by the receive-stations, without going through an explicit estimation phase of the location-related parameters. This method has been shown to outperform the conventional two-step methods under low SNR regime, which characterize the operating conditions of many communication systems. We first give further details on geolocation, in order to precisely define the scope of this dissertation.

Passive vs. Active Localization

In *passive* positioning systems, the signal arriving from the device to be located is emitted by the device itself: depending on the application, the signal characteristics (e.g., waveform, transmit time, carrier frequency) may be partially known (friendly emitter) or totally unknown (unfriendly/foe emitter) at the sensors of the positioning system. In passive localization, the device to be located is frequently called a source; the sensors and arrays of sensors that compose the positioning system are called receivers or base stations.

In *active* positioning systems, the signal arriving from the target is *not* generated by the latter as in passive geolocation; the signal is initially transmitted by the positioning system, then reflected by the target, and finally propagates backward to the positioning system. Radar and sonar are examples of active positioning systems. In active radar systems, the signal waveforms are generated by the system itself and therefore are considered as known. However, *passive radars* rely on “signals of opportunity,” namely signals broadcast by radio or TV stations, for locating targets. In such cases, the signal waveforms may not be considered as known to the geolocation system. The problem of active localization is addressed in chapter 3, in the context of harnessing MIMO Radar technology for direct target positioning.

Cooperative vs. Uncooperative Localization

In *uncooperative* emitter localization, the emitter does not collaborate with the positioning system; it is, therefore, the simplest form of passive localization. Conversely, *cooperative* localization achieves better positioning performance by means of information exchanges between the emitter and the receivers, including a possible feedback to the emitter. An example of cooperation consists of an emitter designed to repeat the positioning signal transmission if its reception is not acknowledged by enough receivers. Of course, the positioning accuracy is improved in cooperative localization at the expense of increased computational costs and communication overloads.

This document focuses on optimal data processing for geolocation. It is assumed that the data is already available; the way the data is obtained, whether

cooperatively or not, does not affect the issues discussed in this document.

Centralized vs. Decentralized Processing

Conventional positioning approaches, known as decentralized methods, are based on two steps. First, each station processes the intercepted signal and provides a measurement related to the emitter localization. Several types of measurements can be obtained in this first step. For example, angle-of-arrival (AOA) data are measurements of the direction of the emitter with regard to the stations [35],[2],[119]. Time-of-arrival (TOA) data are measurements of the propagation times between the emitter and the stations. If the transmit time is not known at the stations, the data are time-difference-of-arrival (TDOA) measurements. Other types of measurements include received-signal-strength (RSS) and differential-Doppler. The measurements realized independently at the different stations are then collected and processed in a second step, which finally provides location estimates for the emitter. All of these techniques can be classified as decentralized processing methods, since the observed signals are exploited independently at each station. It is usually assumed that the measurements are accurate or degraded by small errors only, whereas large errors or biased measurements are overlooked. See papers by Wax and Kailath (1985) [5], and Kozick and Sadler (2004) [6].

Centralized processing methods solve the localization problem using the data collected at all sensors, at all base stations together. As indicated by Wax and Kailath (1983) [7], measuring AOA/TOA at each base station separately and independently is suboptimal since this approach ignores the constraint that the measurements must correspond to the same source position. Therefore, centralized methods outperform decentralized methods. The Direct Position Determination (DPD) algorithm by Weiss (2004) is an efficient centralized location estimator with several side benefits [14].

1.2 The Radio Channel in Geolocation

A propagating signal may experience fluctuations due to three mechanisms: thermal noise, large scale fading, and small scale fading. Large scale fading refers to slow fluctuations due to path loss and shadowing; small scale fading refers to rapid fluctuations due to multipath effects.

Thermal Noise at the Receivers

Thermal noise results from numerous random processes such as: thermal vibrations of atoms in conductors, shot noise and so on. The cumulative effect of these processes invokes the central limit theorem (CLT) and enables us to model this error source as a random Gaussian process. The thermal noise corrupts signals intercepted by receivers and sensors. As a result, the location-related measurements realized by receivers and sensors are all degraded by small errors, even in the case of a signal propagating through an ideal radio channel.

Path Loss and Inaccuracy in RSS Measurements

Path loss is defined as the mean attenuation of a signal due to the physical separation between the transmitter and the receiver. Path loss depends upon the carrier frequency and the physical environment of the radio channel, e.g., urban, indoor, non-line-of-sight, and industrial. There are theoretical models, such as the Friis' formula, that poorly match real-world environments. The path loss models considered in practice have been derived empirically by means of extensive measurement campaigns. Since the actual path loss likely differs from the model, range measurements obtained from RSS data are usually inaccurate.

Shadowing and Inaccuracy in TOA/TDOA/RSS Measurements

The second cause for small scale fading is *shadowing*, and refers to signal attenuation due to obstacles in the propagation path. Since the presence of obstacles is usually unpredictable, shadowing is modeled by random variables.

Their distribution depends upon the nature (walls, furniture, bystanders) and the density (number, size, materials) of these obstacles. Since these obstacles evolve rather slowly, in seconds or minutes, the random attenuations are strongly correlated over time. The signal attenuation due to shadowing obviously degrades RSS measurements.

The physical phenomenon that enables signal propagation behind an obstacle is *diffraction*. When a signal reaches an obstacle, its electromagnetic waves bend around the obstacle and by-pass it to reach the receiver. The propagation path is therefore longer than the direct path. Thus, the actual propagation time to the receiver is longer than the propagation time in line-of-sight conditions. As a result, shadowing also adds measurement errors to TOA and TDOA data.

Multipath and AOA/TOA/RSS

Besides noise and large scale fading, a propagating signal also experiences small scale fading. The latter are often considered as being the most harmful fluctuations. Small scale fading results from multipath propagation between the emitter and the receiver.

Even in the presence of a line-of-sight (LoS) direct path, the transmitted signal is frequently reflected from numerous scatterers. Thus, some duplicate versions of the transmitted signal propagate to the receiver along multiple paths passing through the reflecting scatterers. This phenomenon is called *multipath* propagation. Since the multiple paths differ from each other and depend upon the scatterers randomness, the duplicate versions of the signals are attenuated and delayed by different independent random values. The signal intercepted at the receivers is therefore a superposition of duplicates with random attenuations and delays. It yields unpredictable constructive and destructive self-interferences.

If multipath signals coherently sum into a constructive interference, their overall energy may be greater than that of the direct path signal. Thus, RSS measurements may be inaccurate. Furthermore, this peak of energy corresponds to longer paths, and is therefore observed after the possible arrival of

the direct path signal. In these conditions, a TOA measurement obtained by energy detection necessarily suffers from significant measurement errors. Similarly, a peak of energy may be observed in a direction that is not that of the emitter. Thus AOA measurements are also subject to large measurement errors. Thus, multipath propagation affects all types of measurements.

In the frequency domain, multipath conditions result in frequency selective fading. This is a radio propagation anomaly caused by partial cancellation of a radio signal by itself. In frequency-selective fading, the *coherence bandwidth* of the channel, (i.e., the range of frequencies over which the channel can be considered “flat”), is smaller than the bandwidth of the signal. Different frequency components of the signal therefore experience uncorrelated fading. In contrast, in flat fading, which characterize LoS channels, the coherence bandwidth of the channel is larger than the bandwidth of the signal. Therefore, all frequency components of the signal will experience the same magnitude of fading.

The frequency selectivity phenomena makes multipath channels very challenging for geolocation problems. To combat frequency selectivity, state of the art communication systems employ certain modulation schemes such as orthogonal frequency-division multiplexing (OFDM) and code division multiple access (CDMA) that employ frequency diversity to provide robustness to frequency selective fading. OFDM divides the wideband signal into many slowly modulated narrowband subcarriers, each exposed to flat fading rather than frequency selective fading. Some results for direct positioning of OFDM transmitters have been published in [21] and [23].

Chapter 2

Literature Survey & Dissertation Contributions

In the previous chapter, we defined the challenges in source/target geolocation and explained that:

- Geolocation is realized using intercepted signals and measurements,
- The signals and measurements are degraded by the radio-channel,
- These degradations make localization a complex challenge,
- Geolocation based on a two-step method is inherently suboptimal as it ignores the constraint that the all independently-estimated, location-dependent parameters correspond to the same position.

On the basis of these facts, we ask the following question: could the geolocation estimation results improve, provided that the raw samples of the emitter/target signals collected from all the receive sites, are combined and jointly processed? Answering this question is the motivation and the guideline for this dissertation.

Out of multiple geolocation applications, this research has elected to focus on several novel aspects, to which direct geolocation may be applied. This dissertation describes advances in the fields of:

- Single-step target localization using MIMO Radar,

- Single-step, single platform geolocation using both static and moving receiver,
- Single-step emitter localization in the presence of local scattering,

In this chapter, we first provide a literature survey on geolocation, followed by a literature review of the specific topics dealt with in this dissertation: MIMO Radar, single-station geolocation and signal modeling under local scattering. We then describe in more detail the contribution of this dissertation to the topic.

2.1 Literature Survey of Geolocation

The problem of source localization has received a lot of consideration in scientific literature dealing with signal processing, communications, and underwater acoustics. Military applications date back to World War I. Currently, civilian applications include the localization of cellular phone callers, spectrum monitoring, and law enforcement. Stansfield (1947) submitted one of the first papers on the mathematics of source localization using AOA [1]. Many other publications followed including a fine review paper by Torrieri (1984) [35]. Wax (1995), Krim and Viberg (1996) provided comprehensive review papers on antenna array processing for location by AOA [2]-[3] and Van Trees (2002) published a book exclusively dedicated to array processing [119].

In the recent decades, the extensive development of wireless communications has provided a plethora of infrastructure that incidentally comply with positioning systems. Although communication networks were not designed for geolocation purposes, they are efficiently exploited to that end. The wide coverage of cellular networks motivates a profusion of geolocation applications, e.g. focused advertising and rescue systems. A 1998 review by Bussgang et al., describes the implementation of passive geolocation methods for emergency systems [4]. Another set of comprehensive review papers addressing various aspects of geolocation in wireless networks appeared in the July 2005 issue of the IEEE Signal Processing Magazine, [86]-[89].

Geolocation using MIMO Radar

The idea of multiple-input and multiple-output (MIMO) radar has been proposed as an extension to multi-static radar. Relying on concepts similar to those employed by MIMO communications, MIMO radar uses multiple uncorrelated transmitters and multiple receivers to gain diversity against the Radar Cross Section scintillation and improve radar detection performance [62],[63]. Since its emergence, MIMO radar has attracted significant interest in the academic community, which is indicated by the numerous number of publications on this topic. Several directions have already been addressed in the literature, including: Angle-of-arrival (AOA) estimation accuracy with MIMO radar [64], detection performance [65], optimized signal design [66], effects of co-located antennas [67] and others.

Another radar topic that has re-emerged in recent years is the so-called Passive Coherent Location (PCL) radar (also known as “covert radar”). PCL is an opportunistic method of using existing radio-frequency transmitters (for example, commercial FM radio broadcasts) for the purpose of target detection and tracking. The roots of this idea date back to the seminal experiment of Watson-Watt and Wilkins that was conducted in Daventry, U.K., on the 26th of February 1935. During this experiment, these two radar pioneers managed to detect a bomber in flight using BBC broadcast transmissions [68]. Currently, PCL is becoming more and more popular as low-cost radar for monitoring aviation traffic in developing countries [69], [70]. It is rather obvious that augmenting PCL systems with signal diversity should improve their performance, and, thus, it is of interest to explore the performance of MIMO PCL systems.

The application of MIMO radar for target localization using the conventional AOA method was addressed in [71]. In addition, [72] and [73] developed analysis tools such as the Cramér-Rao bound and Geometric Dilution of Precision (GDOP). This topic was also addressed in papers in PCL literature such as [74], [75] and [76].

Single Platform Geolocation

Single-Site Location (or Single Station Location/SSL) is a concept, which has multiple interpretations. Commonly, it refers to a localization system that enables localizing radio transmitters using a single receiver. That is to distinguish the concept of SSL from radar and sonar systems, which although comprised of a single receiver, are designed to locate passive targets rather than radio transmitters. In the literature SSL is described as a method for over-the-horizon (OTH) geolocation of high-frequency transmitters (HF: 2MHz to 30MHz) [9]-[12],[122]. Relying on the physical phenomenon of ionosphere refractions of HF signals, HF-SSL systems manage to provide an estimate of the HF transmitter position through the use of extremely-large antenna arrays (spanned over hundreds of meters). These arrays enable the estimation of the azimuth and elevation angles of arrival (AOA) of the HF signal multipath with an adequate resolution [13]. The estimated AOA are then embedded into a mathematical model of the ionosphere layers to obtain an estimate of the HF transmitter's location. Due to inaccuracies in the ionosphere model, the rather large distance between the receiver and the transmitter, and AOA estimation errors, the overall HF-SSL geolocation accuracy is rather rough.

In chapter 4, the concept of single-station localization is extended to explore the localization of radio transmitters using common indoor and outdoor RF propagation models. In chapter 4, a novel geolocation system architecture is discussed. This new architecture, termed "single platform geolocation" (SPG) system, can be viewed as an evolution of the SSL idea: similar to HF-SSL, SPG uses a single platform receiver, but in contrast to HF-SSL the signal multipath is not generated through ionospheric refractions. In SPG, the signal multipath is man-made and generated by inexpensive and simple signal transponders (or signal reflectors). These transponders, which are placed at known locations, reflect the emitter's signal towards the single receiver. The single receiver needs to process all the received signals in order to extract the emitter's position.

Since SPG is designed for relatively high radio frequencies and is not intended to be used for HF-OTH applications, it does not require large and expensive antenna arrays. The platform receiver uses an array of only a few

wavelengths, which is relatively small for frequencies above 500 MHz.

Direct Geolocation in the Presence of Local Scattering

The advancement in smart antenna technology during the 1990's has motivated the development of spatial/temporal channel models to facilitate accurate performance prediction of multi-antenna systems. The paper by Ertel *et al.* [42] provides a comprehensive summary of these multi-antenna channel models. Most of these models are based on a combination of spatial and temporal numerical channel modeling, for which analytic analysis is difficult. One of these channel models, termed Gaussian Angle of Arrival (GAA), was proposed by Zetterberg [43], and was later adopted by Ottersten, Trump and others [44]-[50]. The GAA model was developed for obtaining a statistical description of the array correlation under narrow-band Rayleigh fading channels, often characterizing macro-cell cellular environments in suburban areas. The model assumes that the emitter lies within a cluster of scatterers, generating multiple reflections of the emitter's signal. The associated angle of arrival (AOA) at an antenna array has a Gaussian distribution.

Since its publication, the GAA model has been applied to mainly AOA-estimation problems of distributed sources under various channel and signal models [46]-[57]. However, very little attention was given to geolocation of such distributed sources. Chapter 5 aims to bridge this gap by incorporating the GAA model into the geolocation problem model and deriving single-step algorithms for localizing distributed sources under Rayleigh fading channel conditions.

2.2 Dissertation Contributions

In this dissertation, we explore different emitter and target localization problems, where the focus is on single-step localization. This dissertation describes advances in the fields of:

- Single-step target localization using MIMO Radar
 - MIMO Radar with known signal waveforms

- MIMO Radar with unknown (both random and deterministic and unknown) signal waveforms (passive MIMO radar using signals of opportunity)
- Single-step, single platform geolocation (SPG) using a static/moving receiver,
 - SPG with known signal waveforms
 - SPG with deterministic and unknown signal waveforms and fast/slow moving receiver
- Single-step emitter localization in the presence of local scattering
 - Derivation of a spatio-temporal model for emitter geolocation in the presence of local scattering (Rayleigh channel fading)
 - Optimal & sub-optimal algorithms

The theme of the dissertation is the development of powerful algorithmic tools and performance bounds for these localization problems.

Chapter 3

Direct Positioning of Stationary Targets Using MIMO Radar

3.1 Introduction

MIMO Radar is a relatively new concept that has been proposed as an extension to the multi-static Radar systems. In this chapter, we apply the direct position determination (DPD) approach to MIMO Radar and obtain maximum likelihood algorithms for a location estimation of a stationary target. We examine a MIMO radar system with multiple widely separated transmit antennas and multiple, widely separated receiving arrays for locating a stationary target. The receiving arrays do not estimate any parameters of the target, but instead send the raw observed signals to a fusion center (FC). The FC applies the DPD approach in order to estimate the target position directly (i.e., in a single step), given the raw samples supplied by the receiving arrays. Common location algorithms are based on a two-step approach: in the first step, parameter estimation (of TOA, AOA, etc.) is done at each of the receiving arrays, independently. The estimated parameters are then sent by the arrays to the FC. In the second step, a fix is estimated in the FC given the parameters estimated by the arrays in the first step.

It should be emphasized that the proposed system configuration herein differs from the system configurations that have been considered, e.g., in

[77], [78], [79], where the receive side was assumed to consist of individual antennas. The assumption of receiving arrays enables the implicit use of both the TOA and the array responses in the target localization algorithms in order to improve the estimation accuracy. It is also worth noting that an algorithm for direct processing of the received signals for determination of the target position has also been mentioned in [78], [79]. That algorithm, dubbed “direct multilateration”, has the possibility of being a maximum likelihood estimator (MLE) but an explicit derivation of it was not pursued.

Main Contributions

The main contributions of this chapter are novel, maximum-likelihood algorithms for direct target localization using the proposed MIMO radar system configuration. These algorithms are different from the algorithms that have been derived for an emitting target and are shown to outperform the conventional target localization algorithms. Parts of this chapter have been published in [22, 24].

Chapter Organization

The remainder of this chapter is organized as follows. In section 3.2, we formulate the signal and channel model assumed throughout this chapter. Section 3.3 outlines algorithms for Direct Target Position Determination under the assumption that the transmitted waveforms are either known or unknown to the FC. Numerical examples that highlight the superiority of the devised DPD method over the traditional AOA+TOA technique are presented in section 3.4. Discussion of the results is given in 3.5 and a summary with concluding remarks is outlined in section 3.6. The Cramér Rao lower bounds for known and Gaussian signal models are derived in appendix A.1.

3.2 Problem Formulation

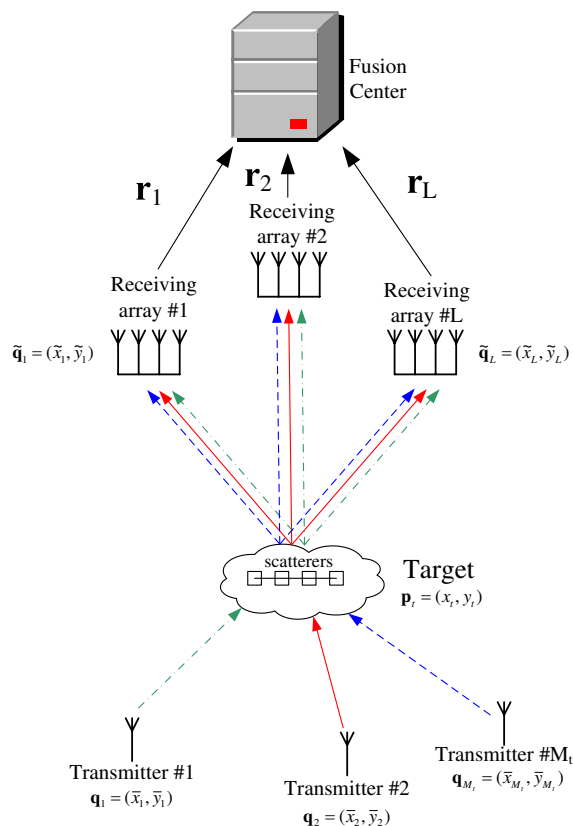


Figure 3.1: System Architecture for Direct Positioning using MIMO Radar

Consider a MIMO radar that consists of M_t , widely separated, transmit antennas and L , widely separated, receiving arrays. Each receiving array is equipped with M_r receive antennas. The receiving arrays intercept echoes from a far-field complex target. The target is illuminated by M_t narrow-band signals. The system architecture is depicted in Figure 3.1.

Each of the transmitted signals is subjected to a delay, which depends on the position of the transmitter and on the (unknown) position of the target. The location of all the transmitters and receivers is known to the FC. It is further assumed that all the receiving arrays are time synchronized.

Given the above assumptions, the time-domain signal received at the ℓ th

array can be described by

$$\mathbf{r}_\ell(t) = \mathbf{a}_\ell(\mathbf{p}_t) \sum_{m=1}^{M_t} \alpha_{\ell,m} s_m(t - \tau_{\ell,m}(\mathbf{p}_t)) + \mathbf{n}_\ell(t), \quad 0 \leq t \leq T \quad (3.1)$$

where, $\mathbf{r}_\ell(t)$ is an $M_r \times 1$ vector of the signals observed at the ℓ th array, $\mathbf{a}_\ell(\mathbf{p}_t)$ is an $M_r \times 1$ vector that denotes the ℓ th array response to the signals backscattered from the target located at position $\mathbf{p}_t = (x_t, y_t)$. Let $\tilde{\mathbf{q}}_\ell = (\tilde{x}_\ell, \tilde{y}_\ell)$ denote the location of the ℓ th array center. Let the \tilde{m} th element in the ℓ th array be located at $\tilde{\mathbf{q}}_{\ell\tilde{m}} = (\tilde{x}_{\ell\tilde{m}}, \tilde{y}_{\ell\tilde{m}})$, defined in local coordinates whose origin is the array center. The response of the \tilde{m} th element to a signal backscattered from the target is given by

$$[\mathbf{a}_\ell]_{\tilde{m}} = \frac{1}{\sqrt{M_r}} e^{-i \frac{2\pi}{\lambda} (\tilde{x}_{\ell\tilde{m}} \cos \tilde{\theta}_\ell + \tilde{y}_{\ell\tilde{m}} \sin \tilde{\theta}_\ell)} \quad (3.2)$$

where λ is the carrier signal wavelength. The angle between the signal direction of arrival and the local x -axis of the ℓ th array is denoted by $\tilde{\theta}_\ell$. Finally, the factor $\frac{1}{\sqrt{M_r}}$ is inserted to conform with $\|\mathbf{a}_\ell(\mathbf{p})\|^2 = 1$.

Further, $\alpha_{m,\ell}$ is an unknown variable representing the fading coefficient of the m th signal, s_m , at the ℓ th receiving array. At this point it is worth emphasizing that for the sake of the derivation of the algorithms, we make no specific assumptions regarding the statistical distribution of the fading coefficients. The assumptions regarding the realizations of the fading coefficients for the numerical performance study will be discussed later in section 3.4. Next, $\tau_{\ell,m}(\mathbf{p}_t)$ is the propagation delay of the signal from the m th transmitter to the ℓ th array. We notice that,

$$\tau_{\ell,m}(\mathbf{p}_t) = \tilde{\tau}_\ell(\mathbf{p}_t) + \tau_m(\mathbf{p}_t) \quad (3.3)$$

where $\tau_m(\mathbf{p}_t)$ is the propagation time from the m th transmitter to the target. Similarly, $\tilde{\tau}_\ell(\mathbf{p}_t)$ is the propagation time from the target to the ℓ th array and is therefore proportional to the distance between the target and that array. Finally, the $M_r \times 1$ additive noise vectors, $\mathbf{n}_\ell(t)$, are i.i.d., zero-mean, complex-Gaussian with covariance $\sigma_n^2 \mathbf{I}$. It is further assumed that the target is either

stationary or slowly moving so that the Doppler effect can be neglected.

The goal is to estimate the target position. The position is estimated using K consecutive samples of the received signals. The total observation time of the signal is $T = K \cdot T_s$, where $T_s = 1/f_s$ and f_s is the sampling rate. It is further assumed that target fading coefficients remain constant across the K samples. In our following analysis, we focus on three scenarios with respect to the receivers. In the first scenario, we assume that the transmitted waveforms are known to the receivers *a priori*. The other two scenarios deal with signal waveforms that are assumed to be unknown to the receivers. The second scenario deals with signals which are non-random but unknown. In the third scenario, we assume that the transmitted signals are yet unknown but are random and modeled as samples of a complex Gaussian process.

3.3 Algorithms for Direct Target Positioning

In the following section, we present direct position determination (DPD) algorithms using signals, which may be either known or unknown to the FC. The DPD belong to the least squares family if the noise statistics are unknown. If the noise is Gaussian, DPD is the exact maximum-likelihood (ML) estimate of location.

In order to obtain an attractive algorithm, it is desirable to separate the delay from the signal waveform. Therefore, we first apply the discrete Fourier transform (DFT) to the received signal and obtain¹,

$$\begin{aligned}\bar{\mathbf{r}}_{\ell,k} &= \mathbf{a}_\ell(\mathbf{p}_t) \sum_{m=1}^{M_t} \alpha_{\ell,m} \bar{s}_{m,k} e^{-i\omega_k \tau_{\ell,m}(\mathbf{p}_t)} + \bar{\mathbf{n}}_{\ell,k} \\ \omega_k &\triangleq \frac{2\pi k}{K \cdot T_s}, \quad 0 \leq k \leq K-1\end{aligned}\quad (3.4)$$

where, $\bar{s}_{m,k}$ is the k th Fourier coefficient of the m th received signal and $\bar{\mathbf{r}}_{\ell,k}$ and $\bar{\mathbf{n}}_{\ell,k}$ are $M_r \times 1$ vectors of the k th Fourier coefficients of $\mathbf{r}_\ell(t)$ and $\mathbf{n}_\ell(t)$, respectively.

In the sequel, the explicit dependence on the position vector, \mathbf{p}_t is frequently suppressed for clarity.

To begin our algorithm derivation, we define the following vectors,

$$\begin{aligned}\bar{\mathbf{s}}_k &\triangleq [\bar{s}_{1,k} e^{-i\omega_k \tau_1(\mathbf{p}_t)}, \dots, \bar{s}_{M_t,k} e^{-i\omega_k \tau_{M_t}(\mathbf{p}_t)}]^T \\ \boldsymbol{\alpha}_\ell &\triangleq [\alpha_{\ell,1}, \alpha_{\ell,2}, \dots, \alpha_{\ell,M_t}]^T \\ \tilde{\mathbf{a}}_{\ell,k} &\triangleq \mathbf{a}_\ell(\mathbf{p}_t) e^{-i\omega_k \tilde{\tau}_\ell(\mathbf{p}_t)}\end{aligned}\quad (3.5)$$

Using these definitions, equation (3.4) can be recast as,

$$\bar{\mathbf{r}}_{\ell,k} = \tilde{\mathbf{a}}_{\ell,k} \bar{\mathbf{s}}_k^T \boldsymbol{\alpha}_\ell + \bar{\mathbf{n}}_{\ell,k}\quad (3.6)$$

We now turn to examine three different cases.

¹Further discussion on the frequency domain model for finite length observations can be found in Appendix G of [16].

3.3.1 Known Signals

In this section, we derive the direct position determination algorithm under the assumption that a perfect knowledge of the signal waveforms exists in the FC. The log likelihood of $\bar{\mathbf{r}}_{\ell,k}$ conditioned on the unknown parameters $\boldsymbol{\alpha}_\ell$ and \mathbf{p} is equivalent, up to an additive constant and scaling to

$$Q(\mathbf{p}) = \sum_{\ell=1}^L \sum_{k=0}^{K-1} \left\| \bar{\mathbf{r}}_{\ell,k} - \tilde{\mathbf{a}}_{\ell,k} \tilde{\mathbf{s}}_k^T \boldsymbol{\alpha}_\ell \right\|^2 \quad (3.7)$$

In order to find the minimum of the cost function expressed in (3.7), we define the following vectors and matrices. Let,

$$\tilde{\mathbf{r}}_\ell \triangleq [\bar{\mathbf{r}}_{\ell,0}^H, \bar{\mathbf{r}}_{\ell,1}^H, \dots, \bar{\mathbf{r}}_{\ell,K-1}^H]^H \quad (3.8)$$

$$\tilde{\mathbf{A}}_\ell \triangleq \text{diag} \{ e^{-j\omega_0 \tilde{\tau}_\ell(\mathbf{p})}, \dots, e^{-j\omega_{K-1} \tilde{\tau}_\ell(\mathbf{p})} \} \otimes \mathbf{a}_\ell(\mathbf{p}) \quad (3.9)$$

$$\tilde{\mathbf{S}} \triangleq [\tilde{\mathbf{s}}_0, \dots, \tilde{\mathbf{s}}_{K-1}]^T \quad (3.10)$$

Using (3.8)-(3.10), we can rewrite the cost function in (3.7) as,

$$Q(\mathbf{p}) = \sum_{\ell=1}^L \left\| \tilde{\mathbf{r}}_\ell - \tilde{\mathbf{A}}_\ell \tilde{\mathbf{S}} \boldsymbol{\alpha}_\ell \right\|^2 \quad (3.11)$$

The vector $\boldsymbol{\alpha}_\ell$ that minimizes $Q(\mathbf{p})$ is given by,

$$\hat{\boldsymbol{\alpha}}_\ell = \left(\tilde{\mathbf{S}}^H \tilde{\mathbf{A}}_\ell^H \tilde{\mathbf{A}}_\ell \tilde{\mathbf{S}} \right)^{-1} \tilde{\mathbf{S}}^H \tilde{\mathbf{A}}_\ell^H \mathbf{r}_\ell \quad (3.12)$$

Using (B.37) we have,

$$\|\mathbf{a}_\ell(\mathbf{p})\|^2 = 1 \quad \forall \ell \quad (3.13)$$

and therefore $\tilde{\mathbf{A}}_\ell^H \tilde{\mathbf{A}}_\ell = \mathbf{I}_K$.

Thus,

$$\hat{\boldsymbol{\alpha}}_\ell = \left(\tilde{\mathbf{S}}^H \tilde{\mathbf{S}} \right)^{-1} \tilde{\mathbf{S}}^H \tilde{\mathbf{A}}_\ell^H \tilde{\mathbf{r}}_\ell \quad (3.14)$$

Substituting (3.14) back into (3.11) yields,

$$\begin{aligned}
 Q(\mathbf{p}) &= \sum_{\ell=1}^L \left\| \tilde{\mathbf{r}}_{\ell} - \tilde{\mathbf{A}}_{\ell} \tilde{\mathbf{S}} \left(\tilde{\mathbf{S}}^H \tilde{\mathbf{S}} \right)^{-1} \tilde{\mathbf{S}}^H \tilde{\mathbf{A}}_{\ell}^H \tilde{\mathbf{r}}_{\ell} \right\|^2 \\
 &= \sum_{\ell=1}^L \left\| \tilde{\mathbf{r}}_{\ell} \right\|^2 - \tilde{\mathbf{r}}_{\ell}^H \tilde{\mathbf{A}}_{\ell} \tilde{\mathbf{S}} \left(\tilde{\mathbf{S}}^H \tilde{\mathbf{S}} \right)^{-1} \tilde{\mathbf{S}}^H \tilde{\mathbf{A}}_{\ell}^H \tilde{\mathbf{r}}_{\ell}
 \end{aligned} \tag{3.15}$$

Define,

$$\mathbf{P} \triangleq \tilde{\mathbf{S}} \left(\tilde{\mathbf{S}}^H \tilde{\mathbf{S}} \right)^{-1} \tilde{\mathbf{S}}^H \tag{3.16}$$

Notice that \mathbf{P} is a projection matrix for which $\mathbf{P}^2 = \mathbf{P}$ (see e.g., [112, p.386]). Therefore (3.15) may be recast as,

$$Q(\mathbf{p}) = \sum_{\ell=1}^L \left\| \tilde{\mathbf{r}}_{\ell} \right\|^2 - \left\| \mathbf{P} \tilde{\mathbf{A}}_{\ell}^H \tilde{\mathbf{r}}_{\ell} \right\|^2 \tag{3.17}$$

Since $\|\tilde{\mathbf{r}}_{\ell}\|^2$ is independent of \mathbf{p} , the minimization of $Q(\mathbf{p})$ is equivalent to the maximization of $\tilde{Q}(\mathbf{p})$ defined by,

$$\tilde{Q}(\mathbf{p}) = \sum_{\ell=1}^L \left\| \mathbf{P} \tilde{\mathbf{A}}_{\ell}^H \tilde{\mathbf{r}}_{\ell} \right\|^2 \tag{3.18}$$

When the signals are *known* to the FC, then for any location \mathbf{p} defined on a search grid, \mathbf{P} can be calculated. The information on the target location is embedded both in \mathbf{P} and in $\tilde{\mathbf{A}}_{\ell}$. The maximum likelihood estimate of the target location is given by,

$$\hat{\mathbf{p}}_t = \underset{\mathbf{p}}{\operatorname{argmax}} \sum_{\ell=1}^L \left\| \mathbf{P} \tilde{\mathbf{A}}_{\ell}^H \tilde{\mathbf{r}}_{\ell} \right\|^2 \tag{3.19}$$

A possible implementation of this algorithm is described in Algorithm 1. This concludes the derivation of the DPD algorithm for known signals.

```

Define the area of interest and determine a suitable grid of locations
 $\mathbf{p}_1, \mathbf{p}_2 \dots \mathbf{p}_g$ 
for  $j = 1$  to  $g$  do
    Set  $C(\mathbf{p}_j) = 0$ 
    Evaluate  $\mathbf{P}(\mathbf{p}_j)$  according to (3.16)
    for  $\ell = 1$  to  $L$  do
        Evaluate  $\tilde{\mathbf{A}}_\ell(\mathbf{p}_j)$  according to (3.9)
        Let  $C(\mathbf{p}_j) = C(\mathbf{p}_j) + \left\| \mathbf{P} \tilde{\mathbf{A}}_\ell^H(\mathbf{p}_j) \tilde{\mathbf{r}}_\ell \right\|^2$ 
    end
end
Find the grid point for which  $C$  is the biggest. This grid point is the
estimated position.

```

Algorithm 1: DPD Algorithm for Known MIMO Radar Signals

3.3.2 Unknown Signals

In conventional radar systems, the receivers have a prior knowledge of the signal waveforms. Yet, in PCL radar systems, which utilize broadcast radio and television signals for target locations, the signal waveforms may not be known in advance. Moreover, the case of unknown signals is also useful for conventional MIMO radar systems in which the transmitted signal replicas that are generated in the central location system are subjected to deformation. Such deformations result in an imperfect knowledge of the signal waveform and may include various kinds of drifts such as: phase, frequency, time or even distortions such as amplitude compression due to non-linear amplification.

In this section, we present two algorithms:

- A deterministic maximum-likelihood (ML) algorithm that utilizes both AOA and TDOA information.
- A stochastic DPD algorithm under the assumption that the signals transmitted are Gaussian random signals.

Deterministic Maximum Likelihood Algorithm

When the signals are *unknown* to the FC, then \mathbf{P} is unknown and its elements must also be estimated. Yet, our interest is in estimating \mathbf{p}_t , while the elements

of \mathbf{P} are considered nuisance parameters. In the following theorems, we prove that by relying on the projection matrix properties, the target position, \mathbf{p}_t , may be estimated directly, *without* explicitly estimating the elements of \mathbf{P} . In our analysis, we distinguish between two cases: $L \leq M_t$ and $L > M_t$.

$$L \leq M_t < K$$

Theorem 3.3.1 *The deterministic maximum likelihood estimator of the target position using $L \leq M_t$ uncorrelated signals is given by*

$$\hat{\mathbf{p}}_t = \underset{\mathbf{P}}{\operatorname{argmax}} \sum_{\ell=1}^L \left\| \tilde{\mathbf{A}}_{\ell}^H \tilde{\mathbf{r}}_{\ell} \right\|^2 \quad (3.20)$$

Proof Straightforward mathematical manipulations of (3.18) yield,

$$\begin{aligned} \tilde{Q}(\mathbf{p}) &= \sum_{\ell=1}^L \left\| \mathbf{P} \tilde{\mathbf{A}}_{\ell}^H \tilde{\mathbf{r}}_{\ell} \right\|^2 \\ &= \sum_{\ell=1}^L \tilde{\mathbf{r}}_{\ell}^H \tilde{\mathbf{A}}_{\ell} \mathbf{P} \tilde{\mathbf{A}}_{\ell}^H \tilde{\mathbf{r}}_{\ell} \\ &= \operatorname{Tr} \left\{ \mathbf{P} \sum_{\ell=1}^L \tilde{\mathbf{A}}_{\ell}^H \tilde{\mathbf{r}}_{\ell} \tilde{\mathbf{r}}_{\ell}^H \tilde{\mathbf{A}}_{\ell} \right\} = \operatorname{Tr} \{ \mathbf{P} \mathbf{D} \} \end{aligned} \quad (3.21)$$

where $\mathbf{D} \triangleq \sum_{\ell=1}^L \tilde{\mathbf{A}}_{\ell}^H \tilde{\mathbf{r}}_{\ell} \tilde{\mathbf{r}}_{\ell}^H \tilde{\mathbf{A}}_{\ell} \triangleq \sum_{\ell=1}^L \mathbf{d}_{\ell} \mathbf{d}_{\ell}^H$ and $\operatorname{tr}\{\cdot\}$ denotes the trace of a matrix.

Since both \mathbf{P} and \mathbf{d}_{ℓ} are \mathbf{p} -dependent and given that \mathbf{P} is a $K \times K$, projection matrix of rank M_t , then provided that $L \leq M_t$ the right hand side (r.h.s.) of (3.21) is maximized if the L vectors \mathbf{d}_{ℓ} , lie within the space spanned by \mathbf{P} . Noticing that $\sum_{\ell=1}^L \mathbf{d}_{\ell}^H \mathbf{d}_{\ell} = \operatorname{Tr}\{\mathbf{D}\}$, then the maximum likelihood estimator of the target location in the case of unknown signals is given by,

$$\hat{\mathbf{p}}_t = \underset{\mathbf{P}}{\operatorname{argmax}} \sum_{\ell=1}^L \left\| \tilde{\mathbf{A}}_{\ell}^H \tilde{\mathbf{r}}_{\ell} \right\|^2 \quad (3.22)$$

This concludes the proof for the case where $L \leq M_t < K$.

$$M_t < L < K$$

Theorem 3.3.2 *The deterministic maximum likelihood estimator of the target position using $M_t < L < K$ uncorrelated signals is given by*

$$\hat{\mathbf{p}}_t = \underset{\mathbf{P}}{\operatorname{argmax}} \sum_{m=1}^{M_t} \lambda_m \{\mathbf{D}\} \quad (3.23)$$

where $\lambda_m \{\mathbf{D}\}$ denotes the m th largest eigenvalue of \mathbf{D} .

Proof Let the singular value decomposition (SVD) of \mathbf{D} be $\mathbf{D} = \mathbf{U}\mathbf{\Delta}\mathbf{U}^H$, where $\mathbf{\Delta}$ is a $K \times K$ diagonal matrix containing the singular values of \mathbf{D} along its diagonal and \mathbf{U} is a $K \times K$ unitary matrix containing K singular vectors for the corresponding singular values. Now (3.21) can be presented as,

$$\operatorname{tr} \{\mathbf{P}\mathbf{D}\} = \operatorname{tr} \{\mathbf{P}\mathbf{U}\mathbf{\Delta}\mathbf{U}^H\} \quad (3.24)$$

Since \mathbf{P} is unknown, we are free to select a projection matrix such that the r.h.s. of (3.21) is maximized. We therefore define the SVD of \mathbf{P} as $\mathbf{P} = \mathbf{U}\mathbf{\Sigma}\mathbf{U}^H$, where $\mathbf{\Sigma}$ is a $K \times K$ diagonal matrix containing the singular values of \mathbf{P} . Since \mathbf{P} is a projection matrix of rank M_t then $\mathbf{\Sigma}$ has exactly M_t elements that are equal to 1 on its diagonal, while the remaining elements are zeros. Since \mathbf{U} is a unitary matrix this selection leads to,

$$\begin{aligned} \operatorname{tr} \{\mathbf{P}\mathbf{U}\mathbf{\Delta}\mathbf{U}^H\} &= \operatorname{tr} \{\mathbf{U}\mathbf{\Sigma}\mathbf{U}^H\mathbf{U}\mathbf{\Delta}\mathbf{U}^H\} \\ &= \operatorname{tr} \{\mathbf{U}\mathbf{\Sigma}\mathbf{\Delta}\mathbf{U}^H\} \\ &= \operatorname{tr} \{\mathbf{\Sigma}\mathbf{\Delta}\} \\ &= \sum_{m=1}^{M_t} \lambda_m \end{aligned} \quad (3.25)$$

where $\lambda_1 \geq \lambda_2 \geq \dots \geq \lambda_L$ are the diagonal elements of $\mathbf{\Delta}$. Since the diagonal elements of $\mathbf{\Delta}$ are also the eigenvalues of \mathbf{D} it follows that the r.h.s of (3.21) is maximized by summing the M_t largest eigenvalues of \mathbf{D} .

This algorithm can be implemented as described in Algorithm 2. This concludes the derivation of the deterministic ML algorithm for unknown signals.

Define the area of interest and determine a suitable grid of locations

$\mathbf{p}_1, \mathbf{p}_2 \dots \mathbf{p}_g$

for $j = 1$ **to** g **do**

 Set $C(\mathbf{p}_j) = 0$

 Set $C_1 = 0$

for $\ell = 1$ **to** L **do**

 Evaluate $\tilde{\mathbf{A}}_\ell$

 Evaluate $\mathbf{d}_\ell = \tilde{\mathbf{A}}_\ell^H(\mathbf{p}_j)\tilde{\mathbf{r}}_\ell$

if $L \leq M_t$ **then**

 | $C_1 = C_1 + \mathbf{d}_\ell^H \mathbf{d}_\ell$

end

else

 | $C_1 = C_1 + \mathbf{d}_\ell \mathbf{d}_\ell^H$

end

end

if $L \leq M_t$ **then**

 | Let $C(\mathbf{p}_j) = C_1$

end

else

 | Calculate SVD for C_1 and find its M_t largest eigenvalues

 | Let $C(\mathbf{p}_j) = \sum_{m=1}^{M_t} \lambda_m \{C_1\}$

end

end

Find the grid point for which C is the biggest. This grid point is the estimated position.

Algorithm 2: DPD Algorithm for Unknown MIMO Radar Signals

Stochastic DPD Algorithm

In the following section, we derive the DPD algorithm under the assumption that the transmitted signals are drawn from a zero-mean, narrow-band, Gaussian process. We assume that the variables of (3.6) satisfy,

$$\begin{aligned}
 E \{ \bar{\mathbf{s}}_k \} &= 0 \quad \forall k \\
 E \{ \bar{\mathbf{n}}_{\ell,k} \} &= 0, \quad \forall \ell, k \\
 E \{ \bar{\mathbf{s}}_k \bar{\mathbf{n}}_{\ell,k}^H \} &= \mathbf{0}, \quad \forall \ell, k \\
 E \{ \bar{\mathbf{s}}_k^H \bar{\mathbf{n}}_{\ell,k} \} &= 0, \quad \forall \ell, k \\
 E \{ \bar{\mathbf{n}}_{\ell,k} \bar{\mathbf{n}}_{i,j}^H \} &= \sigma_n^2 \mathbf{I}_{M_r} \delta_{\ell,i} \delta_{k,j} \\
 E \{ \bar{\mathbf{s}}_k \bar{\mathbf{s}}_j^H \} &= \frac{1}{M_t} \mathbf{I}_{M_t} \delta_{k,j}
 \end{aligned} \tag{3.26}$$

Further, we assume that the vector of the fading coefficients at the ℓ th receiving array, $\boldsymbol{\alpha}_\ell$, is modeled as a vector of unknown parameters. It is assumed that transmitting antennas are located sufficiently apart from each other such that uncorrelated target aspects are received at each of the receiving arrays per each of the transmitted signals [64]. The latter assumption implies that the fading vectors at different arrays are nearly orthogonal. Hence,

$$|\boldsymbol{\alpha}_\ell^H \boldsymbol{\alpha}_i| \ll \|\boldsymbol{\alpha}_\ell\|^2 = M_t \sigma_\ell^2, \quad \forall \ell \neq i \tag{3.27}$$

For a given set of fading vectors $\boldsymbol{\alpha}_\ell, \boldsymbol{\alpha}_i$ the conditioned covariance matrix is given by,

$$\begin{aligned}
 \mathbf{R}_{\ell,i,k,j} |_{\boldsymbol{\alpha}_\ell, \boldsymbol{\alpha}_i} &= E \{ \bar{\mathbf{r}}_{\ell,k} \bar{\mathbf{r}}_{i,j}^H \} \\
 &= E \left\{ \left(\tilde{\mathbf{a}}_{\ell,k} \boldsymbol{\alpha}_\ell^T \bar{\mathbf{s}}_k + \bar{\mathbf{n}}_{\ell,k} \right) \left(\tilde{\mathbf{a}}_{i,j} \boldsymbol{\alpha}_i^T \bar{\mathbf{s}}_j + \bar{\mathbf{n}}_{i,j} \right)^H \right\} \\
 &= \frac{1}{M_t} \boldsymbol{\alpha}_\ell^H \boldsymbol{\alpha}_i \tilde{\mathbf{a}}_{\ell,k} \tilde{\mathbf{a}}_{i,j}^H \delta_{k,j} + \sigma_n^2 \mathbf{I}_{M_r} \delta_{\ell,i} \delta_{k,j}
 \end{aligned} \tag{3.28}$$

Define the vectors and matrices,

$$\begin{aligned}
 \check{\mathbf{r}}_k &\triangleq [\check{\mathbf{r}}_{1,k}^H, \check{\mathbf{r}}_{2,k}^H, \dots, \check{\mathbf{r}}_{L,k}^H]^H \\
 \check{\mathbf{r}} &\triangleq [\check{\mathbf{r}}_0^H, \check{\mathbf{r}}_1^H, \dots, \check{\mathbf{r}}_{K-1}^H]^H \\
 \mathbf{R}_k &\triangleq E \{ \check{\mathbf{r}}_k \check{\mathbf{r}}_k^H \} \\
 \mathbf{R} &\triangleq E \{ \check{\mathbf{r}} \check{\mathbf{r}}^H \}
 \end{aligned} \tag{3.29}$$

Using $\boldsymbol{\alpha} \triangleq [\boldsymbol{\alpha}_1^H, \dots, \boldsymbol{\alpha}_L^H]^H$, the probability density function of the data is given by,

$$f_{\check{\mathbf{r}}}(\check{\mathbf{r}}|\mathbf{p}, \boldsymbol{\alpha}) = (\pi|\mathbf{R}|)^{-1} \exp \{ -\check{\mathbf{r}}^H \mathbf{R}^{-1} \check{\mathbf{r}} \} \tag{3.30}$$

where $|\cdot|$ denotes matrix determinant.

The negative log-likelihood is given, up to an additive constant, by

$$\begin{aligned}
 \mathcal{L}_f(\mathbf{p}, \boldsymbol{\alpha}) &= \ln \{ |\mathbf{R}| \} + \{ \check{\mathbf{r}}^H \mathbf{R}^{-1} \check{\mathbf{r}} \} \\
 &= \ln \left\{ \prod_{k=0}^{K-1} |\mathbf{R}_k| \right\} + \sum_{k=0}^{K-1} \check{\mathbf{r}}_k^H \mathbf{R}_k^{-1} \check{\mathbf{r}}_k
 \end{aligned} \tag{3.31}$$

Let,

$$\mathbf{A}_k \triangleq \begin{bmatrix} \tilde{\mathbf{a}}_{1,k} & \mathbf{0} & \cdots & \mathbf{0} \\ \mathbf{0} & \tilde{\mathbf{a}}_{2,k} & \cdots & \mathbf{0} \\ \vdots & \vdots & \ddots & \vdots \\ \mathbf{0} & \cdots & \mathbf{0} & \tilde{\mathbf{a}}_{L,k} \end{bmatrix} \tag{3.32}$$

$$\mathbf{\Pi} \triangleq \begin{bmatrix} \|\boldsymbol{\alpha}_1\|^2 & \boldsymbol{\alpha}_1^H \boldsymbol{\alpha}_2 & \cdots & \boldsymbol{\alpha}_1^H \boldsymbol{\alpha}_L \\ \boldsymbol{\alpha}_2^H \boldsymbol{\alpha}_1 & \|\boldsymbol{\alpha}_2\|^2 & \cdots & \boldsymbol{\alpha}_2^H \boldsymbol{\alpha}_L \\ \vdots & \vdots & \ddots & \vdots \\ \boldsymbol{\alpha}_L^H \boldsymbol{\alpha}_1 & \boldsymbol{\alpha}_L^H \boldsymbol{\alpha}_2 & \cdots & \|\boldsymbol{\alpha}_L\|^2 \end{bmatrix} \tag{3.33}$$

Now in compact notation we have,

$$\mathbf{R}_k = \mathbf{A}_k \mathbf{\Pi} \mathbf{A}_k^H + \sigma_n^2 \mathbf{I}_{M_r L} \tag{3.34}$$

Define,

$$\mathbf{\Lambda} \triangleq \text{diag}\{\sigma_1^2, \sigma_2^2, \dots, \sigma_L^2\} \quad (3.35)$$

Using our assumption in (3.27) we have $\mathbf{\Pi} \approx \mathbf{\Lambda}$. Thus, the conditioned covariance matrix may be approximated as,

$$\mathbf{R}_k \approx \mathbf{A}_k \mathbf{\Lambda} \mathbf{A}_k^H + \sigma_n^2 \mathbf{I}_{M_r L} \quad (3.36)$$

Using the well-known matrix inversion and matrix determinant lemmas [116], we get,

$$\mathbf{R}_k^{-1} = \sigma_n^{-2} \left(\mathbf{I}_{M_r L} - \mathbf{A}_k \left[\sigma_n^2 \mathbf{\Lambda}^{-1} + \mathbf{A}_k^H \mathbf{A}_k \right]^{-1} \mathbf{A}_k^H \right) \quad (3.37)$$

$$|\mathbf{R}_k| = |\mathbf{\Lambda}^{-1} + \sigma_n^{-2} \mathbf{A}_k^H \mathbf{A}_k| |\mathbf{\Lambda}| |\sigma_n^2 \mathbf{I}_{M_r L}| \quad (3.38)$$

Since the likelihood function now depends both on $\mathbf{\Lambda}$ as well as on \mathbf{p} , we need to find the value of $\hat{\mathbf{\Lambda}}$ that would maximize the likelihood function for any \mathbf{p} . Noting that $\mathbf{A}_k^H \mathbf{A}_k = \mathbf{I}_L$ indicates that $|\mathbf{R}_k|$ is independent of the index k . Thus, the first term in (3.31) is equivalent to $K \ln \left\{ \sigma_n^{2(M_r L - 1)} \prod_{\ell=1}^L (\sigma_n^2 + \sigma_\ell^2) \right\}$.

Further, define the expression in the brackets in (3.37) as,

$$\mathbf{\Gamma} \triangleq \left[\sigma_n^2 \mathbf{\Lambda}^{-1} + \mathbf{I}_L \right]^{-1} \quad (3.39)$$

We notice that $\mathbf{\Gamma}$ is diagonal and its ℓ th diagonal entry equals $\sigma_\ell^2 / (\sigma_n^2 + \sigma_\ell^2)$. Hence (3.37) can be recast as,

$$\mathbf{R}_k^{-1} = \sigma_n^{-2} (\mathbf{I}_{M_r L} - \mathbf{A}_k \mathbf{\Gamma} \mathbf{A}_k^H) \quad (3.40)$$

Plugging these expressions back into (3.31) we get,

$$\begin{aligned} \mathcal{L}_f(\mathbf{p}, \mathbf{\Lambda}) &= K(M_r L - 1) \ln \sigma_n^2 + K \sum_{\ell=1}^L \ln(\sigma_n^2 + \sigma_\ell^2) \\ &\quad + \sigma_n^{-2} \sum_{k=0}^{K-1} \check{\mathbf{r}}_k^H (\mathbf{I}_{M_r L} - \mathbf{A}_k \mathbf{\Gamma} \mathbf{A}_k^H) \check{\mathbf{r}}_k \end{aligned} \quad (3.41)$$

After rearranging and omitting constant terms we have,

$$\begin{aligned} \sigma_n^2 \mathcal{L}_f(\mathbf{p}, \mathbf{\Lambda}) &= K \sigma_n^2 \sum_{\ell=1}^L \ln(\sigma_n^2 + \sigma_\ell^2) \\ &\quad - \sum_{k=0}^{K-1} \text{Tr} \{ \mathbf{\Gamma} \mathbf{A}_k^H \check{\mathbf{r}}_k \check{\mathbf{r}}_k^H \mathbf{A}_k \} \end{aligned} \quad (3.42)$$

To find the optimal $\hat{\sigma}_\ell^2(\mathbf{p})$, we need to differentiate the negative log-likelihood function with respect to σ_ℓ^2 and equate the derivative to 0.

$$\begin{aligned} \sigma_n^2 \frac{\partial \mathcal{L}_f}{\partial \sigma_\ell^2} &= \frac{K}{\sigma_n^2 + \sigma_\ell^2} \\ &\quad - \sum_{k=0}^{K-1} \text{Tr} \left\{ \frac{\sigma_n^2}{(\sigma_n^2 + \sigma_\ell^2)^2} \mathbf{e}_\ell \mathbf{e}_\ell^T \mathbf{A}_k^H \check{\mathbf{r}}_k \check{\mathbf{r}}_k^H \mathbf{A}_k \right\} = 0 \\ K(\sigma_n^2 + \sigma_\ell^2) &= \sum_{k=0}^{K-1} \text{Tr} \{ \mathbf{e}_\ell \mathbf{e}_\ell^T \mathbf{A}_k^H \check{\mathbf{r}}_k \check{\mathbf{r}}_k^H \mathbf{A}_k \} \\ K(\sigma_n^2 + \sigma_\ell^2) &= \mathbf{e}_\ell^T \left(\sum_{k=0}^{K-1} \mathbf{A}_k^H \check{\mathbf{r}}_k \check{\mathbf{r}}_k^H \mathbf{A}_k \right) \mathbf{e}_\ell \\ \hat{\sigma}_\ell^2 &= \frac{1}{K} \mathbf{e}_\ell^T \left(\sum_{k=0}^{K-1} \mathbf{A}_k^H \check{\mathbf{r}}_k \check{\mathbf{r}}_k^H \mathbf{A}_k \right) \mathbf{e}_\ell - \sigma_n^2 \end{aligned} \quad (3.43)$$

where \mathbf{e}_ℓ is $L \times 1$ vector of 0 except for its ℓ th entry, which is 1. Finally, we obtain the estimator for $\mathbf{\Lambda}$ as,

$$\hat{\mathbf{\Lambda}} = \frac{1}{K} \sum_{k=0}^{K-1} \{ \mathbf{A}_k^H \check{\mathbf{r}}_k \check{\mathbf{r}}_k^H \mathbf{A}_k \} \odot \mathbf{I}_L - \sigma_n^2 \mathbf{I}_L \quad (3.44)$$

Recall that the diagonal elements must be positive, then if some happen to be negative they should be replaced by zeros. To obtain the stochastic DPD estimate one has to re-evaluate (3.37)-(3.38) using (3.44) and then minimize (3.31) as,

$$\hat{\mathbf{p}} = \underset{\mathbf{p}}{\text{argmin}} \left\{ \mathcal{L}_f(\mathbf{p}) \right\} \quad (3.45)$$

3.3. Algorithms for Direct Target Positioning

A possible implementation of the stochastic DPD algorithm is described in Algorithm 3. This concludes the DPD algorithms derivation.

```

Define the area of interest and determine a suitable grid of locations
p1, p2 ... pg
for j = 1 to g do
  Set  $C(\mathbf{p}_j) = 0$ 
  Set  $C_1 = 0$ 
  for k = 0 to K - 1 do
    | Let  $C_1 = C_1 + \mathbf{A}_k^H \tilde{\mathbf{r}}_k \tilde{\mathbf{r}}_k^H \mathbf{A}_k$ 
  end
  Obtain  $\hat{\mathbf{A}} = \frac{1}{K\sigma_n^2} C_1 \odot \mathbf{I}_L - \sigma_n^2 \mathbf{I}_L$ 
  Set  $C_2 = 0$ 
  for k = 0 to K - 1 do
    | Evaluate  $\mathbf{R}_k^{-1}$  using  $\hat{\mathbf{A}}$  according to (3.40)
    | Let  $C_2 = C_2 + \tilde{\mathbf{r}}_k^H \mathbf{R}_k^{-1} \tilde{\mathbf{r}}_k$ 
  end
  Let  $C(\mathbf{p}_j) = K \sum_{\ell=1}^L \ln(\sigma_n^2 + \sigma_\ell^2) + C_2$ 
end
Find the grid point for which  $C$  is the smallest. This grid point is the
estimated position.

```

Algorithm 3: DPD Algorithm for Stochastic Signals

3.4 Numerical Examples

In the following section, we demonstrate the estimation performance of the devised algorithms by means of numerical examples. The layout of the MIMO radar system used during the simulations consists of 3 receiving arrays with 3 antennas in each array located at $\{-2000, -2000\}$, $\{-2000, 2000\}$ and $\{2000, -2000\}$, and 4 single-antenna transmitters that are located at $\{-1000, -1000\}$, $\{-1000, 1000\}$, $\{1000, -1000\}$, and $\{1000, 1000\}$. The algorithms outlined in the former sections are used for locating a single target that is located at $\{150.171, -272.135\}$, (all the dimensions are in meters).

In order to gather enough statistics, the simulation results are based on several hundred Monte-Carlo runs. At each run, new channel fading coefficients as well as new additive noise samples are regenerated. The fading coefficients are drawn according to $\alpha_{m,\ell} \sim \mathcal{CN}(0, 1)$ i.e., a complex-Gaussian distribution with zero mean and unit variance. The noise samples are also generated as complex-Gaussian random samples that are distributed according to $\bar{\mathbf{n}}_{\ell,k} \sim \mathcal{CN}(0, \sigma_n^2 \mathbf{I}_{M_r})$. The signal generation is done differently for the stochastic and the deterministic algorithms. For simulating the deterministic algorithms, the signals' frequency-coefficients² are generated once for all the Monte Carlo runs as complex-Gaussian random samples with $\|\bar{\mathbf{s}}_k\|^2 = 1$. When stochastic signals are used, new signal samples are generated at each iteration as complex-Gaussian samples that are distributed as $\bar{s}_{m,k} \sim \mathcal{CN}(0, \frac{1}{M_t})$.

The SNR in the simulation is defined as,

$$\text{SNR} \triangleq E \left\{ \frac{\|\tilde{\mathbf{a}}_{\ell,k} \boldsymbol{\alpha}_{\ell}^T \bar{\mathbf{s}}_k\|^2}{\|\bar{\mathbf{n}}_{\ell,k}\|^2} \right\} \quad (3.46)$$

Recall that $\|\tilde{\mathbf{a}}_{\ell,k}\|^2 = 1$ and assuming that $\sigma_{\ell} = 1$ then $E\{\boldsymbol{\alpha}_{\ell} \boldsymbol{\alpha}_{\ell}^H\} = E\{\boldsymbol{\alpha}_{\ell}^* \boldsymbol{\alpha}_{\ell}^T\} =$

²It should be emphasized, that the choice of using frequency-domain simulation data, generated according to (3.4), is done merely for simplification reasons. In practice, time-domain signal samples are converted into frequency domain coefficients at the receiver. Hence, the direct generation of frequency-domain coefficients, implicitly assumes an ideal time-to-frequency domain conversion. The usage of directly-generated frequency-domain coefficients, eliminates any modeling errors that are likely to be generated during the conversion process. Such errors may, in some cases, exceed the error effects due to additive noise at moderate to higher SNR.

\mathbf{I}_{M_t} . Thus, the SNR is given by

$$\begin{aligned} \text{SNR} &\triangleq \frac{E\{\bar{\mathbf{s}}_k^H \boldsymbol{\alpha}_\ell^* \boldsymbol{\alpha}_\ell^T \bar{\mathbf{s}}_k\}}{M_r \cdot \sigma_n^2} \\ &= \frac{E\{\bar{\mathbf{s}}_k^H \bar{\mathbf{s}}_k\}}{M_r \cdot \sigma_n^2} = \frac{1}{M_r \cdot \sigma_n^2} \end{aligned} \quad (3.47)$$

Hence the noise variance is calculated as,

$$\sigma_n^2 \triangleq \frac{1}{M_r} \cdot 10^{\frac{-\text{SNR}[\text{dB}]}{10}} \quad (3.48)$$

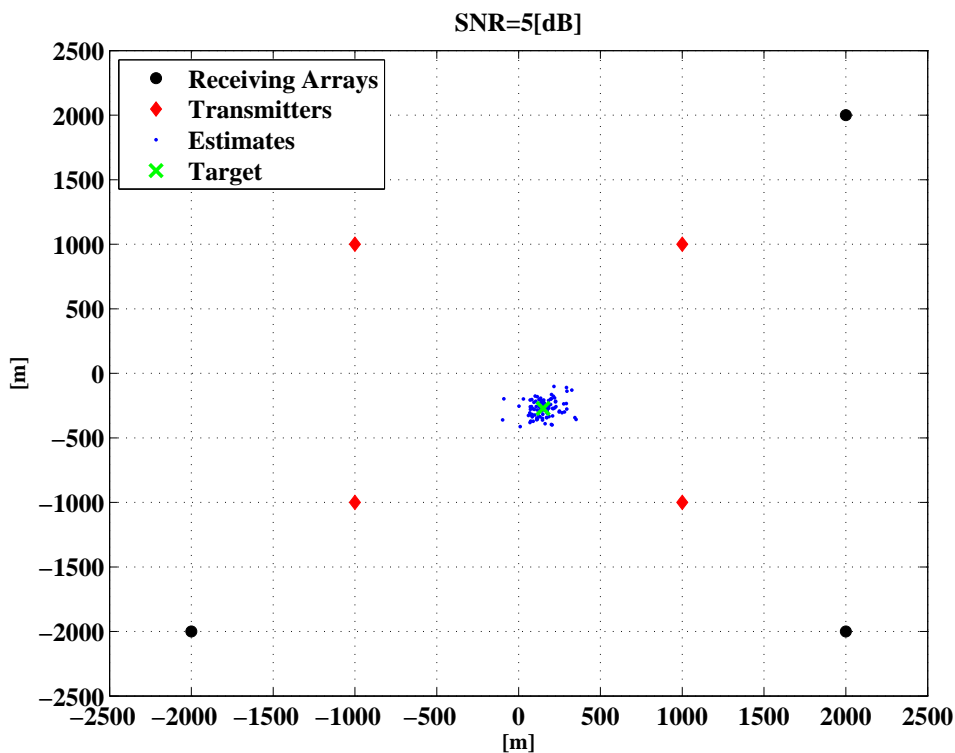


Figure 3.2: DPD Estimation Scatter Plot

Figure 3.3 compares the performance of the devised DPD method with the classical AOA+TOA algorithm under different transmit (TX) diversity levels: $M_t = 1, 2$ and 4 TX antennas with $K = 40$ samples. Both algorithms assume that the transmitted waveforms are non-random and *unknown* to the intercept-

ing arrays. The AOA estimation is done using the well-known beamformer, which is the maximum likelihood algorithm for the case of a single target. The TOA and AOA estimations are weighted optimally in order to produce a joint estimation. Further details of the AOA+TOA algorithm used in this work are described in [22]. The RMSE performance is compared to the average CRLB for known signals, which is averaged over the realizations of the channel fading coefficients. The CRLB derivation can be found in the appendix.

Figure 3.2 provides a visual example for the DPD estimation scattering around the true location of the target for $K = 40$ samples of signals transmitted by $M_t = 4$ transmitters at SNR of 5dB when the signal waveforms are unknown to the FC.

Delving into the results of Fig. 3.3, we notice that under low SNR TX diversity produces a lower performance gain for DPD compared to the gain it generates for the traditional positioning methods. This phenomenon could be explained by considering the similarities between DPD and the well-known maximal ratio combining (MRC) as explained in section 3.5. Considering a DPD-based location system as a "distributed MRC receiver" implies that such a system inherently benefits from receive-combining diversity [121]. Wireless systems that seek average SNR improvement employ diversity techniques to combat the channel fades. Receive or transmit diversity improve the average SNR by effectively "whitening" the channel, i.e., average the channel fluctuations. It is rather obvious that if one compares the performance of an AOA/TOA system without receive-combining diversity to a DPD system that benefits from that, the *incremental* gain of additional transmit diversity would be lower for a DPD system compared to its effect on a system based on conventional location methods. The same holds when considering the incremental gain achieved by doubling the TX diversity level from 2 to 4 TX antennas compared to the gain achieved by doubling the TX diversity from a single TX antenna (i.e., no diversity) into two TX antennas.

The TOA or AOA are estimated by the ℓ th array independently of the other $L - 1$ arrays, without considering the fact that the L estimates refer to the same target location. A weak channel observed by the ℓ th array would lead to an erroneous estimate of the location-related parameter and thus the

AOA/TOA fix algorithm would produce an erroneous location estimate. The transmit diversity reduces the likelihood of observing low SNR at any of the receiving arrays and therefore improves the estimation performance.

Fig. 3.3 also reveals some interesting parallels between MIMO radar using DPD and MIMO communications. Some of these analogies have also been noted in [80]. For example, similar to MIMO communications, the effect of TX diversity is more prominent at high SNR. At low SNR the diversity gain nearly vanishes. Yet, the unification of the DPD's inherent combining diversity along with the TX diversity generates significant gain for DPD over the conventional location techniques under low SNR conditions. Figure 3.4 demonstrates the

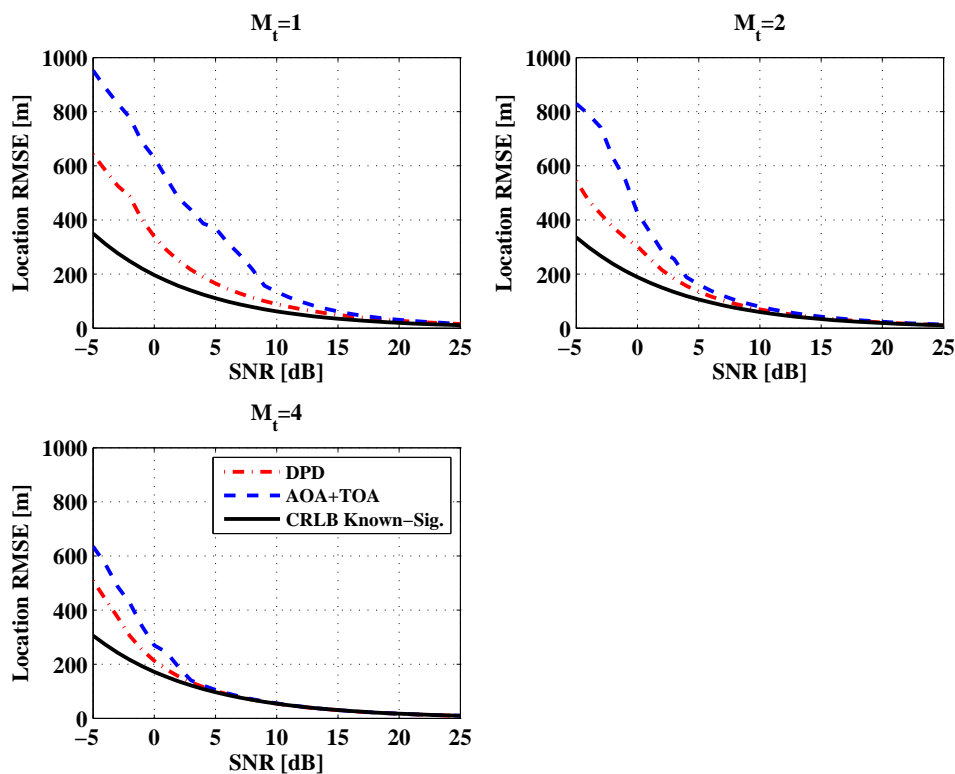


Figure 3.3: Unknown Deterministic Signals: AOA+TOA vs. DPD

effect of prior knowledge of the transmitted signal waveforms on the position estimation accuracy for different TX diversity levels with $K = 40$. The performance of DPD using (3.20) and (4.19), (marked as 'Unknown') are compared to those of (3.19), (marked as 'Known'). As can be seen, prior knowledge of

the signal waveform can improve the performance under low SNR while the effect is diminished as the SNR increases. The comparison of the DPD RMSE performance to the known signals' average CRLB are shown in Fig. 3.4. We notice that the average CRLB is a non-tight bound as discussed e.g., in [81]. Figure 3.5 compares the location estimation performance of the stochastic

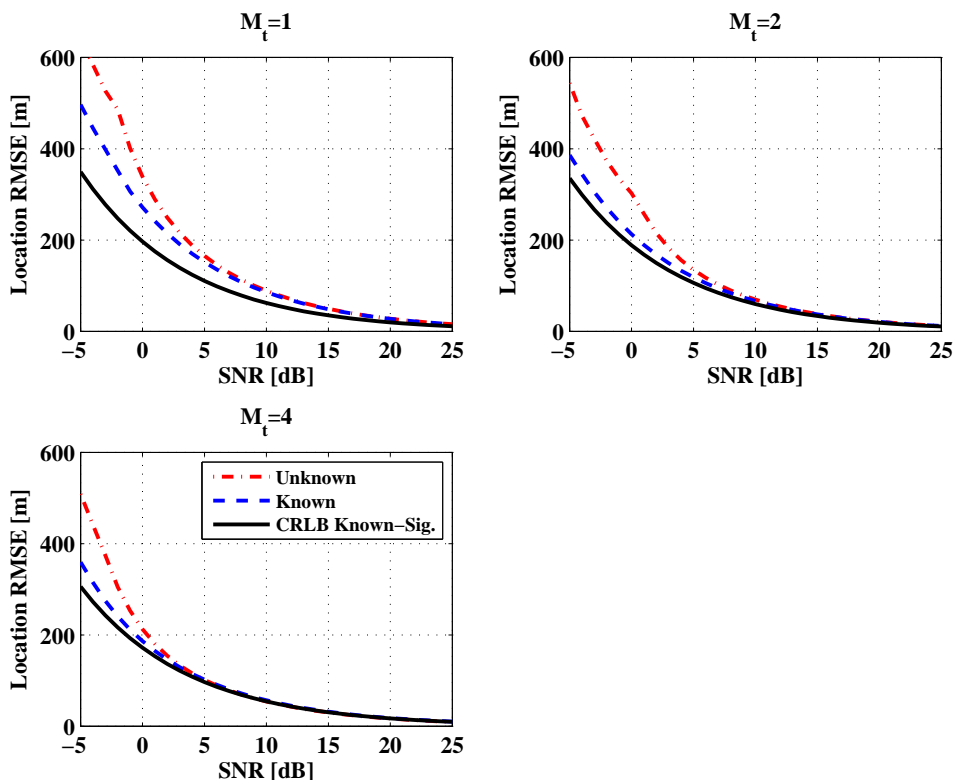


Figure 3.4: DPD using Known and Unknown Deterministic Signals vs. CRLB

DPD of (3.45) for different TX diversity levels. The results are compared to the average CRLB for stochastic Gaussian signals that is derived in the appendix. As shown, the performance of the devised estimator has a very good match with the performance predicted by the average CRLB. The fact that the average CRLB is calculated using the matrix $\mathbf{\Pi}$ (3.33) rather than $\mathbf{\Lambda}$ (3.35) indicates that the approximation used for deriving the estimator ($\mathbf{\Pi} \approx \mathbf{\Lambda}$) is reasonable.

Another way to manifest the superior performance and gain of transmit diversity is to examine the location outage probability. The outage probability

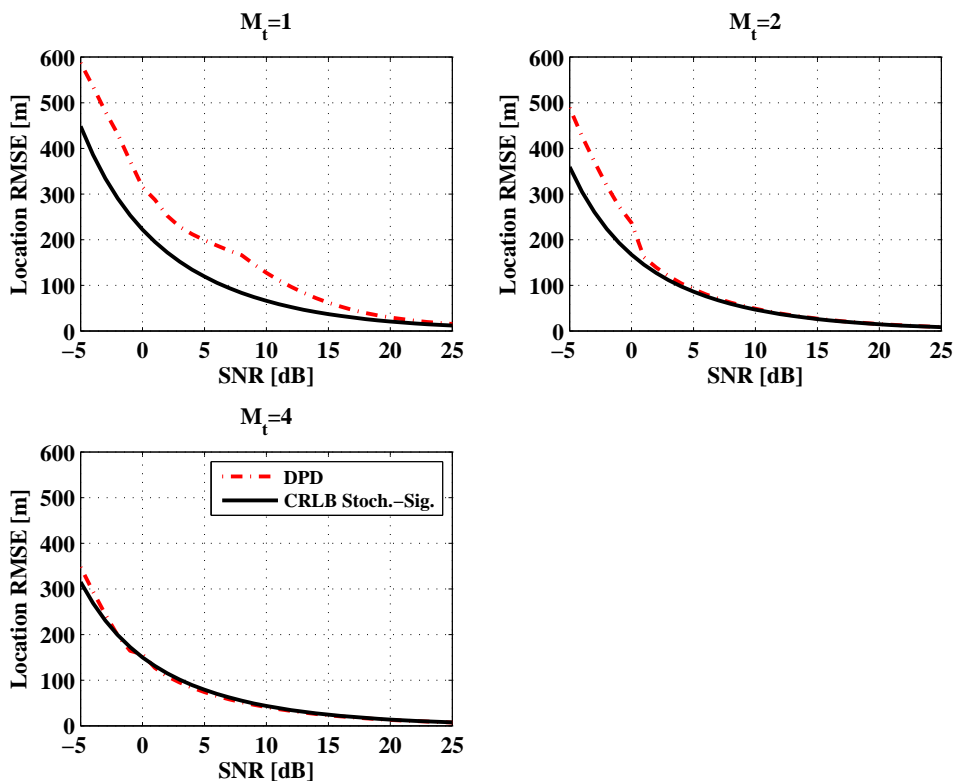


Figure 3.5: Stochastic DPD Performance

in this case is defined as the probability that the location error would be larger than a certain distance from the true position of the target. The outage probability estimations for deterministic ML DPD and for AOA+TOA with 1, 2 and 4 transmit antennas are compared in Figure 3.6. The complementary cumulative distribution functions are calculated using 5000 Monte Carlo runs for $K = 40$ snapshots of unknown signals at SNR of 0dB.

The phenomenon that TX diversity effectively "whitens" the channel and converts it from a fading channel into a pure AWGN channel can also be demonstrated by considering the behavior of the term $\|\alpha_\ell^T \mathbf{s}_k\|^2$. Under AWGN, we may consider an equivalent system that consists of an emitting target that transmits a *single* Gaussian waveform $\bar{s}_k \sim \mathcal{CN}(0, 1)$, which is subjected only to AWGN and hence $\alpha_\ell = 1$. With $\alpha_{\ell,m} \sim \mathcal{CN}(0, 1)$, the expected value of both $\|\alpha_\ell^T \mathbf{s}_k\|^2$ and $|\bar{s}_k|^2$ is 1. However the law of large numbers [111] states that the expected value for $\|\alpha_\ell^T \mathbf{s}_k\|^2$ can only be attained for a large number

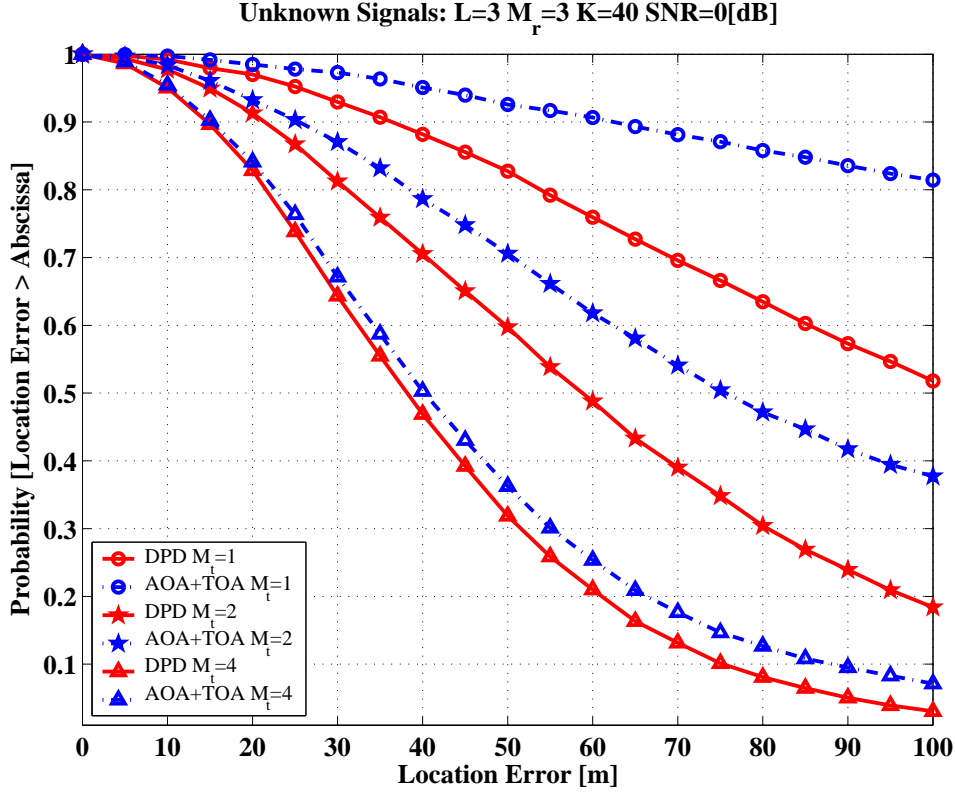


Figure 3.6: Location Error Probability for Unknown Signals

of TX diversity levels. In order to demonstrate this, in Fig. 3.7 the standard deviations of $\|\alpha_\ell^T \mathbf{s}_k\|^2$ and $|\bar{s}_k|^2$ are compared. The waveforms are complex Gaussian and are generated such that $\|\bar{\mathbf{s}}_k\|^2 = |\bar{s}_k|^2 = 1$. The fading coefficients are randomly selected according to $\alpha_{\ell,m} \sim \mathcal{CN}(0, 1)$. As shown, the standard deviations of the two terms coincide approximately for $M_t = 1000$.

This proves the claim that TX diversity effectively whitens the channel so that for $M_t \rightarrow \infty$, the noise-free received signal at the ℓ th array, $\tilde{\mathbf{a}}_{\ell,k} \bar{\mathbf{s}}_k^T \alpha_\ell$, effectively becomes $\tilde{\mathbf{a}}_{\ell,k} \bar{s}_k$. In the next section, we further discuss the integrated effect of whitening of the channel due to the TX diversity and the combining diversity of DPD that enable these excellent estimation performance results.

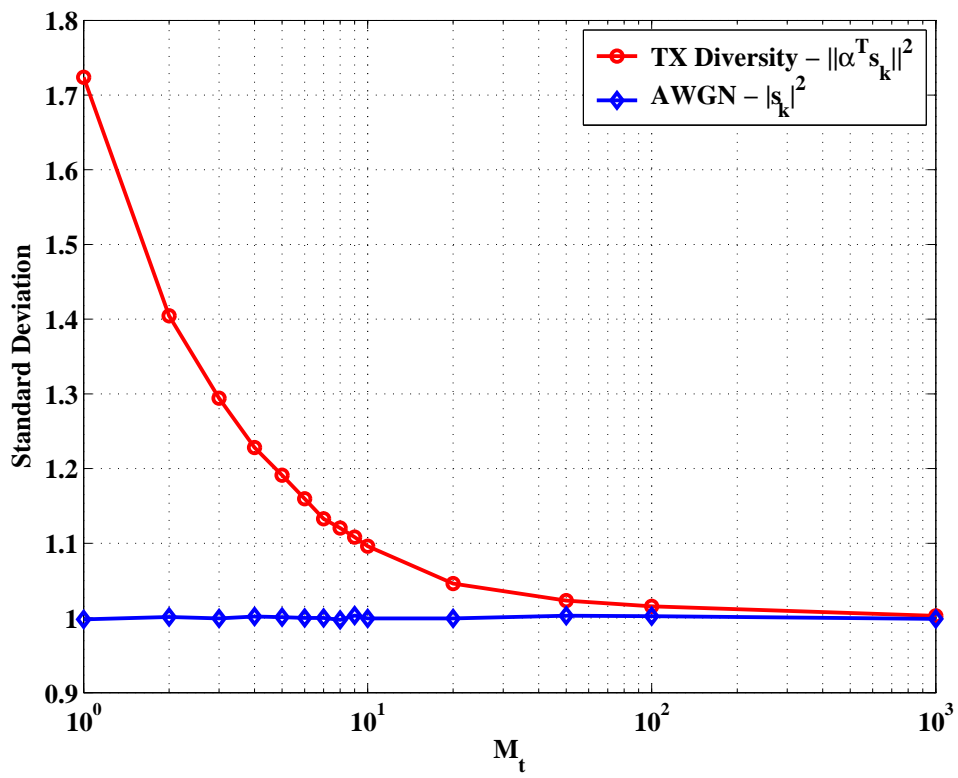


Figure 3.7: Effect of TX Diversity on the "Whiteness" of the Channel

3.5 Discussion

The basic idea common to the various DPD algorithms outlined in this chapter is the attempt to estimate the target location by coherently summing the delayed replicas of the transmitted signal. The location for which the coherent summation is maximized is the maximum likelihood estimate of the target location. The coherent summation is obtained using the match-field processing principle, which is well known in under-water location applications [82]. Thus DPD can also be considered as a variant of the well-known maximal ratio combining (MRC) technique, which is widely used by Code Division Multiple Access (CDMA) rake receivers [121]. Rake receivers use channel estimations of all their fingers to cancel out the phase shifts introduced by the multiple channel paths. The rake receiver then coherently combines the finger outputs together and performs maximum likelihood detection of the transmitted symbol. The detection is performed by finding the constellation point that minimizes its Euclidean distance to the received symbol. If we compare the algorithmic steps taken by a rake receiver with L fingers to those taken by a DPD system with L receiving arrays, we can easily see that the MRC act of multiplying the faded signal received by ℓ th finger with the estimate of the ℓ th path has a similar effect as the DPD algorithm act of multiplying the ℓ th array response by “the expected ℓ th array response to a signal backscattered from a target located at \mathbf{p} ”. In both cases, this multiplication cancels out the phase shift introduced into the received signal. In both algorithms, the elimination of the channel-induced phase shift is followed by summing up the products of all the L fingers/arrays in order to maximize the SNR for the detection/estimation step. It is also interesting to observe the analogy between a search grid employed by DPD and the symbol constellation map used by MRC. This implies that both symbol detection and parameters estimation are done out of a finite set of values (although, unlike the symbol constellation map, which is predefined for both the receiver and transmitter, the grid granularity can be refined by the FC as needed).

As has already been discussed in former papers (see e.g., [15]), the cost of the improved DPD performance incurs in an increased transmission band-

width between the receiving arrays and the FC that calculates the fix. Whilst conventional location methods require the transmission of only the measured parameters (AOA, TOA, received signal strength etc.), DPD requires the transmission of the raw samples of the received emitter signals.

3.6 Summary

We presented maximum likelihood algorithms for direct position determination of a passive, stationary target using MIMO radar. The algorithms are suitable for both PCL (passive) MIMO radar as well as for conventional MIMO radar, and are shown to benefit from the MIMO radar TX diversity under both low and high SNR conditions. Their advantage over the conventional, two-step, location methods is manifested mainly under low SNR.

Chapter 4

Emitter Geolocation using Single Moving Receiver

4.1 Introduction

In this chapter, the passive emitter geolocation problem is analyzed for a novel geolocation architecture termed “single platform geolocation” (SPG). The SPG system consists of a single receiver (equipped with an antenna array) and multiple, passive signal transponders, which are placed at known locations and may be either static or dynamic. The concept of SPG was first introduced in [25], where the analysis assumed that the Doppler shifts were negligible. In contrast, in the following chapter, we discuss a fast-moving receiver (w.r.t. the emitter), which enables us to augment the emitter position estimation with Doppler frequency-shifts information.

As will be demonstrated later on, the SPG algorithms achieve similar performance to multiple-RX DPD algorithms. This manifests the main advantage of using SPG over multiple-RX geolocation: the reduced system cost. The multiple-RX geolocation algorithms are developed under the general assumption that multiple, synchronized receivers observe the emitter’s signal simultaneously. The receivers either estimate position-dependent parameters embedded in the captured signal, or simply capture and transfer the raw signal to a central mobile location center (MLC), where the emitter location is

estimated. This implies that network connectivity between all the receivers and the MLC is required (a.k.a., “backbone network”). Transferring the information from the receivers to the MLC in real-time has to be done over an out-of-band (OOB) channel (i.e., outside the wireless channel occupied by the emitter and the receivers, e.g., an IP-based wired connection). The OOB bandwidth requirements vary depending on whether the MLC uses two-step or single-step geolocation (i.e., DPD), where in the latter case the OOB bandwidth significantly increases due to the transfer of raw signal samples vs. few parameters in the former case. Furthermore, when considering military geolocation applications operating in a hostile environment, such a backbone network is more vulnerable to be detected by the enemy

In contrast, with SPG not only are most of the receivers replaced with much-cheaper signal transponders, but the system deployment costs including the backbone network infrastructure are significantly reduced. Since in SPG, the raw signal samples are transferred “in-band” (i.e., as multipath), the backbone connectivity is required only between the (single) receiver and the MLC. Compared to multiple-RX, for single-step geolocation, when using SPG, the amount of raw signal data that needs to be transferred over the SPG backbone is also reduced by a factor of L , (which corresponds to the number of signal-transponders in the SPG system). It should also be noted that in multiple-RX geolocation architectures, the receivers are required to be tightly synchronized in time and frequency - a task that requires means such as atomic clocks, GPS receivers and message exchange protocols. This requirement is accomplished implicitly with SPG and without extra cost.

As will be described in the sequel, the SPG scheme does not require any synchronization between the emitter and the receiver. In that sense, SPG may be considered as a type of an asynchronous geolocation system. Such systems, which have been drawing increasing interest recently (see, e.g., [38]-[40]), are based on cooperation between various nodes constructing the network (e.g., “anchor nodes,” that are placed in locations known to a central location server). Typically, these systems rely on time-difference measurements provided by the “anchor nodes” to locate so-called “blind nodes” within the network. In many cases, these “blind nodes” also need to actively participate in their own geolo-

cation process (e.g., by referencing their own timing measurements to signals transmitted by the “anchor nodes”, by reporting these timing measurements back to a location server, and so on).

Though the SPG transponders may be viewed as a type of “cooperative anchor nodes,” there are several fundamental differences that distinguish SPG from those systems. First, unlike the anchor nodes aforementioned, the transponders do not conduct any measurement of the emitter signal. Conversely, they are used only to form a multipath channel for the receiver. Second, in the SPG scheme, except for transmitting its signal, the emitter is completely passive during the location process: it does not need to actively participate in its location process; further, it is even unaware of being located. This makes SPG suitable for various kinds of military and security location applications. Third, as opposed to the approach pursued by [38]-[40], which relies on a two-step location estimation via time-difference measurements, all the algorithms discussed in this chapter are based on single-step location, in which the emitter position is extracted directly from the received signal samples.

Main Contributions

We derive a novel received signal model for transponder-aided geolocation using a single moving receiving station. Based on this model, we derive novel maximum-likelihood (ML), single-step (direct) geolocation algorithms for known and unknown (deterministic) signals. We also provide a detailed (textbook) derivation of the ‘concentrated’ Cramér Rao lower bound (CRLB) on the emitter position estimation for the received signal model. Using numerical analysis of the CRLB expressions, we highlight and demonstrate the system layout limitation when using transponder-aided geolocation. Parts of this chapter have been published in [26].

Chapter Organization

Section 4.2 outlines the problem formulation. Single-step algorithms for SPG of a static emitter under the assumptions of known and unknown signal waveforms are derived in section 4.3. Numerical performance examples of these

algorithms are given in section 4.4. The final conclusions are given in section 4.5. Finally, in the appendix, we provide the derivation of the CRLB, along with the reference multiple-RX DPD algorithms used for comparison with the devised SPG algorithms.

4.2 Problem Formulation

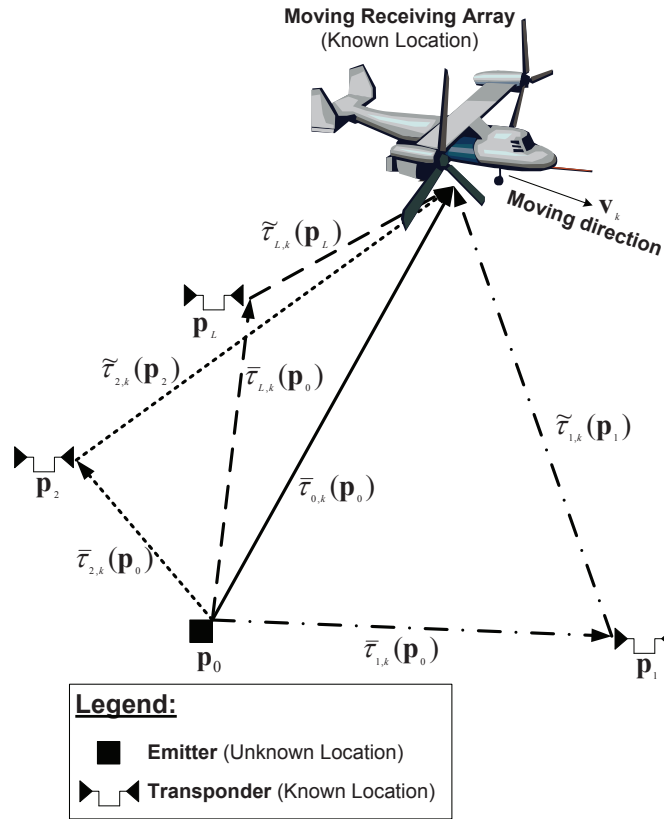


Figure 4.1: SPG Geometry with Moving Receiver & Static Transponders

Consider a stationary source transmitting a narrow band signal whose carrier frequency is f_c and its envelope is $s(t)$. The bandwidth of $s(t)$ is W , which satisfies $W \ll f_c$. An appropriate signal model would be $s(t)e^{i2\pi f_c t}$. When the signal is observed by a moving receiver, the observed signal becomes $s(\beta t)e^{i2\pi f_c \beta t}$, which is an expansion or compression of the signal time

scale, known as the Doppler effect. Let v be the sensor-source relative velocity and c the signal propagation velocity, then $\beta = 1 + v/c$. Since β is nearly one, the effect on the slowly varying envelope will be negligible; however, the carrier frequency will be shifted considerably (see e.g., [118, p. 241]). In this case, the observed signal can be approximated by $s(t)e^{i2\pi f_c \beta t}$. When the distance between the source and the receiver is considerable, the signal will be delayed by τ and the observed signal becomes $s(t - \tau)e^{i2\pi f_c \beta t}$ up to the complex constant $e^{-i2\pi f_c \beta \tau}$, which has no effect on the signal amplitude, the signal delay or the signal frequency. This simple model will be used in the sequel.

The location of the static emitter is estimated using a geolocation system that consists of a single (moving) receiver, and L static, passive signal-transponders acting as ideal signal reflectors. The transponders reflect the emitter signal towards the receiver and assist in the geolocation of the transmitter. This scenario is depicted in Fig. 4.1. Our model assumes that the transponders do not amplify the signal and therefore do not generate any further processing delay. Furthermore, any random noise that may be added to the signal samples while passing through the transponder, may be considered as an “additional” additive noise at the receiver.

Assume that the emitter is located at $\mathbf{p}_0 = [x_0, y_0, z_0]^T$, and let \mathbf{p}_ℓ , $\ell = 1 \dots L$ denote the position of the ℓ th transponder. The transponders implicitly generate a multipath signal propagation channel with $L + 1$ paths. We reserve $\ell = 0$ for the direct/line-of-sight (LoS) path between the receiver and the emitter, while $\ell = 1 \dots L$ designates the indirect (Non-line of sight/NLoS) paths through the transponders.

The receiver is moving in a known direction and speed. It intercepts the transmitted signal at K short intervals along its trajectory. Let \mathbf{q}_k denote the coordinates vector of the receiver during the k th interception interval. It is assumed that the transponders locations are known to the receiver and so is its own (instantaneous) location.

As explained, the motion of the receiver w.r.t., the emitter and the transponders, generates Doppler frequency shifts associated with each signal path. Let $\mathbf{v}_k = [v_{k,x}, v_{k,y}, v_{k,z}]^T$ denote the velocity vector of the moving receiving-array during the k th observation interval.

The Doppler-shift of the ℓ th signal path during the k th observation interval, $f_{\ell,k}$ is given by,

$$f_{\ell,k} \triangleq f_c \bar{\mu}_{\ell,k} \quad (4.1)$$

with $\bar{\mu}_{\ell,k}$ being the Doppler coefficient defined as,

$$\bar{\mu}_{\ell,k} \triangleq \frac{1}{c} \mathbf{v}_k^T \frac{\mathbf{p}_{\ell,k} - \mathbf{q}_k}{\|\mathbf{p}_{\ell,k} - \mathbf{q}_k\|}, \quad \ell = 0 \dots L \quad (4.2)$$

Next, let $\tau_{\ell,k}$ denote the total propagation delay of the ℓ th path at the k th interception interval defined as,

$$\tau_{\ell,k}(\mathbf{p}_0) = \bar{\tau}_{\ell,k}(\mathbf{p}_0) + \tilde{\tau}_{\ell,k} \quad (4.3)$$

where $\bar{\tau}_{\ell,k}$ denotes the signal propagation-delay between the emitter and the ℓ th transponder (or the receiver) during the k th interval, and $\tilde{\tau}_{\ell,k}$ denotes the propagation-delay between the ℓ th transponder and the receiver. These parameters are defined as follows.

$$\begin{aligned} \bar{\tau}_{\ell,k} &\triangleq \bar{\tau}_\ell \triangleq \frac{1}{c} \|\mathbf{p}_0 - \mathbf{p}_\ell\|^2, \quad \forall \ell \neq 0 \\ \bar{\tau}_{0,k} &\triangleq \frac{1}{c} \|\mathbf{p}_0 - \mathbf{q}_k\|^2 \\ \tilde{\tau}_{\ell,k} &\triangleq \frac{1}{c} \|\mathbf{p}_\ell - \mathbf{q}_k\|^2, \quad \forall \ell \neq 0 \\ \tilde{\tau}_{0,k} &\triangleq 0 \end{aligned} \quad (4.4)$$

Notice that since the transponder locations are known, $\tilde{\tau}_{\ell,k}$ is independent of the emitter's position. Similarly to [36], we assume that $\tau_{\ell,k} \ll T$, where T is the observation time during the k th interception interval. This condition ensures that all the signal replicas observed during the observation window are similar up to a small shift. Further, note that we assumed that $\tau_{\ell,k}$ is quasi-constant during the observation time. This means that the observation time must be short enough to ensure that the platform position does not change more than the desired positioning error during the observation time.

Under the assumption that the receiver integrates an array of M antennas and the emitter begins transmitting at an unknown time, t_0 , then after frequency down-conversion by a known carrier frequency f_c , the complex signal vector observed by the receiving array during the k th interception interval at time t is given by,

$$\mathbf{r}_k(t) = \sum_{\ell=0}^L \alpha_{\ell,k} \mathbf{a}_{\ell,k}(\mathbf{p}_\ell) s_k(t - \tau_{\ell,k} - t_0) e^{i2\pi t f_{\ell,k}(\mathbf{p}_\ell)} + \mathbf{n}_k(t),$$

$$-T/2 \leq t \leq T/2 \quad (4.5)$$

where,

- $\mathbf{r}_k(t)$ - is an $M \times 1$ observation vector at the k th interception interval.
- $\alpha_{\ell,k}$ - is the complex attenuation of the ℓ th signal path during the k th interception interval. The scalar, $\alpha_{\ell,k}$, is assumed to be deterministic and unknown¹.
- $\mathbf{a}_{\ell,k}(\mathbf{p}_\ell)$ - is an $M \times 1$ vector denoting the array response to the signals arriving from position \mathbf{p}_ℓ during the k th observation interval. Without loss of generality we assume that $\|\mathbf{a}_{\ell,k}\|^2 = 1$.
- $s_k(t)$ - is the observed signal complex-envelope during the k th interception interval.
- $\mathbf{n}_k(t)$ - is an $M \times 1$ vector representing the additive noise during the k th observation interval. It is further assumed that the additive noise is wide sense stationary, zero mean, complex Gaussian noise with flat spectrum.

The problem discussed herein can be stated as follows: Given $\{\mathbf{r}_k\}_{k=1}^K$ estimate the emitter's position \mathbf{p}_0 .

¹Notice that we make no path-loss modeling assumption regarding the complex path attenuation. Hence, we implicitly ignore any effect on the SNR that may be caused by distance. Further, the performance bounds derived in Appendix B.1, are also developed under this assumption.

4.3 Positioning Algorithms

We shall consider the waveform received by each sensor to be represented by its Fourier coefficients defined by

$$\bar{\mathbf{r}}_k(f_n) \triangleq \frac{1}{T} \int_{-T/2}^{T/2} \mathbf{r}_k(t) e^{-i2\pi f_n t} dt, \quad (4.6)$$

where $f_n = n/T$, $n = 0, \pm 1, \pm 2, \dots$ is the frequency associated with the n th coefficient. The Fourier coefficients of $s_k(t)$ and of $\mathbf{n}_k(t)$ are denoted by $\bar{s}_k(f_n)$ and by $\bar{\mathbf{n}}_k(f_n)$, respectively.

In the frequency domain (4.5) becomes,

$$\bar{\mathbf{r}}_k(f_n) = \sum_{\ell=0}^L \alpha_{\ell,k} \mathbf{a}_{\ell,k} \bar{s}_k(f_n - f_{\ell,k}) e^{-i2\pi f_n (\tau_{\ell,k} + t_0)} + \bar{\mathbf{n}}_k(f_n). \quad (4.7)$$

where $\alpha_{\ell,k}$ also accounts for $e^{-i\phi_{\ell,k}}$ representing the ℓ th signal path phase-shift, $\phi_{\ell,k}$, due to the Doppler frequency offset.

4.3.1 Known Signal Waveform

In this section, the waveforms transmitted by the emitter at each of the K interception segments are known to the receiver. This could be the case where the emitter transmits a synchronization sequence or a known message. Yet, the time at which the emitter begins its transmission, t_0 , is unknown to the receiver.

Next, let $\tilde{\mathbf{F}}_{\ell,k}$ be a cyclic-shift operator such that,

$$\begin{bmatrix} \bar{s}_k(f_{-N} - f_{\ell,k}) \\ \bar{s}_k(f_{-N+1} - f_{\ell,k}) \\ \vdots \\ \bar{s}_k(f_N - f_{\ell,k}) \end{bmatrix} \triangleq \tilde{\mathbf{F}}_{\ell,k} \bar{\mathbf{S}}_k \quad (4.8)$$

where,

$$\bar{\mathbf{s}}_k \triangleq [\bar{s}_k(f_{-N}), \dots, \bar{s}_k(f_N)]^T \quad (4.9)$$

This operator $\tilde{\mathbf{F}}_{\ell,k}$ may be viewed as a linear time-invariant (LTI) system consisting of a filter and a sampler that re-samples the shifted vector $\bar{\mathbf{s}}_k$ at the frequency sampling points of the DFT.

This operator may be approximated as a line-permuted identity matrix that is used for down-shifting. The product $\tilde{\mathbf{F}}_{\ell,k}\bar{\mathbf{s}}_k$ shifts the vector $\bar{\mathbf{s}}_k$ by $\text{sgn}\{f_{\ell,k}\} \cdot \lfloor T \cdot |f_{\ell,k}| \rfloor$ indices.

Now (4.7) can be recast as,

$$\bar{\mathbf{r}}_k(f_n) = \sum_{\ell=0}^L \alpha_{\ell,k} \mathbf{a}_{\ell,k} \underbrace{\mathbf{e}_n^T \tilde{\mathbf{F}}_{\ell,k} \bar{\mathbf{s}}_k}_{\bar{s}_k(f_n - f_{\ell,k})} e^{-i2\pi f_n(\tau_{\ell,k} + t_0)} + \bar{\mathbf{n}}_k(f_n). \quad (4.10)$$

where \mathbf{e}_n is the n th column of an identity matrix of order $2N + 1$.

We define the following vectors and matrices:

$$\begin{aligned} \bar{\mathbf{r}}_k &\triangleq [\bar{\mathbf{r}}_k^T(f_{-N}), \dots, \bar{\mathbf{r}}_k^T(f_N)]^T \\ \bar{\mathbf{n}}_k &\triangleq [\bar{\mathbf{n}}_k^T(f_{-N}), \dots, \bar{\mathbf{n}}_k^T(f_N)]^T \\ \tilde{\mathbf{E}}_{\ell,k} &\triangleq \text{diag}\{e^{-i2\pi f_{-N}\tau_{\ell,k}}, \dots, e^{-i2\pi f_N\tau_{\ell,k}}\} \\ \tilde{\mathbf{Z}} &\triangleq \text{diag}\{e^{-i2\pi f_{-N}t_0}, \dots, e^{-i2\pi f_N t_0}\} \end{aligned} \quad (4.11)$$

Next, define:

$$\tilde{\mathbf{d}}_{\ell,k} \triangleq (\tilde{\mathbf{F}}_{\ell,k} \tilde{\mathbf{E}}_{\ell,k} \tilde{\mathbf{Z}} \bar{\mathbf{s}}_k) \otimes \mathbf{a}_{\ell,k} \quad (4.12)$$

$$\mathbf{D}_k(\mathbf{p}) \triangleq [\tilde{\mathbf{d}}_{0,k}, \tilde{\mathbf{d}}_{1,k}, \dots, \tilde{\mathbf{d}}_{L,k}] \quad (4.13)$$

In vectorized form, (4.10) can be recast using (4.11)-(4.13) as,

$$\bar{\mathbf{r}}_k = \mathbf{D}_k \boldsymbol{\alpha}_k + \bar{\mathbf{n}}_k \quad (4.14)$$

The emitter position can be found by minimizing the cost function,

$$Q(\mathbf{p}, t_0) = \sum_{k=0}^{K-1} \|\bar{\mathbf{r}}_k - \mathbf{D}_k \boldsymbol{\alpha}_k\|^2 \quad (4.15)$$

The Least-Squares (LS) estimate of the complex attenuation coefficients vector is given by,

$$\hat{\boldsymbol{\alpha}}_k = (\mathbf{D}_k^H \mathbf{D}_k)^{-1} \mathbf{D}_k^H \bar{\mathbf{r}}_k \quad (4.16)$$

Minimizing $Q(\mathbf{p}, t_0)$ is equivalent to maximizing,

$$\begin{aligned} \tilde{Q}(\mathbf{p}, t_0) &= \sum_{k=1}^K \bar{\mathbf{r}}_k^H \mathbf{D}_k (\mathbf{D}_k^H \mathbf{D}_k)^{-1} \mathbf{D}_k^H \bar{\mathbf{r}}_k \\ &= \sum_{k=1}^K \text{Tr}\{\tilde{\boldsymbol{\Pi}}_k \bar{\mathbf{r}}_k \bar{\mathbf{r}}_k^H\} \end{aligned} \quad (4.17)$$

where,

$$\tilde{\boldsymbol{\Pi}}_k \triangleq \mathbf{D}_k (\mathbf{D}_k^H \mathbf{D}_k)^{-1} \mathbf{D}_k^H \quad (4.18)$$

The joint ML estimate for the emitter position and the emitter-receiver clock offset t_0 is given by,

$$\hat{\mathbf{p}} = \underset{\mathbf{p}, t_0}{\text{argmax}} \sum_{k=1}^K \text{Tr}\{\tilde{\boldsymbol{\Pi}}_k \bar{\mathbf{r}}_k \bar{\mathbf{r}}_k^H\} \quad (4.19)$$

An example of implementing this algorithm is described in Algorithm 4.

4.3.2 Unknown Signal Waveform

In contrast to the main assumption in the previous section, we will now derive a direct geolocation algorithm under the assumption that the transmitted signal waveform is deterministic but unknown to the receiver.

We notice that in the absence of prior knowledge of the emitter signal,

```

Define the area of interest and determine a suitable grid of locations
 $\mathbf{p}_1, \mathbf{p}_2 \dots \mathbf{p}_g$ 
Define a suitable grid of time of transmission  $0 \dots t_{0\max}$ 
for  $j = 1$  to  $g$  do
     $\tilde{Q}(\mathbf{p}_j) = 0$ 
    for  $i = 1$  to  $t$  do
        1. For an emitter located at  $\mathbf{p}_j$ , evaluate:
            (a) The delay  $\tau_{\ell,k}$ ,
            (b) The Doppler-shift  $\mu_{\ell,k}$ ,
            (c) The AOA steering vectors  $\mathbf{a}_k(\mathbf{p}_\ell)$ 
        2.  $c(i) = 0$ 
        for  $k = 1$  to  $K$  do
            1. Evaluate  $\mathbf{D}_k, \tilde{\mathbf{\Pi}}_k(\mathbf{p}_j, t_i)$ 
            2.  $c(i) = c(i) + \text{Tr}\{\tilde{\mathbf{\Pi}}_k \bar{\mathbf{r}}_k \bar{\mathbf{r}}_k^H\}$ 
        end
    end
     $\tilde{Q}(\mathbf{p}_j) = \tilde{Q}(\mathbf{p}_j) + \max\{c\}$ 
end
Find the grid point for which  $\tilde{Q}$  is the biggest. This grid point is the
estimated position.

```

Algorithm 4: Direct SPG Algorithm for Known Emitter Signal and Unknown Transmission Time

a direct evaluation of (4.19) would require per each candidate position to search over the complex signal spectrum (a total of $2 \cdot (2N + 1)$ unknown parameters, and search over t_0 at some pre-defined resolution). This would make the geolocation in such cases impractical.

In the following section, we derive ML algorithms for two cases: one in which the Doppler-shift information is significant and may be utilized to enhance position estimation, and another for the case in which the Doppler shift may be overlooked.

Non-Negligible Doppler Shift

To begin our analysis, we first notice that since the waveform is unknown to the receiver, the receiver clock phase-shift due to the time of transmission t_0 , is immaterial and may be absorbed into the unknown waveform, such that $\tilde{s}_k(f_n) \triangleq \bar{s}_k(f_n)e^{-i2\pi f_n t_0}$. Each of the $L + 1$ vectors constructing the matrix \mathbf{D}_k embeds a shifted version of the vector $\tilde{\mathbf{s}}_k$. In order to obtain an attractive direct-positioning algorithm, we need to recast the matrix \mathbf{D}_k such that the vector $\tilde{\mathbf{s}}_k$ would be separated. Recall from (4.12) that,

$$\begin{aligned} \tilde{\mathbf{d}}_{\ell,k} &\triangleq \underbrace{(\tilde{\mathbf{F}}_{\ell,k} \tilde{\mathbf{E}}_{\ell,k})}_{\tilde{\mathbf{W}}_{\ell,k}} \underbrace{(\tilde{\mathbf{Z}} \tilde{\mathbf{s}}_k)}_{\tilde{\mathbf{s}}_k} \otimes \mathbf{a}_{\ell,k} \\ &\triangleq (\tilde{\mathbf{W}}_{\ell,k} \tilde{\mathbf{s}}_k) \otimes \mathbf{a}_{\ell,k} \end{aligned} \quad (4.20)$$

The matrix $\tilde{\mathbf{W}}_{\ell,k}$ is a $(2N + 1) \times (2N + 1)$ matrix. Denote the n th line of $\tilde{\mathbf{W}}_{\ell,k}$ as $\tilde{\mathbf{w}}_{\ell,k}^T(f_n) \triangleq \mathbf{e}_n^T \tilde{\mathbf{W}}_{\ell,k}$. Since $\tilde{\mathbf{w}}_{\ell,k}^T(f_n) \tilde{\mathbf{s}}_k$ is a scalar, one may write:

$$[\tilde{\mathbf{w}}_{\ell,k}^T(f_n) \tilde{\mathbf{s}}_k] \otimes \mathbf{a}_{\ell,k} = \underbrace{\mathbf{a}_{\ell,k} \tilde{\mathbf{w}}_{\ell,k}^T(f_n)}_{\tilde{\mathbf{B}}_{\ell,k}(f_n)} \tilde{\mathbf{s}}_k \triangleq \tilde{\mathbf{B}}_{\ell,k}(f_n) \tilde{\mathbf{s}}_k$$

Stacking all the $2N + 1$ lines of the matrix $\tilde{\mathbf{B}}_{\ell,k}$ we get,

$$\tilde{\mathbf{B}}_{\ell,k} \triangleq \begin{bmatrix} \tilde{\mathbf{B}}_{\ell,k}(f_{-N}) \\ \tilde{\mathbf{B}}_{\ell,k}(f_{-N+1}) \\ \vdots \\ \tilde{\mathbf{B}}_{\ell,k}(f_N) \end{bmatrix} \quad (4.21)$$

Now the matrix \mathbf{D}_k can be recast as,

$$\mathbf{D}_k = \left[\underbrace{\tilde{\mathbf{B}}_{1,k}\tilde{\mathbf{s}}_k}_{\tilde{\mathbf{d}}_{1,k}}, \tilde{\mathbf{B}}_{2,k}\tilde{\mathbf{s}}_k, \dots, \tilde{\mathbf{B}}_{L,k}\tilde{\mathbf{s}}_k \right] \quad (4.22)$$

By applying the $\text{vec}\{\mathbf{D}_k\}$ operator we can stack the L column vectors constructing the \mathbf{D}_k :

$$\text{vec}\{\mathbf{D}_k\} = \begin{bmatrix} \tilde{\mathbf{d}}_{1,k} \\ \tilde{\mathbf{d}}_{2,k} \\ \vdots \\ \tilde{\mathbf{d}}_{L,k} \end{bmatrix} = \begin{bmatrix} \tilde{\mathbf{B}}_{1,k} \\ \tilde{\mathbf{B}}_{2,k} \\ \vdots \\ \tilde{\mathbf{B}}_{L,k} \end{bmatrix} \tilde{\mathbf{s}}_k \triangleq \tilde{\mathbf{B}}_k \tilde{\mathbf{s}}_k \quad (4.23)$$

Notice that,

$$\begin{aligned} \mathbf{D}_k \boldsymbol{\alpha}_k &= \text{vec}\{\mathbf{D}_k \boldsymbol{\alpha}_k\} \\ &= (\boldsymbol{\alpha}_k^T \otimes \mathbf{I}_{(2NM+M)}) \text{vec}\{\mathbf{D}_k\} \end{aligned} \quad (4.24)$$

Now, (4.14) may be recast as,

$$\bar{\mathbf{r}}_k = (\boldsymbol{\alpha}_k^T \otimes \mathbf{I}_{(2NM+M)}) \tilde{\mathbf{B}}_k \tilde{\mathbf{s}}_k + \bar{\mathbf{n}}_k \quad (4.25)$$

Using (4.25) the cost function defined in (4.15) may be recast as,

$$\begin{aligned} Q(\mathbf{p}) &= \sum_{k=0}^{K-1} \|\bar{\mathbf{r}}_k - \mathbf{D}_k \boldsymbol{\alpha}_k\|^2 \\ &= \sum_{k=0}^{K-1} \|\bar{\mathbf{r}}_k - (\boldsymbol{\alpha}_k^T \otimes \mathbf{I}_{(2NM+M)}) \tilde{\mathbf{B}}_k \tilde{\mathbf{s}}_k\|^2 \end{aligned} \quad (4.26)$$

The LS estimate of $\tilde{\mathbf{s}}_k$ that minimizes this cost function is given by,

$$\begin{aligned} \hat{\tilde{\mathbf{s}}}_k &= \left(\tilde{\mathbf{B}}_k^H [\boldsymbol{\alpha}_k^* \boldsymbol{\alpha}_k^T \otimes \mathbf{I}_{(2NM+M)}] \tilde{\mathbf{B}}_k \right)^{-1} \\ &\quad \cdot \tilde{\mathbf{B}}_k^H (\boldsymbol{\alpha}_k^* \otimes \mathbf{I}_{(2NM+M)}) \bar{\mathbf{r}}_k \end{aligned} \quad (4.27)$$

Substituting (4.27) back into (4.26), the position-dependent cost function to be maximized is obtained as,

$$\tilde{Q}(\mathbf{p}) = \sum_{k=0}^{K-1} \text{Tr} \{ \check{\mathbf{\Pi}}_k \bar{\mathbf{r}}_k \bar{\mathbf{r}}_k^H \} \quad (4.28)$$

where,

$$\begin{aligned} \check{\mathbf{\Pi}}_k &\triangleq (\boldsymbol{\alpha}_k^T \otimes \mathbf{I}_{(2NM+M)}) \tilde{\mathbf{B}}_k \\ &\quad \cdot \left(\tilde{\mathbf{B}}_k^H [\boldsymbol{\alpha}_k^* \boldsymbol{\alpha}_k^T \otimes \mathbf{I}_{(2NM+M)}] \tilde{\mathbf{B}}_k \right)^{-1} \\ &\quad \cdot \tilde{\mathbf{B}}_k^H (\boldsymbol{\alpha}_k^* \otimes \mathbf{I}_{(2NM+M)}) \end{aligned} \quad (4.29)$$

All the information describing the emitter position, including: TOA, AOA and Doppler shift, is embedded in the matrix $\tilde{\mathbf{B}}_k$. The unknowns are \mathbf{p} , $\tilde{\mathbf{s}}_k$ and $\boldsymbol{\alpha}_k$. To find the direct ML estimate for \mathbf{p} , we propose the following alternating-maximization (AM) scheme. The technique is iterative; at every iteration, a maximization is performed with respect to a single parameter while all the other parameters are held fixed. When applied in the context of direct positioning, the maximization with respect to $\tilde{\mathbf{s}}_k$ and $\boldsymbol{\alpha}_k$ is performed at every candidate position on the search grid (that is, \mathbf{p} is held fixed). The maximization process continues iteratively until a local maxima at candidate \mathbf{p}_i is attained. Once the per-point maximization process is done, a search for the global maxima is performed in order to obtain the ML estimate for \mathbf{p} .

The proposed technique may be implemented as described in Algorithm 5. We notice that implementing this ML algorithm incurs in a high computational complexity, due to the inversion and multiplication of relatively large matrices in an iterative manner.

In many cases, signals transmitted by communication systems include syn-

```

Define the area of interest and determine a suitable grid of locations
 $\mathbf{p}_1, \mathbf{p}_2 \dots \mathbf{p}_g$ 
for  $j = 1$  to  $g$  do
     $\tilde{Q}(\mathbf{p}_j) = 0$ 
    for  $k = 1$  to  $K$  do
        1. Evaluate the delay  $\tau_{\ell,k}$ ,  $f_{\ell,k}$  and,
            $L + 1$  AOA's for an emitter located at  $\mathbf{p}_j$ 
        2. Choose  $\hat{\boldsymbol{\alpha}}_k^0$ 
        3.  $\tilde{Q}_k^0 = 0$ ,  $\tilde{Q}_k^1 = 0$ 
        while  $|\tilde{Q}_k^i(\mathbf{p}_j) - \tilde{Q}_k^{i-1}(\mathbf{p}_j)| > \epsilon \cdot \tilde{Q}_k^{i-1}(\mathbf{p}_j)$  do
            1. Evaluate:  $\tilde{\boldsymbol{\Pi}}^i$  according to (4.29).
            2. Set:  $\tilde{Q}_k^i = \text{Tr}\{\tilde{\boldsymbol{\Pi}}_k^i \bar{\mathbf{r}}_k \bar{\mathbf{r}}_k^H\}$ 
            3. Set:  $\hat{\mathbf{s}}^i$  according to (4.27).
            4. Evaluate:  $\mathbf{D}_k$  according to (4.13) and (4.20).
            5. Set:  $\hat{\boldsymbol{\alpha}}_k^i = (\mathbf{D}_k^H \mathbf{D}_k)^{-1} \mathbf{D}_k^H \bar{\mathbf{r}}_k$ 
            6. Set:  $\tilde{Q}_k^{i+1} = \text{Tr}\{\tilde{\boldsymbol{\Pi}}_k^i \bar{\mathbf{r}}_k \bar{\mathbf{r}}_k^H\}$ 
        end
         $\tilde{Q}(\mathbf{p}_j) = \tilde{Q}(\mathbf{p}_j) + \tilde{Q}_k(\mathbf{p}_j)$ 
    end
end
Find the grid point for which  $\tilde{Q}$  is the biggest. This grid point is the
estimated position.

```

Algorithm 5: Direct SPG Algorithm for Unknown Emitter Signal using a Moving Receiver

chronization sequences. These sequences consist of symbols known to the receiver (pilot symbols) that enable the estimation of the channel characteristics. The estimation is carried out under the assumption that these characteristics remain constant at least for several data symbols that follow the pilot symbols. For these kinds of transmission systems, a position estimation strategy such as the one described in Algorithm 7 may be applied. The position estimation scheme first estimates the channel coefficients based on known synchronization symbols. Then, it estimates the unknown data symbols using the estimated channel coefficients. The position estimation in this case is based on the maximization of the sum of the cost functions that are based on either the known signal symbols or unknown signal symbols.

Negligible Doppler Shift

The high computational complexity of the ML solution as described in Algorithm 5 may be relaxed in certain scenarios, in which the Doppler offset may effectively be neglected. This could result from either a slow-moving receiver or a relatively short observation time. While the observation time has to be long enough to ensure that the entire delay-spread is captured, an observation time that is too long may violate the underlying assumption that the receiver is fairly motionless during the observation period. Furthermore, the observation duration T is related to the number of samples N as, $T = N/f_s$. A long observation time combined with a high sampling frequency (beyond the Nyquist rate) results in a large amount of signal samples that need to be processed, thereby increasing the system processing speed requirements. Recall that the operator $\tilde{\mathbf{F}}_{\ell,k}$ shifts the observed signal spectrum by $\text{sgn}\{f_{\ell,k}\} \cdot [T \cdot |f_{\ell,k}|]$; the condition for the Doppler offset negligibility may be stated as,

$$\lfloor T \cdot \max\{|f_{\ell,k}|\} \rfloor = 0 \quad (4.30)$$

This implies that for an observation duration T , the minimal distinguishable Doppler shift should satisfy the following condition:

$$\min\{|f_{\ell,k}|\} \geq \frac{1}{T} \quad (4.31)$$

In case (4.31) does not hold, the Doppler shift may effectively be neglected such that:

$$\tilde{s}_k(f_n - f_{\ell,k}) \approx \tilde{s}_k(f_n)$$

and (4.7) may be recast as,

$$\bar{\mathbf{r}}_{k,n} = \sum_{\ell=0}^L \alpha_{\ell,k} \mathbf{a}_{\ell,k} \tilde{s}_{k,n} e^{-i2\pi f_n \tau_{\ell,k}} + \bar{\mathbf{n}}_{k,n} \quad (4.32)$$

The LS estimate for the signal frequency coefficient is given by,

$$\hat{\tilde{s}}_{k,n} = \left(\boldsymbol{\alpha}_k^H \tilde{\mathbf{A}}_{k,n}^H \tilde{\mathbf{A}}_{k,n} \boldsymbol{\alpha}_k \right)^{-1} \boldsymbol{\alpha}_k^H \tilde{\mathbf{A}}_{k,n}^H \bar{\mathbf{r}}_{k,n} \quad (4.33)$$

Substituting (4.33) back in (4.15) we obtain the cost function for the k th interval as,

$$Q_k(\boldsymbol{\alpha}_k, \mathbf{p}) = \sum_n \left\| \bar{\mathbf{r}}_{k,n} - \tilde{\mathbf{A}}_{k,n} \boldsymbol{\alpha}_k \left(\boldsymbol{\alpha}_k^H \tilde{\mathbf{A}}_{k,n}^H \tilde{\mathbf{A}}_{k,n} \boldsymbol{\alpha}_k \right)^{-1} \boldsymbol{\alpha}_k^H \tilde{\mathbf{A}}_{k,n}^H \bar{\mathbf{r}}_{k,n} \right\|^2 \quad (4.34)$$

The minimization of $Q_k(\boldsymbol{\alpha}_k, \mathbf{p})$ is equivalent to maximizing $\tilde{Q}_k(\boldsymbol{\alpha}_k, \mathbf{p})$, which is given by,

$$\begin{aligned} \tilde{Q}_k(\boldsymbol{\alpha}_k, \mathbf{p}) &= \sum_n \bar{\mathbf{r}}_{k,n}^H \tilde{\mathbf{A}}_{k,n} \boldsymbol{\alpha}_k \left(\boldsymbol{\alpha}_k^H \tilde{\mathbf{A}}_{k,n}^H \tilde{\mathbf{A}}_{k,n} \boldsymbol{\alpha}_k \right)^{-1} \cdot \boldsymbol{\alpha}_k^H \tilde{\mathbf{A}}_{k,n}^H \bar{\mathbf{r}}_{k,n} \\ &= \sum_n \frac{\boldsymbol{\alpha}_k^H \mathbf{f}_{k,n} \mathbf{f}_{k,n}^H \boldsymbol{\alpha}_k}{\boldsymbol{\alpha}_k^H \mathbf{C}_{k,n} \boldsymbol{\alpha}_k} \end{aligned} \quad (4.35)$$

where $\mathbf{f}_{k,n} \triangleq \tilde{\mathbf{A}}_{k,n}^H \bar{\mathbf{r}}_{k,n}$, $\mathbf{C}_{k,n} \triangleq \tilde{\mathbf{A}}_{k,n}^H \tilde{\mathbf{A}}_{k,n}$.

An iterative solution for maximizing the cost function in the form of (4.35) is derived in appendix B.3, (see also [25]). Here, this iterative solution is extended to a case where the receiver is moving along K interception intervals. Since the emitter is assumed to be static, the position estimate in this case is obtained through the maximization of the sum of K distinct cost functions at

a specific position \mathbf{p} :

$$\hat{\mathbf{p}} = \underset{\mathbf{p}}{\operatorname{argmax}} \sum_k \tilde{Q}_k(\boldsymbol{\alpha}_k, \mathbf{p}) \quad (4.36)$$

A possible implementation of the proposed maximization procedure is outline in Algorithm 6.

```

Define the area of interest and determine a suitable grid of locations


$\mathbf{p}_1, \mathbf{p}_2 \dots \mathbf{p}_g$

for  $j = 1$  to  $g$  do
   $\tilde{Q}(\mathbf{p}_j) = 0$ 
  for  $k = 1$  to  $K$  do
    1. Set  $\mathbf{f}_{k,n} = \tilde{\mathbf{A}}_{k,n}^H \bar{\mathbf{r}}_{k,n}$  ;  $\mathbf{C}_{k,n} = \tilde{\mathbf{A}}_{k,n}^H \tilde{\mathbf{A}}_{k,n}$ 
    2. Choose  $\alpha_{k,0}$ 
    while  $|\tilde{Q}_k^i(\alpha_k, \mathbf{p}_j) - \tilde{Q}_k^{i-1}(\alpha_k, \mathbf{p}_j)| > \epsilon \cdot \tilde{Q}_k^{i-1}(\alpha_k, \mathbf{p}_j)$  do
      1. Evaluate:  $w_n \triangleq \mathbf{f}_{k,n}^H \alpha_{k,0} (\alpha_{k,0}^H \mathbf{C}_{k,n}^H \alpha_{k,0})$ 
      2. Evaluate:  $\mathbf{C}_k = \sum_n |w_n|^2 \mathbf{C}_{k,n}$ 
      3.  $\beta = \sum_n w_n \mathbf{f}_{k,n}$ 
      4. Find:  $\hat{\alpha}_k = \mathbf{C}^{-1} \beta$ 
      5. Set:  $\alpha_{k,0} = \hat{\alpha}_k$ 
      6. Evaluate:
         
$$\tilde{Q}_k^i(\alpha_k, \mathbf{p}_j) = \sum_n \frac{\alpha_{k,0}^H \mathbf{f}_{k,n} \mathbf{f}_{k,n}^H \alpha_{k,0}}{\alpha_{k,0}^H \mathbf{C}_{k,n} \alpha_{k,0}}$$

    end
     $\tilde{Q}(\mathbf{p}_j) = \tilde{Q}(\mathbf{p}_j) + \tilde{Q}_k(\mathbf{p}_j)$ 
  end
end

```

Find the grid point for which \tilde{Q} is the biggest. This grid point is the estimated position.

Algorithm 6: Direct SPG Algorithm for Unknown, Arbitrary Emitter Signal and Slowly Moving Receiver

Define the area of interest and determine a suitable grid of locations

$\mathbf{p}_1, \mathbf{p}_2 \dots \mathbf{p}_g$

for $j = 1$ **to** g **do**

$\tilde{Q}(\mathbf{p}_j) = 0$

for $k = 1$ **to** K **do**

1. Evaluate the delay $\tau_{\ell,k}$, $f_{\ell,k}$ and, $L + 1$ AOA's for an emitter located at \mathbf{p}_j
2. Evaluate: \mathbf{D}_k according to (4.13).
3. Estimate: $\hat{\boldsymbol{\alpha}}_k = (\mathbf{D}_k^H \mathbf{D}_k)^{-1} \mathbf{D}_k^H \bar{\mathbf{r}}_k$
4. Evaluate: $\tilde{\boldsymbol{\Pi}}_k$ according to (4.18).
5. Evaluate: $\tilde{Q}_k^{known} = \text{Tr}\{\tilde{\boldsymbol{\Pi}}_k \bar{\mathbf{r}}_k \bar{\mathbf{r}}_k^H\}$
6. Evaluate: $\tilde{\boldsymbol{\Pi}}_k^i$ according to (4.29) using $\hat{\boldsymbol{\alpha}}_k$.
7. Evaluate: $\tilde{Q}_k^{unknown} = \text{Tr}\{\tilde{\boldsymbol{\Pi}}_k \bar{\mathbf{r}}_k \bar{\mathbf{r}}_k^H\}$

$\tilde{Q}(\mathbf{p}_j) = \tilde{Q}(\mathbf{p}_j) + \tilde{Q}_k^{known} + \tilde{Q}_k^{unknown}$

end

end

Find the grid point for which \tilde{Q} is the biggest. This grid point is the estimated position.

Algorithm 7: Pilot-Aided Direct SPG Algorithm for Unknown Emitter Signal using a Moving Receiver

4.3.3 Computational Complexity Analysis

As explained in the introduction to this chapter, the main advantage of the SPG system stems from its reduced hardware costs. Yet, as one might expect, this reduction in hardware costs does not come for free; as in many other cases, the reduced hardware complexity is traded off for increased computational complexity. We will now analyze the computational load imposed by the algorithms outlined in this chapter. In algorithms 4 & 7, (as well as the DPD algorithm for known signal derived in B.2), the main computation is based on computing a projection matrix of different orders. It is well known that if the singular value decomposition (SVD) of a matrix $\mathbf{A} \in \mathbb{C}^{m \times n}$ is given by $\mathbf{A} = \mathbf{U}\mathbf{\Sigma}\mathbf{V}^H$, then one may obtain the projection matrix as: $\mathbf{A}(\mathbf{A}^H\mathbf{A})^{-1}\mathbf{A}^H = \mathbf{U}\mathbf{U}^H$. According to Golub & Van Loan [113, p. 254], the minimal number of FLOPS required for calculating the (complex) SVD using the R-SVD algorithm equals $4mn^2 + 22n^3$. In algorithm 6, each iteration is based on simple matrix multiplications. The running time for multiplying rectangular matrices (one $m \times p$ -matrix with one $p \times n$ -matrix) is $O(mnp)$. Table 5.1 lists the number of FLOPS consumed by each of the algorithms described.

Table 4.1: Computational Complexity of SPG using Moving Receiver

Algorithm	Primary Computation	# FLOPS	Comments
SPG Known Signal	$\tilde{\mathbf{\Pi}}_k$ $\mathbf{D}_{k(2N+1)M \times (L+1)}$	$O(K[8NML^2 + 22L^3])$	- per grid point
SPG Unknown Signal - Non negligible Doppler	$\tilde{\mathbf{\Pi}}_k$ $\mathbf{D}_{k(2N+1)M \times (L+1)}$ $\tilde{\mathbf{\Pi}}_k$ $\mathbf{B}_{k(2N+1)M \times (2N+1)(L+1)M}$	$O(K[NML]^3)$	- per grid point, - per iteration (number of iterations is SNR-dependent)
SPG Unknown Signal - Negligible Doppler	$M \times (L + 1)$ matrix multiplications per frequency coefficient	$O(K[NML])$	- per grid point, - per iteration (number of iterations is SNR-dependent [25])
DPD Known Signal	$(2N + 1)M \times (2N + 1)M$ matrix multiplication	$O(K[N^2M])$	- per grid point
DPD Unknown Signal	SVD, $\mathbf{U}_{k(2N+1) \times L}$	$O(K[8NL^2 + 22L^3])$	- per grid point

4.4 Numerical Examples

In this section, we demonstrate the estimation performance of the devised algorithms using some numerical simulations examples. The system layout is illustrated in Fig. 4.2. The system consists of a single receiver equipped with a pentagon antenna array of 5 elements and two passive signal transponders. The system aims to determine the location of a single emitter placed at [2000, 2000]. The signal transmitted by the emitter is a modulated carrier at

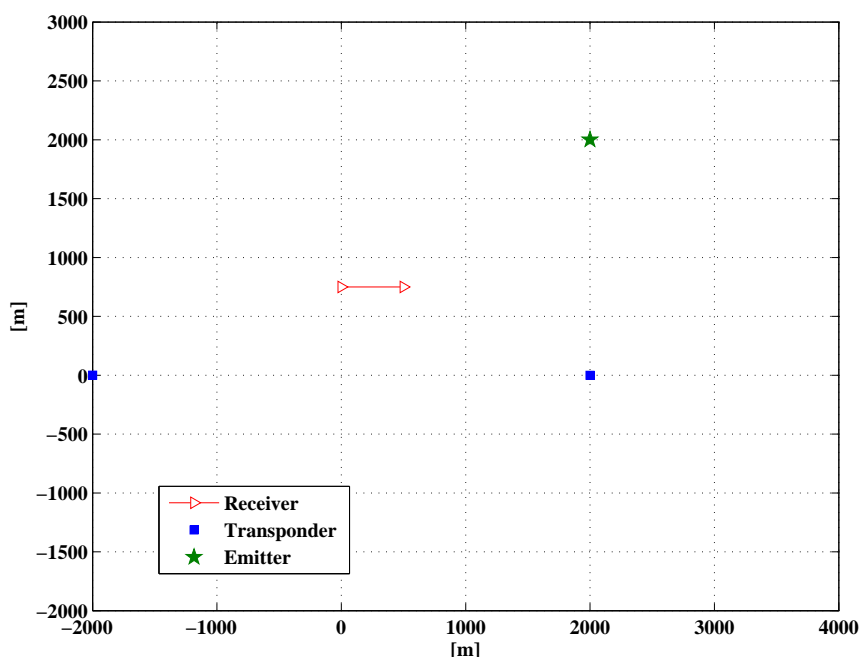


Figure 4.2: System Layout

1.0GHz. Throughout the numerical analysis the propagation speed is assumed to be $c = 3 \cdot 10^8$ [meters/sec]. The modulating signal is a pulse train with a bandwidth of 1.0MHz and duty cycle of 5%. The sampling rate used by the receiver is 2.56MHz. The observation time interval is $50\mu\text{sec}$. As shown in Fig. 4.2, the receiver intercepts the signal twice, once every 500 [meters]. For the simulations in Fig. 4.3, the signal was modulated with a similar waveform but with bandwidth of 300KHz. The sampling frequency in these test cases was 768KHz and the observation time interval is $167\mu\text{sec}$.

In order to gather enough statistics, the simulation results are based on

200 Monte-Carlo runs per each SNR value. At each run, new channel fading coefficients as well as new additive noise samples are regenerated. The fading coefficients are drawn from a complex-Gaussian distribution with zero mean and unit variance². The signal is normalized such that $\|\mathbf{s}_k\|^2 = 1$, where $\mathbf{s}_k \triangleq [s_k(t_1), \dots, s_k(t_N)]^T$. The noise coefficients are drawn from zero mean, circular, complex Gaussian distribution with scaled identity matrix covariance.

Fig. 4.3-Fig. 4.5 depict the root-mean-squared-error (RMSE) of the estimated position that is given by,

$$\text{RMSE}(\mathbf{p}) \triangleq \sqrt{\frac{1}{N_{\text{exp}}} \sum_{i=1}^{N_{\text{exp}}} [(\hat{x}_i - x_0)^2 + (\hat{y}_i - y_0)^2]} \quad (4.37)$$

where N_{exp} denotes the number of Monte-Carlo runs, $\hat{\mathbf{p}} \triangleq [\hat{x}_i, \hat{y}_i]$ denotes the estimated position at the i th trial and $\mathbf{p}_0 \triangleq [x_0, y_0]$ denotes the true emitter position. Fig. 4.3-Fig. 4.5 demonstrate 3 different scenarios:

1. Figure 4.3 - Large Doppler shift, long observation time
2. Figure 4.4 - Small Doppler shift, short observation time
3. Figure 4.5 - Large Doppler shift, short observation time

Results in Fig. 4.3-Fig. 4.5 correspond to the following algorithms

1. The result curves marked as "SPG Known Sig." refer to the estimation results using Algorithm 4.
2. The result curves marked as "SPG Unknown Sig." refer to the estimation results using Algorithm 7.
3. The result curves marked as "SPG Unknown Sig. - Iter." refer to the estimation results using Algorithm 6 and Algorithm 5. Both algorithms yielded identical results using $\epsilon = 10^{-4}$.

²As explained in sec. 4.2, the choice of modeling the attenuation coefficients as complex-Gaussian scalars, overlooks any path-loss effects. Thus, it eliminates any position-dependent information from the attenuation coefficients. The attenuation of distant emitters, (which is expected to be larger than the attenuation of closer emitters), may be quantified through lower SNR levels. Hence, low SNR level in the simulation may account for either high noise level at the receiver or for low signal level due to distant emitter.

4. The result curves marked as "DPD Unknown Sig." refer to the estimation results using the DPD algorithm derived in Appendix B.2, which maximizes the cost function defined in (B.60).
5. The result curves marked as "DPD Known Sig." refer to the estimation results using (B.61).

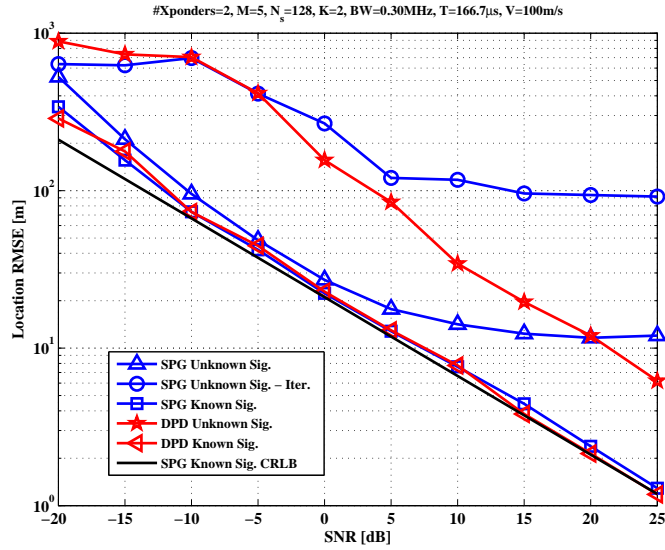


Figure 4.3: RMSE $T = 166.7\mu s$, Bandwidth = 300[KHz], $V=100\frac{m}{s}$

As shown in Fig. 4.3, the combination of large Doppler-shift and long observation time causes algorithm 6, which relies on a low Doppler shifts assumption, and does not attempt to estimate the Doppler-shift, to exhibit irreducible estimation error under high SNR. In contrast, when the observation time is relatively short, such that the product $[T \cdot \max\{|f_{\ell,k}|\}]$ is 0 (as in Fig. 4.4 & Fig. 4.5), this algorithm achieves similar performance as the DPD algorithm that implicitly estimates and compensates for Doppler-shift (see B.2). In all test cases, the performance of SPG algorithm for known signals is tightly bounded by the CRLB (derived in B.1)³.

³The choice of comparing the RMSE results in Fig. 4.3-Fig. 4.5, only against known-signal CRLB, was made due to simulation run-time considerations. Given the deterministic signal assumption, each frequency coefficient of the transmitted signal, becomes a (complex) unknown parameter. Hence, the FIM would become unreasonably large for large observation

4.4. Numerical Examples

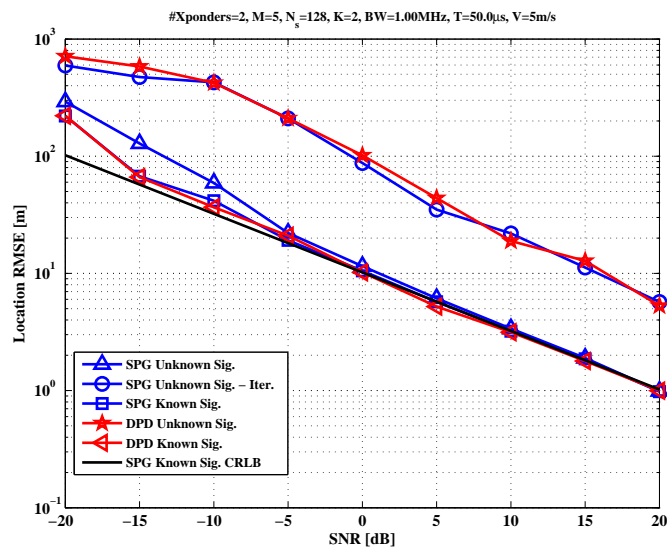


Figure 4.4: RMSE $T = 50\mu\text{s}$, Bandwidth = 1 [MHz], $V=5\frac{m}{s}$

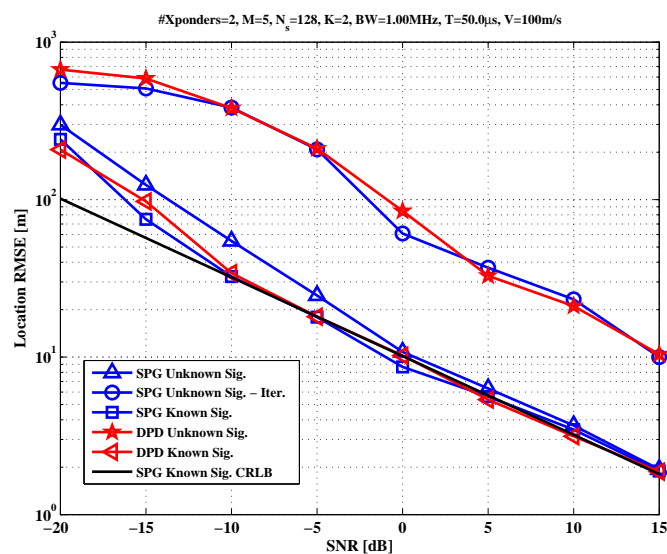


Figure 4.5: RMSE $T = 50\mu\text{s}$, Bandwidth = 1 [MHz], $V=100\frac{m}{s}$

Fig. 4.6 and Fig. 4.7 depict the CRLB for different locations over a grid of $2[\text{km}] \times 2[\text{km}]$. The CRLB is evaluated for a single observation interval ($K = 1$), in which the receiver (captured at $[0, 0]$), is moving at a speed of

intervals, resulting in excessively long simulation execution-time. While maintaining the execution-time within reasonable bounds, the known-signal CRLB also serves as a (non-tight) lower bound for the unknown signal case.

$100\frac{m}{s}$. The transmitted waveform is the 1.0MHz, 5% duty-cycle pulse train and the SNR is 25[dB]. In Fig. 4.6, the receiving array is equipped with 5 antennas circular array and uses two transponders located at $\{\pm 500[m], -500[m]\}$. It is interesting to notice the trails 'dragged behind' the transponders. These trails represent areas of ambiguity: in these locations the angular and temporal resolution of the system is relatively low and does not enable us to distinguish between close grid locations. At the center of each trail there is a line, along which the error is minimized: an emitter placed along this line co-aligns with the receiver. With this constellation the system has 'side-information' about the emitter position - the AOA of the LoS path and one of the NLoS paths overlap, which indicates that the emitter must lie on the imaginary line connecting the receiving array and the transponder. Hence, the ambiguity in such cases is eliminated. A similar phenomenon is also observed in Fig. 4.7, where there are 4 transponders located at $\{\pm 500[m], \pm 500[m]\}$. As expected, the additional transponders reduce the overall ambiguity errors in the transponder trails. These figures also hint at the recommended system layout and receiver path for minimizing the position estimation error.

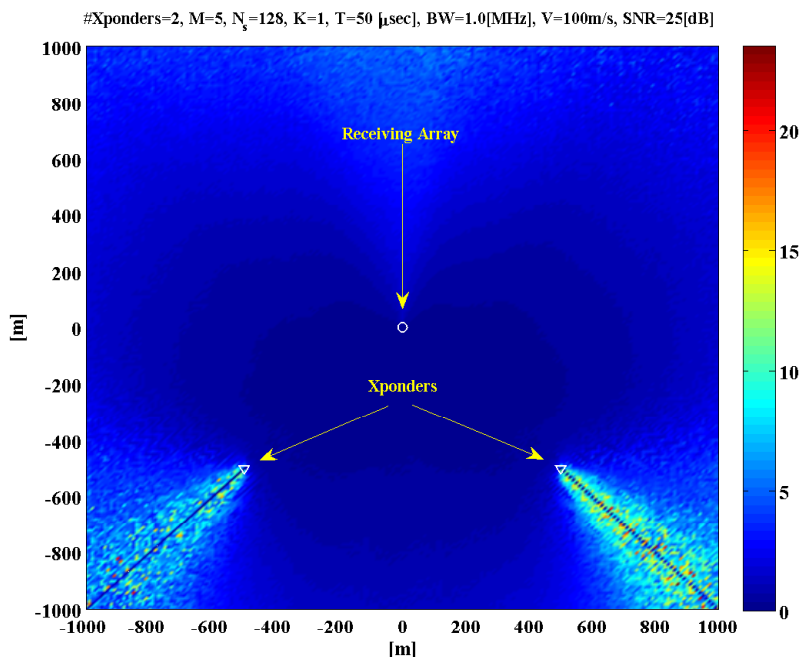


Figure 4.6: Known Signal CRLB for 2 Transponders and a receiver moving at $V = 100 \frac{m}{s}$, $SNR = 25[dB]$)

Finally, Fig. 4.8 and Fig. 4.9 depict the cumulative distribution function (CDF) for the positioning error bound predicted by the CRLB. The CDF, $F(x)$, is defined as follows:

$$F(x) = \frac{\text{Number of grid locations where position error} \leq x}{\text{Total number of grid locations}} \quad (4.38)$$

The error values were calculated for the system layouts described in Fig. 4.6 and Fig. 4.7, respectively, over the $2[km] \times 2[km]$ grid in steps of $20[m]$ (forming a total of 10,000 different locations). Each of these figures depicts CDF curves at 4 different SNR levels: $-10[dB]$, $0[dB]$, $10[dB]$ and $20[dB]$. As anticipated, the expected positioning error level decreases with increase in SNR or with increase in the number of transponders.

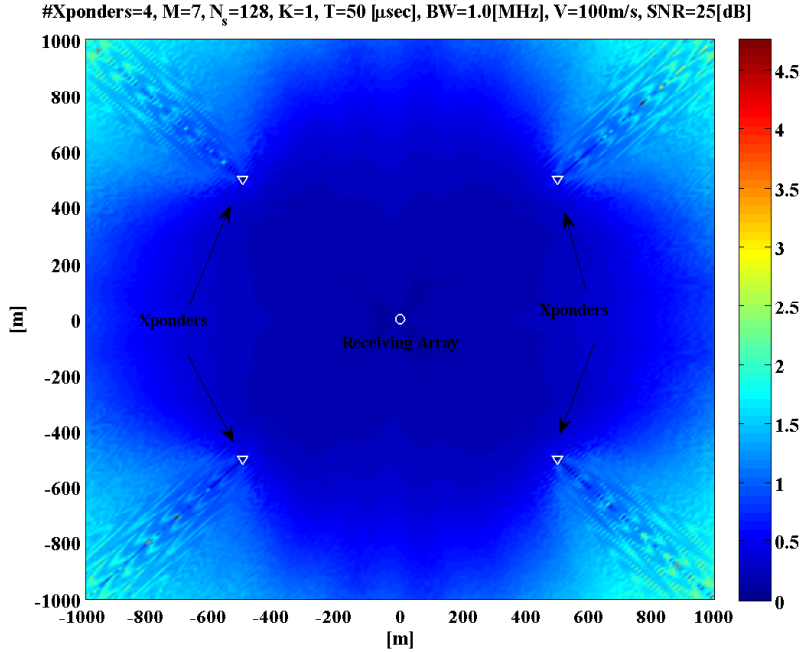


Figure 4.7: Known Signal CRLB for 4 Transponders and a receiver moving at $V = 100 \frac{m}{s}$, $SNR = 25[dB]$)

4.5 Summary

In this chapter, we presented maximum likelihood algorithms for direct geolocation of a stationary radio emitter using a single-platform geolocation (SPG) system. The system consists of a single moving receiver and multiple, passive signal transponders, (which may be either static or in motion). Numerical analysis indicates that SPG location accuracy performances are similar to the accuracy that can be achieved by a costly, comparative multiple-receivers geolocation system. The analysis of the Wideband SPG CRLB reveals the preferable system layouts for minimizing the position estimation error over a large area. The advantage of SPG stems from its ease of deployment and its reduced cost.

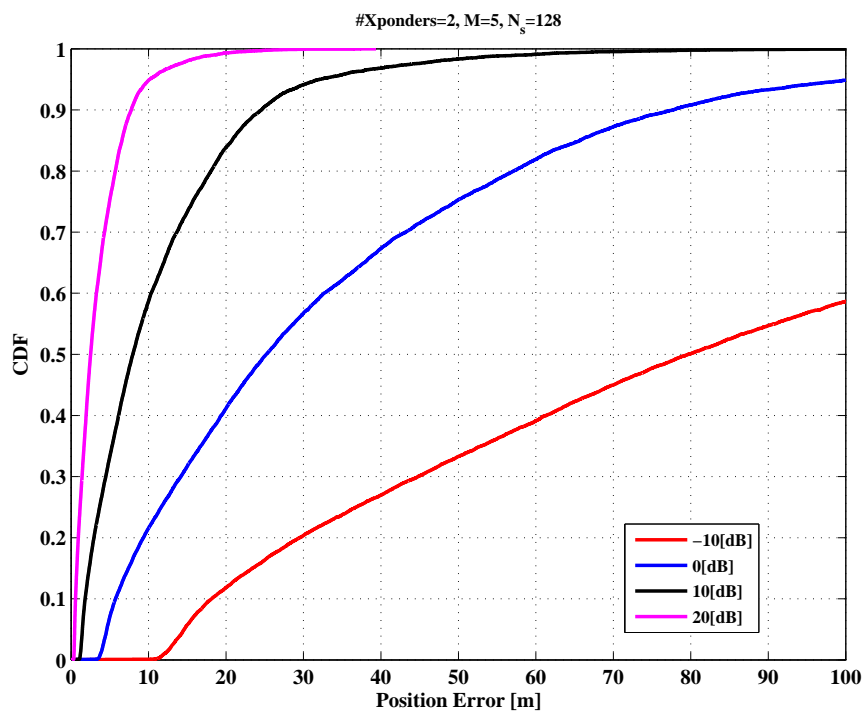


Figure 4.8: Empirical CDF for 2 Transponders

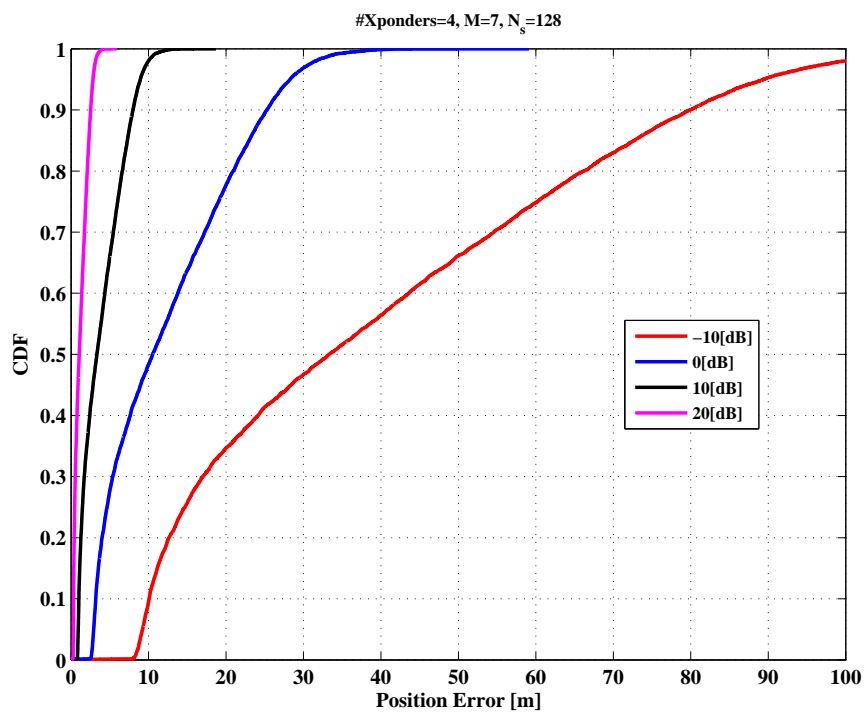


Figure 4.9: Empirical CDF for 4 Transponders

Chapter 5

Direct Emitter Geolocation under Local Scattering

5.1 Introduction

As described in previous chapters, the method of single-step geolocation has been shown to be an efficient geolocation method that outperforms conventional two-step geolocation methods in a variety of systems and applications [14]-[31]. Yet, in most of the publications investigating DPD performance, the emitting source is modeled as a point source. While enabling some important insights into the fundamental limitations of single-step emitter geolocation, the rather simplistic point-source model rarely provides a high-fidelity representation of the emitter signal in a multipath-dense environment. Such an environment is typically crowded with scatterers surrounding the emitter and reflecting its signal towards the receiving array. In such case, the emitter is not perceived as a point but rather as a “scattered” or as a “distributed” source.

In this chapter we explore the problem of emitter geolocation in the local scattering environment. We derive an analytic model for the received signal where the local scattering environment is modeled as a stochastic process using the Gaussian Angle of Arrival (GAA) model. For the signal model, we provide both optimal and sub-optimal, computationally-simpler, 1-step (direct) emitter geolocation algorithms. The proposed algorithms enable estimation of the

emitter's position directly, using the received signal samples. The algorithms extract the emitter position information from both fading channel statistics, as well as temporal correlations when the fading channel is quasi-static. It is shown that the devised 1-step algorithms outperform 2-step emitter geolocation algorithms, formerly proposed for the problem.

Main Contributions

We formulate the signal model for geolocation of an emitting source in the presence of local scattering under quasi-static temporal Rayleigh fading, using multiple base-station antenna arrays. We extend the GAA model covariance matrix derivation, originally developed for uniform-linear arrays (ULA), to arbitrary-shaped antenna arrays. For this model, we derive both optimal and computationally-simpler, sub-optimal, single-step (direct) geolocation algorithms for emitter geolocation. Based on both numerical performance and complexity analysis, we introduce the recommended algorithm for the problem. In addition, a detailed derivation of the Cramér Rao lower bound (CRLB) for the received signal model is provided in appendix C.1. Using numerical analysis of the CRLB expressions, we highlight expected estimation accuracy under different temporal-fading and scattering conditions. Parts of this chapter have been published in [27].

Chapter Organization

The remainder of this chapter is organized as follows: Section 5.2 outlines the problem formulation. Then section 5.3 provides several optimal and sub-optimal algorithms for 1-step geolocation of a static emitter under local scattering. Numerical performance examples of the devised algorithms are given in section 5.4, and their computational-complexity is analyzed in section 5.5. The CRLB for the problem is derived in appendix C.1.

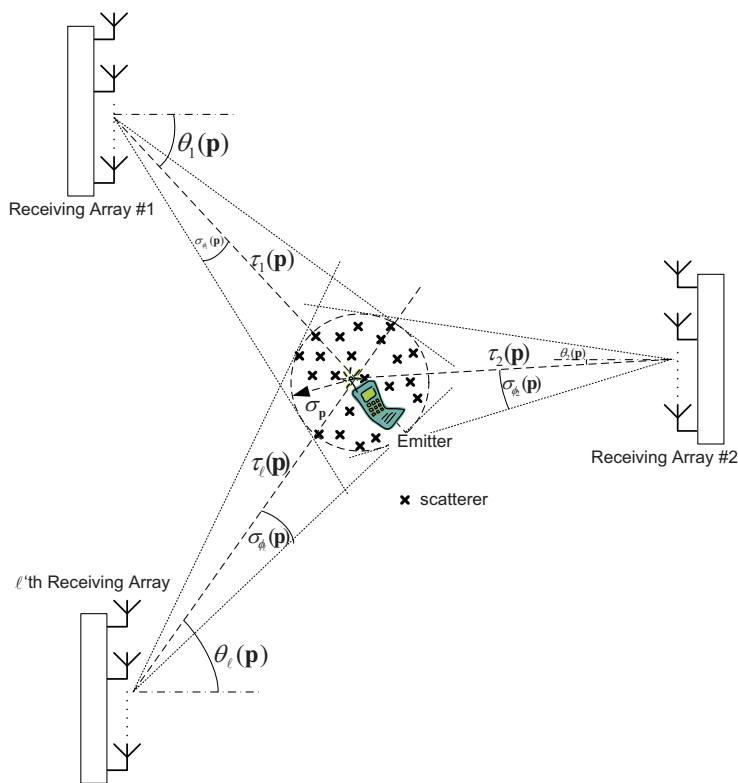


Figure 5.1: Emitter Geolocation in Presence of Local Scattering - Problem Definition

5.2 Problem Formulation

5.2.1 Spatial Model

Consider a stationary emitter that at an unknown time, t_0 , begins to transmit a narrow band signal with an envelope of $s(t)$. The signal bandwidth is W , which satisfies the condition $W \ll f_c$, where f_c is the carrier frequency¹. The emitter's signal is intercepted by L geographically separated Base-Station (BS), each equipped with an antenna-array with M antenna elements.

As depicted in Fig. 5.1, the emitter is surrounded by \bar{N}_{sc} closely spaced

¹The propagation time of the signal across the array must be small compared to the signal's envelope rate of change, given by $1/W$. Let the array aperture be $Y = \tilde{A} \cdot \lambda$, where \tilde{A} is an integer, which usually varies between 1-10. Then, at the propagation speed, c , we have $Y/c \ll 1/W \Rightarrow \tilde{A}/f_c \ll 1/W$. Thus, we have $W/f_c \ll 1/\tilde{A} \leq 1 \Rightarrow W \ll f_c$.

scatterers, (which are assumed to be about the same height or higher than the emitter). The scatterers generate multiple reflection rays of the emitter’s signal around the emitter. The emitter signal observed by each of the receiving arrays is built up by a super-position of these independent rays. This phenomenon is known as “local scattering”. The emitter is assumed to be completely obscured by the scatterers such that there is no direct line of sight (LoS) between the emitter and any of the receiving arrays. In case there is a LoS between the scattered emitter and any of the arrays, the formed fading channel is called Ricean [50, 55].

The rays emanating from the scatterers impinge on each array with a delay associated with the propagation time. The ray originating from the n th scatterer hits the ℓ th array after $(\tau_\ell + \Delta\tau_{\ell n})$ seconds, where τ_ℓ denotes the nominal propagation time from the emitter located at $\mathbf{p} = [x, y]^T$ to the ℓ th BS located at $\mathbf{q}_\ell = [\bar{x}_\ell, \bar{y}_\ell]^T$, (both defined in a global coordinates-system), and $\Delta\tau_{\ell n}$ denotes the excess time delay due to the signal reflected by the n th scatterer.

The nominal propagation time is given by,

$$\begin{aligned}\tau_\ell &= \frac{d_\ell}{c} \\ d_\ell &= \|\mathbf{p} - \mathbf{q}_\ell\|^2 = \sqrt{(x - \bar{x}_\ell)^2 + (y - \bar{y}_\ell)^2}\end{aligned}\quad (5.1)$$

where c denotes the propagation speed.

Commonly, it is assumed that all the time delays of the independent rays generated by the scatterers are small in comparison with the reciprocal of the signal bandwidth and therefore are unresolvable [51, 52]. Thus, the following approximation may be used:

$$s(t - \tau_\ell - \Delta\tau_{\ell n} - t_0) \approx s(t - \tau_\ell - t_0) \triangleq s(t - \tilde{\tau}_\ell) \quad (5.2)$$

where $\tilde{\tau}_\ell \triangleq \tau_\ell - t_0$.

The noise-free signal received by the ℓ th BS array can be described as,

$$\mathbf{x}_\ell(t) = \mathbf{b}_\ell(t) \cdot s(t - \tilde{\tau}_\ell) \quad (5.3)$$

where $\mathbf{b}_\ell(t)$ is a $M \times 1$ vector describing the array's response to the channel at time t . Assuming that the n th ray received by the ℓ th array has a complex gain, $\beta_{\ell,n}(t)$, and an angular perturbation $\phi_{\ell,n}$, then array response may be described as a superposition of all the rays impinging on the array given by:

$$\mathbf{b}_\ell(t) = \sum_{n=1}^{\tilde{N}_{sc}} \beta_{\ell,n}(t) \mathbf{a}_\ell(\theta_\ell(\mathbf{p}) + \phi_{\ell,n}) \quad (5.4)$$

with $\mathbf{a}_\ell(\theta)$ is the ℓ th array $M \times 1$ steering vector with its m th element located at, $\mathbf{q}_{\ell,m} = [\bar{x}_{\ell,m}, \bar{y}_{\ell,m}]^T$, (where $\mathbf{q}_{\ell,m}$ is defined w.r.t. the array center located at \mathbf{q}_ℓ). The response of this element to a signal arriving from position $\mathbf{p} = [x, y]^T$ is given by:

$$[\mathbf{a}_\ell]_m = \frac{1}{\sqrt{M}} e^{\frac{i2\pi}{\lambda} [\bar{x}_{\ell,m} \cos \theta_\ell(\mathbf{p}) + \bar{y}_{\ell,m} \sin \theta_\ell(\mathbf{p})]} \quad (5.5)$$

where $i = \sqrt{-1}$ and λ is the transmitted signal wavelength and, (see e.g., [35])

$$\theta_\ell(\mathbf{p}) = \tan^{-1} \left(\frac{y - \bar{y}_\ell}{x - \bar{x}_\ell} \right) \quad (5.6)$$

In the sequel, we adopt the GAA model for obtaining a closed-form analytic expressions for the statistical distribution of the array response vectors. These expressions are shown to be position-dependent and therefore enable one to extract the emitter position from multiple observations of the channel. The GAA model assumes that the n th ray complex gain is distributed as $\beta_{\ell,n}(t) \sim \mathcal{CN}(0, \frac{1}{\tilde{N}_{sc}})$, and the distribution of the angle perturbations generated by the scatterers is Gaussian with zero mean and standard deviation of σ_{ϕ_ℓ} .

For simplicity, it is assumed that the distribution of the scatterers around the emitter is circular-symmetric (i.e., the scatterers' locations are equally spread in x and y dimensions, namely $\sigma_x^2 = \sigma_y^2 \equiv \sigma_{\mathbf{p}}^2$, $\sigma_{xy} \equiv 0$)², the angular

²A generalization of this model could be made by dropping the circularity assumption and assuming a 2-D Gaussian distribution. In such case, in the vector of unknown parameters, $\sigma_{\mathbf{p}}^2$ would be replaced by σ_x^2 , σ_y^2 and σ_{xy} .

spread observed by the ℓ th receiving array may be approximated as,

$$\sigma_{\phi_\ell} \triangleq \tan \phi_\ell \approx \frac{\sigma_{\mathbf{p}}}{d_\ell} \quad (5.7)$$

It should be noted that the approximation in (5.7) is based on the first-order Taylor expansion of $\theta \approx \tan \theta$, which holds when θ is in the order of ~ 0.1 radians (or ≈ 6 degrees). This approximation holds well for angular-spreading measured for macrocell base-station arrays (see e.g., [46], [51]).

Assuming that the number of scatterers is large ($\bar{N}_{sc} \rightarrow \infty$, [42]), the superposition of the large number of independent rays generated by the local scatterers allows us to invoke a central limit theorem (CLT) argument. Using the CLT, $\mathbf{b}_\ell(t)$ can be modeled as a complex multivariate, normally distributed vector. The variation of the vector components with time gives rise to so-called Rayleigh amplitude fading. The multivariate normal distribution is parameterized by only its mean and covariance matrix.

Recall that $\beta_{\ell,n}(t) \sim \mathcal{CN}(0, \frac{1}{\bar{N}_{sc}})$, therefore:

$$E\{\mathbf{b}_\ell(t)\} = E\{\beta_{\ell,n}(t)\} \cdot E\{\mathbf{a}_\ell(\theta_\ell + \phi_{\ell,n})\} = \mathbf{0} \quad (5.8)$$

Next, we derive the covariance matrix.

$$\mathbf{R}_{b,\ell} \triangleq E\{\mathbf{b}_\ell \mathbf{b}_\ell^H\} \quad (5.9)$$

The m, l th element of array covariance matrix is given by,

$$E\{b_{\ell,m} b_{\ell,l}^*\} = E \left\{ \sum_n \sum_i \beta_{\ell,n}(t) \beta_{\ell,i}^*(t) \cdot e^{i \frac{2\pi}{\lambda} [\bar{x}_{\ell,m} \cos(\theta_\ell + \phi_{\ell,n}) + \bar{y}_{\ell,m} \sin(\theta_\ell + \phi_{\ell,n})]} \cdot e^{-i \frac{2\pi}{\lambda} [\bar{x}_{\ell,l} \cos(\theta_\ell + \phi_{\ell,i}) + \bar{y}_{\ell,l} \sin(\theta_\ell + \phi_{\ell,i})]} \right\} \quad (5.10)$$

where $(\cdot)^*$ denotes the complex-conjugate.

Since the rays originating from the different scatterers are independent, $E\{\beta_{\ell,n}(t) \beta_{\ell,i}^*(t)\} = \frac{1}{\bar{N}_{sc}} \delta_{n,i}$ and $E\{\sum_n |\beta_{\ell,n}(t)|^2\} = \sum_n E\{|\beta_{\ell,n}(t)|^2\} = 1$.

Recall that $\phi_\ell \sim \mathcal{N}(0, \sigma_{\phi_\ell})$, then the expectation in (5.10) is given by,

$$E\{b_{\ell,m} b_{\ell,l}^*\} \approx \int_{-\infty}^{\infty} \frac{1}{\sqrt{2\pi}\sigma_{\phi_\ell}} e^{-\frac{\phi_\ell^2}{2\sigma_{\phi_\ell}^2}} \cdot e^{i\frac{2\pi}{\lambda} [\Delta_{\ell,x}^{m,l} \cos(\theta_\ell + \phi_\ell) + \Delta_{\ell,y}^{m,l} \sin(\theta_\ell + \phi_\ell)]} d\phi_\ell \quad (5.11)$$

where $\Delta_{\ell,x}^{m,l} \triangleq \bar{x}_{\ell,m} - \bar{x}_{\ell,l}$, $\Delta_{\ell,y}^{m,l} \triangleq \bar{y}_{\ell,m} - \bar{y}_{\ell,l}$.

The integral in (5.11) should be evaluated numerically³. However, we may utilize the assumption that the angular spread is small in order to obtain an approximated, closed-form, analytic expression for the array covariance matrix. Under the assumption that the angular spread, σ_{ϕ_ℓ} , is small, the terms $\sin \phi_\ell$ and $\cos \phi_\ell$ may be approximated using their first-order Taylor series expansions:

$$\begin{aligned} \sin(\theta_\ell + \phi_\ell) &\approx \sin \theta_\ell + \cos \theta_\ell \phi_\ell \\ \cos(\theta_\ell + \phi_\ell) &\approx \cos \theta_\ell - \sin \theta_\ell \phi_\ell \end{aligned} \quad (5.12)$$

Plugging (5.12) back into (5.11) and using the formula (see e.g., [115, p. 98, eq. 15.75]):

$$\int_{-\infty}^{\infty} e^{-(ax^2+bx+c)} dx = \sqrt{\frac{\pi}{a}} e^{(b^2-4ac)/4a} \quad (5.13)$$

³We notice that the assumption normal distribution for the AOA perturbations leads to an integral with infinite support, which strictly speaking, is physically impossible. Yet, considering the fact that large deviations from the nominal AOA are less likely than small deviations, and that the spread of rays around the nominal AOA is assumed to be relatively small, we may neglect the emitter power scattered outside the physically possible limits. The infinite-support approximation has been widely used [43]-[50] and was found useful in approximating the case in which, a slowly moving emitter is located between closely-spaced reflectors and scatterers. This has also been validated in a field measurement campaign conducted by Ericsson Radio Systems during the 1990's [45]. Furthermore, for indoor channel scenarios, the Laplacian angle distribution is commonly employed (see e.g., [104]).

it is easy to verify that this integral equals,

$$\begin{aligned}
 E\{b_{\ell,m}b_{\ell,l}^*\} &\approx \frac{1}{\sqrt{2\pi}\sigma_{\phi_\ell}} \int_{-\infty}^{\infty} e^{-\frac{\phi_\ell^2}{2\sigma_{\phi_\ell}^2}} \\
 &\cdot e^{i\frac{2\pi}{\lambda} [(\Delta_{\ell,x}^{m,l} \cos \theta_\ell + \Delta_{\ell,y}^{m,l} \sin \theta_\ell) - \phi_\ell (\Delta_{\ell,x}^{m,l} \sin \theta_\ell - \Delta_{\ell,y}^{m,l} \cos \theta_\ell)]} d\phi_\ell \\
 &= e^{i\frac{2\pi}{\lambda} [\Delta_{\ell,x}^{m,l} \cos \theta_\ell + \Delta_{\ell,y}^{m,l} \sin \theta_\ell]} \\
 &\cdot e^{-\frac{2\pi^2}{\lambda^2} \sigma_{\phi_\ell}^2 [\Delta_{\ell,x}^{m,l} \sin \theta_\ell - \Delta_{\ell,y}^{m,l} \cos \theta_\ell]^2}
 \end{aligned} \tag{5.14}$$

We now see that the ℓ th array covariance matrix can be expressed as,

$$\mathbf{R}_{b,\ell} = \mathbf{a}_\ell(\mathbf{p})\mathbf{a}_\ell^H(\mathbf{p}) \odot \mathbf{B}_\ell(\mathbf{p}, \sigma_{\mathbf{p}}) \tag{5.15}$$

where the (m, l) th element of the $M \times M$ matrix \mathbf{B}_ℓ is given by:

$$[\mathbf{B}_\ell]_{m,l} = e^{-\frac{2\pi^2}{\lambda^2} \sigma_{\phi_\ell}^2 [\Delta_{\ell,x}^{m,l} \sin \theta_\ell - \Delta_{\ell,y}^{m,l} \cos \theta_\ell]^2} \tag{5.16}$$

The result in (5.15) is similar in structure to the result obtained by Zetterberg [45] and Trump & Ottersten [47], but (5.16) holds for an arbitrary-shaped, planar array, not only ULA. An extension to an arbitrary 3-dimensional array is straightforward.

5.2.2 Temporal Model

The spatial model assumptions outlined in the former section indicate that the position-dependent information is embedded in the sampled data covariance. This implies that multiple temporal observations are required to gather sufficient statistics for estimating the position. In the following section, we define assumptions of the temporal model.

1. The total observation time, T , is divided into K disjoint sub-intervals of length ΔT . It is assumed that $\Delta T \gg \max\{\tau_{\ell,j}\}$ where $\tau_{\ell,j}$ is the propagation time between the ℓ th and j th BS.

Remark: The number of frequency bins, N_s , in the signal spectrum that differ from 0 is given by $N_s = \lfloor W \cdot \Delta T \rfloor + 1$, where $\lfloor W \cdot \Delta T \rfloor$ denotes

the largest integer smaller than the observation time-bandwidth product $W \cdot \Delta T$, (see [119, sec. 5.2.1], [17], [41]).

2. The channel coherence time $T_c > \Delta T$, so that the array response vector \mathbf{b}_ℓ remains constant during an observation sub-interval, but may vary between observation sub-intervals. This assumption ensures that the N_s frequency bins are subjected to single realization of the channel vector, \mathbf{b}_ℓ , which implies flat spectral fading. This type of fading channel is commonly referred to as “quasi-static” fading channel or “block-fading” channel (see, e.g., [58], [59]).
3. Finally, it is assumed that the spectrum of the signal observed during each of the ΔT sub-intervals is constant, and is known *a priori* to the receivers. This assumption typically holds for most communication systems. See proposition 5.2.1 for proof.

Proposition 5.2.1 *The spectrum of signal with infinite support is constant.*

Proof Assume $s(t)$ has infinite support. The Fourier transform of this signal is given by: $\mathcal{F}\{s(t)\} = \tilde{S}(f)$. The k th observation of the signal is equivalent to multiplying the signal by a window $w(t)$ of length ΔT . In the frequency domain, this becomes a convolution between $\tilde{S}(f)$ and the Fourier transform of the window, $\tilde{W}(f)$. Since the same window is used for all snapshots, up to delay that can be compensated, the signal representation in the frequency domain is identical for all snapshots.

Problem Statement

Assuming that the signals intercepted by the ℓ th array are corrupted by spatially and temporally white noise with variance σ_n^2 , the time-domain signal of the k th sub-interval (a.k.a., “snapshot”) received by the ℓ th array can be

expressed as,

$$\begin{aligned} \mathbf{y}_{\ell,k}(t) &= \mathbf{b}_{\ell,k} \cdot s(t - \tau_\ell - t_0) + \mathbf{n}_{\ell,k}(t), \\ &\quad (k-1) \cdot \Delta T \leq t \leq k \cdot \Delta T \\ &\quad k = 1 \dots K \end{aligned} \tag{5.17}$$

where,

$$\mathbf{b}_{\ell,k} \in \mathcal{CN}(\mathbf{0}, \mathbf{R}_{b,\ell}(\mathbf{p}, \sigma_{\mathbf{p}})) \tag{5.18}$$

Concatenating all the synchronized observations into a single vector,

$$\mathbf{y}_\ell \triangleq [\mathbf{y}_{\ell,1}^T, \mathbf{y}_{\ell,2}^T, \dots, \mathbf{y}_{\ell,K}^T]^T \tag{5.19}$$

The problem discussed herein may be stated as follows: Given $\{\mathbf{y}_\ell\}_{\ell=1}^L$, estimate the emitter's position, \mathbf{p} , where the vector of unknown parameters is defined as,

$$\boldsymbol{\eta} \triangleq [\mathbf{p}^T, \sigma_{\mathbf{p}}, t_0]^T \tag{5.20}$$

The value of the additive noise variance, σ_n^2 , is assumed to be known *a priori*, as it is a function of the RF chain at the BS receivers.

5.3 Positioning Algorithms

In the following section we derive direct (single-step) positioning algorithms for a single emitting source subjected to a local scattering that forms a Rayleigh fading channel complying with the assumptions outlined in section 5.2.

5.3.1 Maximum Likelihood Estimation

In this section, we derive the Maximum Likelihood Estimator (MLE) for the problem at hand. The information on the emitter position is embedded both in the fading channel statistics, as well as in the time delay of the received signal. Under the assumption that the channel coherence time, T_c is longer than the snapshot observation time, ΔT , the time delay information embedded in the received signal may be extracted for improving the geolocation performance.

To separate the time delay τ_ℓ from the signal's complex envelope, we shall consider the waveform received by each sensor to be represented by its Fourier coefficients defined by

$$\bar{\mathbf{y}}_{\ell,k}(f_n) \triangleq \frac{1}{\Delta T} \int_{(k-1)\Delta T}^{k\Delta T} \mathbf{y}_{\ell,k}(t) e^{-i2\pi f_n t} dt, \quad (5.21)$$

where $f_n = n/\Delta T$, $n = 0, \pm 1, \pm 2, \dots$ is the frequency associated with the n th coefficient. Under assumption A-3, the spectrum of the transmitted signal is constant across the snapshots. Thus, using assumption A-2, the frequency domain model of the signal received by the ℓ th array during the k th observation interval is given by,

$$\bar{\mathbf{y}}_{\ell,k}(f_n) = \mathbf{b}_{\ell,k} \bar{s}(f_n) e^{-j2\pi f_n (\tau_\ell + t_0)} + \bar{\mathbf{n}}_{\ell,k}(f_n) \quad (5.22)$$

where, $\bar{s}(f_n)$ is the n th frequency coefficient. Define,

$$\tilde{\mathbf{y}}_{\ell,k} \triangleq [\bar{\mathbf{y}}_{\ell,k}^T(f_0), \bar{\mathbf{y}}_{\ell,k}^T(f_1), \dots, \bar{\mathbf{y}}_{\ell,k}^T(f_{N-1})]^T \quad (5.23)$$

Notice the relation,

$$\begin{aligned}\tilde{\mathbf{y}}_{\ell,k} &= [(\mathbf{D}_\ell \bar{\mathbf{s}}) \otimes \mathbf{I}_M] \mathbf{b}_{\ell,k} + \tilde{\mathbf{n}}_{\ell,k} \\ &= \mathbf{G}_\ell \mathbf{b}_{\ell,k} + \tilde{\mathbf{n}}_{\ell,k}\end{aligned}\quad (5.24)$$

where,

$$\begin{aligned}\bar{\mathbf{s}} &\triangleq [\bar{s}(f_0), \bar{s}(f_1), \dots, \bar{s}(f_{N-1})]^T \\ \mathbf{D}_\ell(\mathbf{p}, t_0) &\triangleq \text{diag}\{e^{-j2\pi f_0(\tau_\ell(\mathbf{p})+t_0)}, e^{-j2\pi f_1(\tau_\ell(\mathbf{p})+t_0)}, \\ &\quad \dots, e^{-j2\pi f_{N-1}(\tau_\ell(\mathbf{p})+t_0)}\} \\ \mathbf{G}_\ell &= (\mathbf{D}_\ell \bar{\mathbf{s}}) \otimes \mathbf{I}_M \\ \tilde{\mathbf{n}}_{\ell,k} &\triangleq [\tilde{\mathbf{n}}_{\ell,k}^T(f_0), \tilde{\mathbf{n}}_{\ell,k}^T(f_1), \dots, \tilde{\mathbf{n}}_{\ell,k}^T(f_{N-1})]^T\end{aligned}\quad (5.25)$$

Further, define:

$$\begin{aligned}\mathbf{G} &\triangleq \begin{bmatrix} \mathbf{G}_1 & \mathbf{0} & \dots & \mathbf{0} \\ \mathbf{0} & \mathbf{G}_2 & & \vdots \\ \vdots & & \ddots & \mathbf{0} \\ \mathbf{0} & \dots & \mathbf{0} & \mathbf{G}_L \end{bmatrix} \\ \tilde{\mathbf{b}}_k &\triangleq [\mathbf{b}_{1,k}^T, \mathbf{b}_{2,k}^T, \dots, \mathbf{b}_{L,k}^T]^T \\ \tilde{\mathbf{y}}_k &\triangleq [\tilde{\mathbf{y}}_{1,k}^T, \tilde{\mathbf{y}}_{2,k}^T, \dots, \tilde{\mathbf{y}}_{L,k}^T]^T \\ \tilde{\mathbf{n}}_k &\triangleq [\tilde{\mathbf{n}}_{1,k}^T, \tilde{\mathbf{n}}_{2,k}^T, \dots, \tilde{\mathbf{n}}_{L,k}^T]^T\end{aligned}\quad (5.26)$$

Using (5.26), (5.24) may be recast as,

$$\tilde{\mathbf{y}}_k = \mathbf{G} \tilde{\mathbf{b}}_k + \tilde{\mathbf{n}}_k \quad (5.27)$$

The first and second order moments of the noise and spatial signature vectors

are summarized by,

$$\begin{aligned}
E\{\tilde{\mathbf{n}}_{\ell,k}\} &= \mathbf{0}. \quad \forall \ell, k \\
E\{\tilde{\mathbf{n}}_{\ell,k}\tilde{\mathbf{n}}_{i,j}^H\} &= \sigma_n^2 \mathbf{I}_{MN} \delta_{\ell,i} \delta_{k,j} \\
E\{\mathbf{b}_{\ell,k}\} &= \mathbf{0}. \quad \forall \ell, k \\
E\{\mathbf{b}_{\ell,k}\mathbf{b}_{i,j}^H\} &= \mathbf{R}_{b,\ell} \delta_{\ell,i} \delta_{k,j} \\
E\{\mathbf{b}_{\ell,k}\tilde{\mathbf{n}}_{\ell,k}^H\} &= \mathbf{0}. \quad \forall \ell, k
\end{aligned} \tag{5.28}$$

where $\mathbf{R}_{b,\ell}$ is defined in (5.15). Using (5.28) we have:

$$\begin{aligned}
\tilde{\mathbf{R}}_{\ell,k,i,j} &\triangleq E\{\tilde{\mathbf{y}}_{\ell,k}\tilde{\mathbf{y}}_{i,j}^H\} \\
&= E\{(\mathbf{G}_\ell \mathbf{b}_{\ell,k} + \tilde{\mathbf{n}}_{\ell,k})(\mathbf{G}_i \mathbf{b}_{i,j} + \tilde{\mathbf{n}}_{i,j})^H\} \\
&= \mathbf{G}_\ell \mathbf{R}_{b,\ell} \mathbf{G}_i^H \delta_{\ell,i} \delta_{k,j} + \sigma_n^2 \mathbf{I}_{NM} \delta_{\ell,i} \delta_{k,j}
\end{aligned} \tag{5.29}$$

Hence,

$$\tilde{\mathbf{R}}_\ell = \mathbf{G}_\ell \mathbf{R}_{b,\ell} \mathbf{G}_\ell^H + \sigma_n^2 \mathbf{I}_{NM} \tag{5.30}$$

Since the snapshots are independent and identically distributed, the likelihood of the complete data set $\tilde{\mathbf{y}}_1, \tilde{\mathbf{y}}_2, \dots, \tilde{\mathbf{y}}_K$ is given by,

$$f(\tilde{\mathbf{y}}_1, \tilde{\mathbf{y}}_2, \dots, \tilde{\mathbf{y}}_K | \boldsymbol{\eta}) = \prod_{i=1}^K \frac{1}{\pi^{NML} |\tilde{\mathbf{R}}|} e^{-\tilde{\mathbf{y}}_i^H \tilde{\mathbf{R}}^{-1} \tilde{\mathbf{y}}_i} \tag{5.31}$$

where,

$$\tilde{\mathbf{R}} \triangleq \begin{bmatrix} \tilde{\mathbf{R}}_1 & \mathbf{0} & \cdots & \mathbf{0} \\ \mathbf{0} & \tilde{\mathbf{R}}_2 & & \vdots \\ \vdots & & \ddots & \mathbf{0} \\ \mathbf{0} & \cdots & \mathbf{0} & \tilde{\mathbf{R}}_L \end{bmatrix} \tag{5.32}$$

and $|\mathbf{X}|$ denotes the determinant of the matrix \mathbf{X} .

The negative log-likelihood is given, up to an additive constant, by (see

e.g., [117]),

$$\begin{aligned}
 \mathcal{L}_f(\boldsymbol{\eta}) &= \ln \left\{ |\tilde{\mathbf{R}}| \right\} + \left\{ \tilde{\mathbf{y}}^H \tilde{\mathbf{R}}^{-1} \tilde{\mathbf{y}} \right\} \\
 &= \ln \left\{ \prod_{\ell=1}^L |\tilde{\mathbf{R}}_{\ell}| \right\} + \sum_{\ell=1}^L \text{Tr} \left[\tilde{\mathbf{R}}_{\ell}^{-1} \hat{\mathbf{R}}_{\ell} \right] \\
 &= \sum_{\ell=1}^L \ln \left\{ |\tilde{\mathbf{R}}_{\ell}| \right\} + \text{Tr} \left[\tilde{\mathbf{R}}_{\ell}^{-1} \hat{\mathbf{R}}_{\ell} \right]
 \end{aligned} \tag{5.33}$$

where $\hat{\mathbf{R}}_{\ell} = \frac{1}{K} \sum_{k=1}^K \tilde{\mathbf{y}}_{\ell,k} \tilde{\mathbf{y}}_{\ell,k}^H$. The MLE of the parameter vector $\boldsymbol{\eta}$ is the minimizing argument of $\mathcal{L}_f(\boldsymbol{\eta})$,

$$\hat{\boldsymbol{\eta}} = \underset{\boldsymbol{\eta}}{\text{argmin}} \{ \mathcal{L}_f(\boldsymbol{\eta}) \} \tag{5.34}$$

This minimization requires a 3-dimensional search (or 4-dimensional, if the z -coordinate is required as well).

The implementation of the criterion specified in (5.33) may be simplified by “castling” between the terms inside the trace operator: namely, replacing the inverse covariance matrix with its consistent estimate, $\hat{\mathbf{R}}_{\ell}^{-1}$ (see [60] for proof), while the sample covariance is replaced by the true covariance term. The new criteria referred to as “approximate MLE” (AMLE), is stated as follows:

$$\hat{\boldsymbol{\eta}} = \underset{\boldsymbol{\eta}}{\text{argmin}} \left\{ \sum_{\ell=1}^L \ln \left\{ |\tilde{\mathbf{R}}_{\ell}| \right\} + \text{Tr} \left[\hat{\mathbf{R}}_{\ell}^{-1} \tilde{\mathbf{R}}_{\ell} \right] \right\} \tag{5.35}$$

Notice that for $K \rightarrow \infty$, (5.35) and (5.33) are asymptotically equivalent:

$$\text{Tr} \left[\hat{\mathbf{R}}_{\ell}^{-1} \tilde{\mathbf{R}}_{\ell} \right] = \text{Tr} \left[\tilde{\mathbf{R}}_{\ell}^{-1} \hat{\mathbf{R}}_{\ell} \right] = \mathbf{I}. \tag{5.36}$$

The advantage of (5.35) over (5.33) lies in the fact that $\hat{\mathbf{R}}_{\ell}^{-1}$ is free of parameters and therefore may be inverted outside the search loop, thereby saving the computational cost incurred by inverting the covariance matrix for every grid point.

5.3.2 Sub-Optimal Estimators

In the following section we outline several types of sub-optimal estimators for the geolocation problem at hand:

- Estimators utilizing both time-delay and angle of arrival statistical information.
- An estimator utilizing only time-delay information.
- Estimators utilizing only angle of arrival statistical information.

Weighted Least Squares Estimation

In this section, estimators based on least squares fits of the theoretical and sample covariances are investigated with the aim of finding less computationally demanding approximations to MLE. Consider the following cost function:

$$\tilde{Q}(\boldsymbol{\eta}) = \sum_{\ell=1}^L \|\mathbf{W}_\ell^{H/2}(\tilde{\mathbf{R}}_\ell(\boldsymbol{\eta}) - \hat{\hat{\mathbf{R}}}_\ell)\mathbf{W}_\ell^{1/2}\|_F^2 \quad (5.37)$$

where \mathbf{W}_ℓ is a positive definite weighting matrix, and $\|\mathbf{X}\|_F^2 = \text{Tr}\{\mathbf{X}^H\mathbf{X}\}$.

The choice of \mathbf{W}_ℓ is usually made such that the error-covariance of the parameter vector, $\boldsymbol{\eta}$, is minimized. It can be shown that the optimal choice for $\tilde{\mathbf{W}}_\ell$ would be $\mathbf{W}_\ell = \tilde{\mathbf{R}}_\ell^{-1}$ [47]. Viberg and Ottersten [60] have shown that \mathbf{W}_ℓ may be replaced by a consistent estimate $\hat{\mathbf{W}}_\ell = \hat{\hat{\mathbf{R}}}_\ell^{-1}$ without affecting the asymptotic properties of the estimator. Substituting $\hat{\mathbf{W}}_\ell$ back into (5.37) and using the fact that both the sample and the true covariance matrices are hermitian we obtain,

$$\begin{aligned} \tilde{Q}(\boldsymbol{\eta}) &= \sum_{\ell=1}^L \tilde{Q}_\ell = \sum_{\ell=1}^L \|\tilde{\mathbf{R}}_\ell(\boldsymbol{\eta})\hat{\hat{\mathbf{R}}}_\ell^{-1} - \mathbf{I}\|_F^2 \\ &= \sum_{\ell=1}^L \text{Tr} \left\{ \left(\tilde{\mathbf{R}}_\ell(\boldsymbol{\eta})\hat{\hat{\mathbf{R}}}_\ell^{-1} - \mathbf{I} \right)^2 \right\} \end{aligned} \quad (5.38)$$

Thus, the WLS criterion may be stated as:

$$\hat{\boldsymbol{\eta}} = \underset{\boldsymbol{\eta}}{\operatorname{argmin}} \left\{ \sum_{\ell=1}^L \operatorname{Tr} \left[\left(\tilde{\mathbf{R}}_{\ell}(\boldsymbol{\eta}) \hat{\mathbf{R}}_{\ell}^{-1} - \mathbf{I} \right)^2 \right] \right\} \quad (5.39)$$

Least Squares Estimation

An even less computational-intensive estimator (see sec. 5.5 for more details) may be obtained by setting $\mathbf{W} = \mathbf{I}$. This is known as the least squares estimator (LSE).

$$\hat{\boldsymbol{\eta}} = \underset{\boldsymbol{\eta}}{\operatorname{argmin}} \left\{ \sum_{\ell=1}^L \operatorname{Tr} \left[\left(\tilde{\mathbf{R}}_{\ell} - \hat{\mathbf{R}}_{\ell} \right)^2 \right] \right\} \quad (5.40)$$

Time-Delay based Geolocation

A different suboptimal location estimator may be obtained by treating the vector $\tilde{\mathbf{b}}_k$ as an unknown deterministic vector. By making this assumption the estimator effectively ignores the location-dependent information embedded in $\tilde{\mathbf{b}}_k$, and thus becomes suboptimal. In such case, the likelihood function becomes:

$$\begin{aligned} f(\tilde{\mathbf{y}}|\boldsymbol{\zeta}) &= f(\tilde{\mathbf{y}}_1, \tilde{\mathbf{y}}_2, \dots, \tilde{\mathbf{y}}_K|\boldsymbol{\zeta}) \\ &= \prod_{k=1}^K \frac{1}{|\pi\sigma_n^2\mathbf{I}|} \exp \left\{ -\sigma_n^{-2} \|\tilde{\mathbf{y}}_k - \mathbf{G}\tilde{\mathbf{b}}_k\|^2 \right\} \end{aligned} \quad (5.41)$$

where $\boldsymbol{\zeta} \triangleq [\mathbf{p}^T, t_0]^T$.

The negative log-likelihood cost function (up to an additive constant), is given by,

$$Q(\boldsymbol{\zeta}) = \sum_{k=1}^K \|\tilde{\mathbf{y}}_k - \mathbf{G}\tilde{\mathbf{b}}_k\|^2 \quad (5.42)$$

It is easy to verify that $Q(\boldsymbol{\zeta})$ is minimized by selecting $\tilde{\mathbf{b}}_k$ as the least-

squares estimate:

$$\hat{\mathbf{b}}_k = (\mathbf{G}^H \mathbf{G})^{-1} \mathbf{G}^H \tilde{\mathbf{y}}_k \quad (5.43)$$

Plugging back (5.43) into (5.42), the MLE for the deterministic, unknown channel vector case is obtained as,

$$\begin{aligned} \hat{\boldsymbol{\zeta}} &= \underset{\boldsymbol{\zeta}}{\operatorname{argmax}} \left\{ \sum_{k=1}^K \tilde{\mathbf{y}}_k^H \mathbf{G} (\mathbf{G}^H \mathbf{G})^{-1} \mathbf{G}^H \tilde{\mathbf{y}}_k \right\} \\ &= \underset{\boldsymbol{\zeta}}{\operatorname{argmax}} \left\{ \operatorname{Tr} \left[\mathbf{\Pi}_G \sum_{k=1}^K \tilde{\mathbf{y}}_k \tilde{\mathbf{y}}_k^H \right] \right\} \\ &= \underset{\boldsymbol{\zeta}}{\operatorname{argmax}} \left\{ \operatorname{Tr} \left[\mathbf{\Pi}_G \hat{\mathbf{R}} \right] \right\} \end{aligned} \quad (5.44)$$

where $\mathbf{\Pi}_G \triangleq \mathbf{G}(\mathbf{G}^H \mathbf{G})^{-1} \mathbf{G}^H$ is the projection matrix onto the column subspace of the matrix \mathbf{G} . The estimator in (5.44) requires maximization of the cost function over the parameters space of interest.

Angle-based Geolocation

An alternative family of sub-optimal position estimators may be derived by ignoring the temporal coherence information embedded in the signal received at each snapshot. The advantage of these estimators is reduced computational complexity compared to the estimators that take the temporal coherence into account, (see sec. 5.5 for more details). In this case, it is assumed that $T_c \ll \Delta T$. Namely, the fading channel varies rapidly such that each time-sample is subjected to a different, independent channel realization. This assumption precludes the time-delay information from being extracted. Hence, the emitter position may be estimated only from the AOA statistical information. Since the position estimation does not rely on temporal correlations there is no need to transform the received signal from the time-domain to the frequency domain, as is done in all of the algorithms aforementioned.

The processing is carried out in the time-domain; we collect K temporal observations (snapshots) of each of the L arrays, (sampled at instants $t_1 \dots t_K$).

Define the following matrices:

$$\begin{aligned}
 \mathbf{y}(t_k) &\triangleq [\mathbf{y}_1^T(t_k), \mathbf{y}_2^T(t_k), \dots, \mathbf{y}_L^T(t_k)]^T \\
 \mathbf{n}(t_k) &\triangleq [\mathbf{n}_1^T(t_k), \mathbf{n}_2^T(t_k), \dots, \mathbf{n}_L^T(t_k)]^T \\
 \mathbf{b}(t_k) &\triangleq [\mathbf{b}_1^T(t_k), \mathbf{b}_2^T(t_k), \dots, \mathbf{b}_L^T(t_k)]^T
 \end{aligned} \tag{5.45}$$

Using (5.45), the model in (5.17) may be written in vector notation as,

$$\mathbf{y}(t_k) = \mathbf{b}(t_k)s(t_k - \tilde{\tau}_\ell) + \mathbf{n}(t_k), \quad k = 1, \dots, K \tag{5.46}$$

MLE Applying the assumptions outline in (5.28) we have:

$$\begin{aligned}
 \mathbf{R}_{\ell,i}(t_k, t_j) &\triangleq E\{\mathbf{y}_\ell(t_k)\mathbf{y}_i^H(t_j)\} \\
 &= E\left\{ [s(t_k - \tilde{\tau}_\ell)\mathbf{b}_\ell(t_k) + \mathbf{n}_\ell(t_k)] \right. \\
 &\quad \left. [s(t_j - \tilde{\tau}_i)\mathbf{b}_i(t_j) + \mathbf{n}_i(t_j)]^H \right\} \\
 &= s(t_k - \tilde{\tau}_\ell) \cdot s^*(t_j - \tilde{\tau}_i) \cdot \mathbf{R}_{b,\ell}\delta_{\ell,i}\delta_{k,j} \\
 &\quad + \sigma_n^2 \mathbf{I}_{NM}\delta_{\ell,i}\delta_{k,j}
 \end{aligned} \tag{5.47}$$

From (5.47) we have,

$$\mathbf{R}_\ell(t_k) = |s(t_k - \tilde{\tau}_\ell)|^2 \cdot \mathbf{R}_{b,\ell} + \sigma_n^2 \mathbf{I}_M \tag{5.48}$$

For mathematical convenience it is common to assume constant-modulus signal (see, [47, 56, 55]), for which $|s(t)|^2 = 1$. Under this assumption (5.48) becomes,

$$\mathbf{R}_\ell(t_k) = \mathbf{R}_\ell = \mathbf{R}_{b,\ell} + \sigma_n^2 \mathbf{I}_M \tag{5.49}$$

Notice that under the constant-modulus assumption (5.49) depends only on the vector, $\boldsymbol{\psi} \triangleq [\mathbf{p}^T, \sigma_p]^T$.

Since the snapshots are independent and identically distributed, the likeli-

hood function of the complete data set $\mathbf{y}(t_1), \mathbf{y}(t_2), \dots, \mathbf{y}(t_K)$ is given by,

$$f(\mathbf{y}(t_1), \mathbf{y}(t_2), \dots, \mathbf{y}(t_K) | \boldsymbol{\psi}) = \prod_{i=1}^K \frac{1}{\pi^{ML} |\mathbf{R}|} e^{-\mathbf{y}^H(t_i) \mathbf{R}^{-1} \mathbf{y}(t_i)} \quad (5.50)$$

where,

$$\mathbf{R} \triangleq \begin{bmatrix} \mathbf{R}_1 & \mathbf{0} & \cdots & \mathbf{0} \\ \mathbf{0} & \mathbf{R}_2 & & \vdots \\ \vdots & & \ddots & \mathbf{0} \\ \mathbf{0} & \cdots & \mathbf{0} & \mathbf{R}_L \end{bmatrix} \quad (5.51)$$

The negative log-likelihood is given, up to an additive constant, by,

$$\begin{aligned} \mathcal{L}_f(\boldsymbol{\psi}) &= \ln \{|\mathbf{R}|\} + \{\mathbf{y}^H \mathbf{R}^{-1} \mathbf{y}\} \\ &= \ln \left\{ \prod_{\ell=1}^L |\mathbf{R}_\ell| \right\} + \sum_{\ell=1}^L \text{Tr} \left[\mathbf{R}_\ell^{-1} \hat{\mathbf{R}}_\ell \right] \\ &= \sum_{\ell=1}^L \ln \{|\mathbf{R}_\ell|\} + \text{Tr} \left[\mathbf{R}_\ell^{-1} \hat{\mathbf{R}}_\ell \right] \end{aligned} \quad (5.52)$$

where $\hat{\mathbf{R}}_\ell = \frac{1}{K} \sum_k \mathbf{y}_\ell(t_k) \mathbf{y}_\ell^H(t_k)$.

The MLE of $\boldsymbol{\psi}$ is obtained as minimizing argument of $\mathcal{L}_f(\boldsymbol{\psi})$,

$$\hat{\boldsymbol{\psi}} = \underset{\boldsymbol{\psi}}{\text{argmin}} \left\{ \sum_{\ell=1}^L \ln \{|\mathbf{R}_\ell|\} + \text{Tr} \left[\mathbf{R}_\ell^{-1} \hat{\mathbf{R}}_\ell \right] \right\} \quad (5.53)$$

This requires a 3-dimensional search (or a 4-dimensional, if z -coordinate is required as well), The criteria defined in (5.53) is considered as suboptimal for the quasi-static fading channel case, yet this is the MLE/optimal criteria for the ‘fast-fading’ channel case.

Least Squares Estimators The LS estimators derived in section 5.3.2 may also be adopted for the ‘fast-fading’ channel case.

From (5.39), the WLS estimator is given by:

$$\hat{\boldsymbol{\psi}} = \underset{\boldsymbol{\psi}}{\operatorname{argmin}} \left\{ \sum_{\ell=1}^L \operatorname{Tr} \left[\left(\mathbf{R}_{\ell}(\boldsymbol{\psi}) \hat{\mathbf{R}}_{\ell}^{-1} - \mathbf{I} \right)^2 \right] \right\} \quad (5.54)$$

The LSE for this case can be derived from (5.40):

$$\hat{\boldsymbol{\psi}} = \underset{\boldsymbol{\psi}}{\operatorname{argmin}} \left\{ \sum_{\ell=1}^L \operatorname{Tr} \left[\left(\mathbf{R}_{\ell}(\boldsymbol{\psi}) - \hat{\mathbf{R}}_{\ell} \right)^2 \right] \right\} \quad (5.55)$$

This concludes the positioning algorithms section.

5.4 Numerical Examples

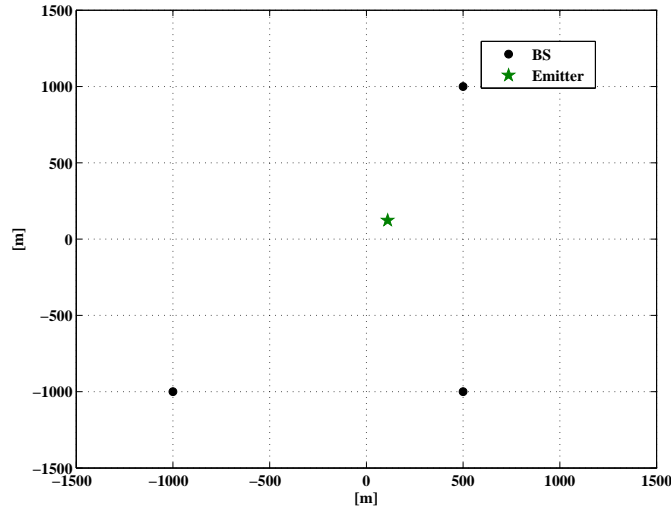


Figure 5.2: Geolocation of Emitter under Local Scattering - System Layout

In this section, we demonstrate the estimation performance of the devised algorithms using some numerical simulation examples. The system layout is illustrated in Fig. 5.2. The system consists of 3 base-stations (BS) that are located at $\{-1, -1\}, \{0.5, 1\}, \{0.5, -1\} \cdot 1000[\text{m}]$. Each BS is equipped with a circular antenna array of 5 elements. The system aims to determine the location of a single emitter placed at $\{111[\text{m}], 123[\text{m}]\}$. The signal transmitted

5.4. Numerical Examples

by the emitter is a modulated carrier at 1.0GHz. Throughout the numerical analysis the propagation speed is assumed to be $c = 3 \cdot 10^8$ [meters/sec] and, for simplicity, $t_0 = 0$. The baseband modulating signal is constant modulus with $|s(t)|^2 = 1$. The additive noise variance at each antenna element in every array is calculated as,

$$\sigma_n^2 \triangleq \frac{1}{M} \cdot 10^{\frac{-\text{SNR}[\text{dB}]}{10}} \quad (5.56)$$

In order to gather enough statistics, the simulation results are based on 500 Monte-Carlo runs per each SNR value. At each run new channel fading coefficients, as well as new additive noise samples are regenerated. The noise coefficients are drawn from zero mean, circular, complex Gaussian distribution with scaled identity matrix covariance. Fig. 5.3 - Fig. 5.4 depict the root-mean-squared-error (RMSE) of the estimated position that is given by (4.37).

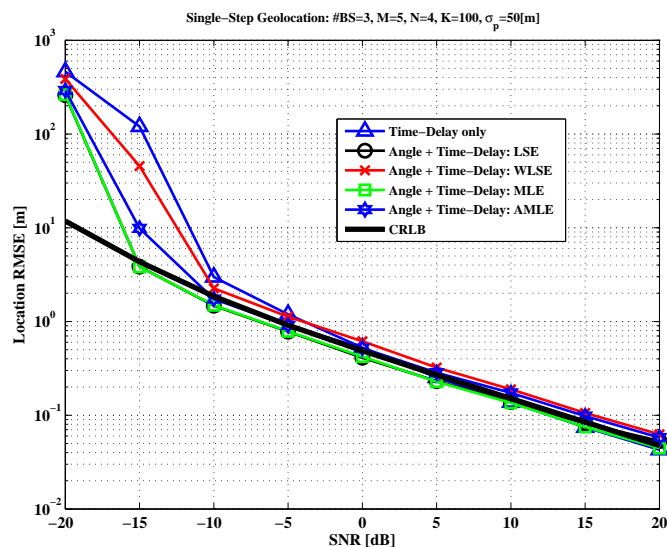


Figure 5.3: RMSE Performance for Quasi-Static Channel ($N_S = 4$), $L = 3$ and $\sigma_p = 50\text{m}$

Fig. 5.3 - Fig. 5.4 depict the RMSE performance for quasi-static fading channel. In these figures, it is assumed that time-bandwidth product is $N_s = 4$ and the number of snapshots is $K = 100$. In both figures, the scatterers are assumed to be distributed around the emitter with a position spread standard deviation

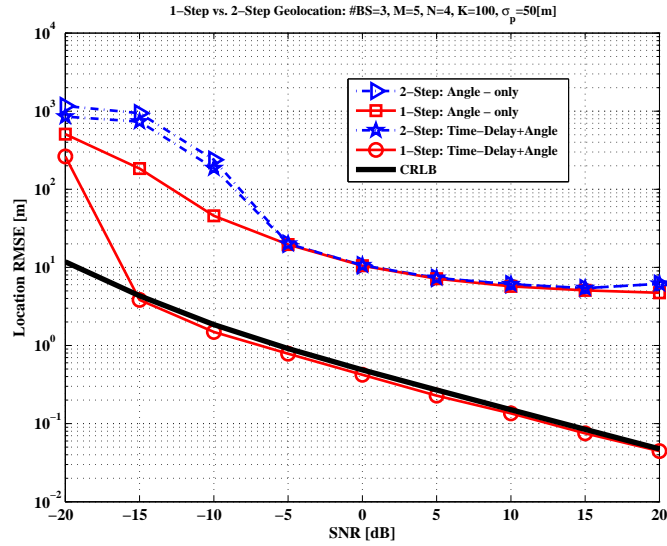


Figure 5.4: 1-Step vs. 2-Step Position Estimation with $L = 3$ Base-Station.

of 50[m].

As seen in Fig. 5.3, while MLE, AMLE and LSE estimators coincide with the CRLB, the WLS exhibits slightly inferior performance compared to these 3 estimators. This also agrees with the observation of Hari & Ottersten [50] regarding the inferior performance of WLS compared to MLE and LSE. It is also evident that the AMLE and LSE attain similar performance as MLE with the advantage of lower computational complexity.

The advantage of the angle-related information comes into play under low SNR regime, as indicated by the lower performance of the time-delay only estimator, which lacks that information. We may conclude that although it has no optimality claim, the LSE is the preferred approach as it achieves the best performance at the lowest computational complexity. (This will be explained in the next section).

Fig. 5.4 compares 1-step geolocation estimators to 2-Step geolocation estimators that are based on AOA-only and AOA+TOA estimation. The 1-step, angle-based geolocation is accomplished using (5.55) and the 1-step angle+time delay geolocation is done using (5.40). The AOA estimation in the 2-step geolocation is performed using the LSE algorithm proposed by Trump & Ottersten in [47]. The TOA estimation at each of the L BS is accomplished

by evaluating,

$$\hat{\tau}_\ell = \underset{\tau_\ell}{\operatorname{argmax}} \left\{ \operatorname{Tr} \left[\mathbf{\Pi}_{G_\ell} \hat{\mathbf{R}}_\ell \right] \right\} \quad (5.57)$$

where $\mathbf{\Pi}_{G_\ell} \triangleq \mathbf{G}_\ell (\mathbf{G}_\ell^H \mathbf{G}_\ell)^{-1} \mathbf{G}_\ell^H$, and \mathbf{G}_ℓ is defined in (5.25). Notice that in order to make a fair comparison with the time-delay + angle 1-step estimator, both AOA and angle-dependent position estimation were done for $(K \cdot N_s)$ snapshots of the array, (which contained only K different channel realizations).

As demonstrated, the devised 1-step estimator, which combines both time-delay and angle information, outperforms both the AOA-based and AOA+TOA, 2-step estimators. This is expected as the latter ignore the position information embedded in the time-delay, as well as the phase information of the known signal (recall that the signal has constant modulus, hence this information is lost in the structure of the covariance matrix). Notwithstanding, even the sub-optimal 1-step LSE estimator, which is based only on angle-information, excels over the 2-step estimator under a low SNR regime. This can be attributed to the 2-step estimation approach, which overlooks the fact that all the L independent angle estimations must correspond to a single emitter location, but also to the fact that the 2-step estimator cannot utilize the distance information embedded in the angular spread parameter, while the 1-step estimator can extract that.

Finally, Fig. 5.5 - Fig. 5.6 depict the cumulative distribution function (CDF) for the positioning error bound predicted by the CRLB. The CDF, $F(x)$, is defined in (4.38). The error values are calculated for the system layouts described in Fig. 5.2, over a $2[\text{km}] \times 2[\text{km}]$ grid in steps of $20[\text{m}]$ (forming a total of 10,000 different locations). Each of these figures depicts the CDF curves at 4 different position-spread levels ranging from 0 spread (i.e., the case when the local scattering causes no angular spreading but only fading), to a spread of $600[\text{m}]$ around the emitter. Fig. 5.5 depicts the CDFs for a quasi-static fading channel scenario with time-bandwidth product of $N_s = 4$. Fig. 5.6 depicts the CDFs a fast-fading channel scenario, which is simulated via signal with a time-bandwidth product of $N_s = 1$. In both cases, the SNR is 10dB and $K = 100$.

It is interesting to note the difference between the two fading-type cases: while for the fast-fading channel a clear dependence of the estimation error in the angular spread can be observed, in the quasi-static channel case the positioning error is less sensitive to large angular spreads. This phenomenon can be attributed to the time-delay information that can only be utilized in the quasi-static case and effectively bounds the positioning error. When the time delay information is lost due to lack of temporal channel coherence, the estimation error is strongly affected by the scattering environment parameters.

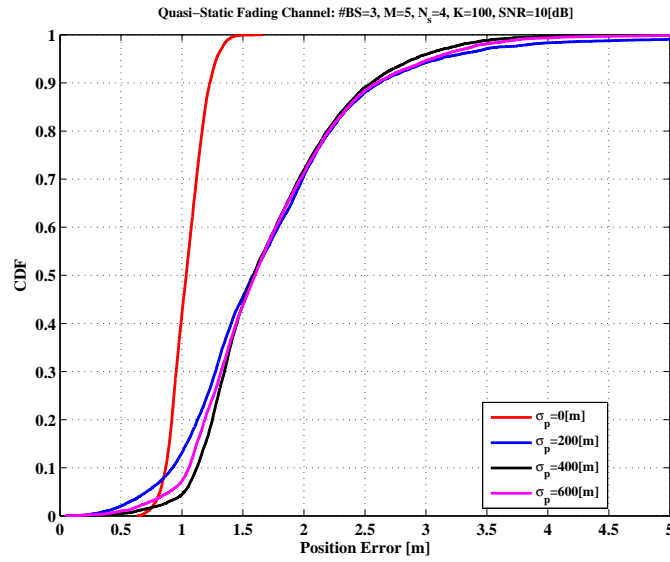


Figure 5.5: CRLB for Quasi-Static Fading Channel $N_s = 4$, $K = 100$, $L = 3$ @ SNR = 10[dB]

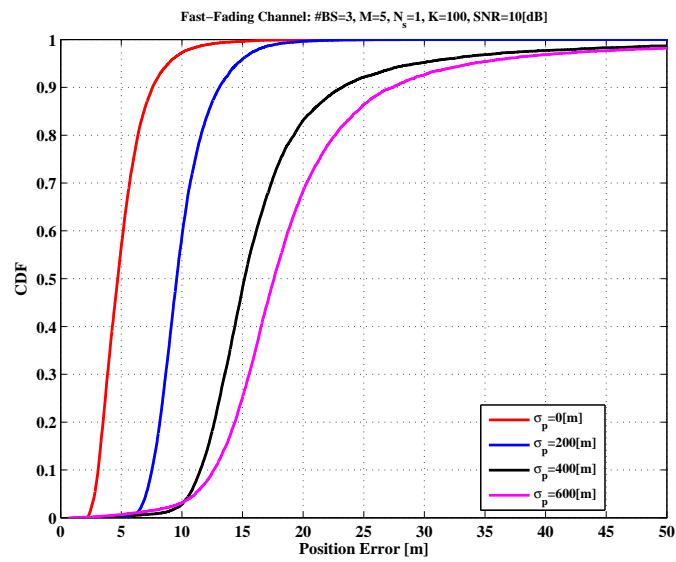


Figure 5.6: CRLB for Fast-Fading Channel $N_s = 1, K = 100, L = 3$ @ SNR = 10[dB]

5.5 Computational Complexity Analysis

In this section, we analyze the computational load imposed by the algorithms outlined in this chapter. These algorithms require maximization or minimization of cost functions via a grid-search process. A typical implementation of this search process loops over the parameter set of interest. The length of this search depends on the granularity of the grid and various grid-search techniques may be employed to facilitate this activity (e.g., Newton-type search [47], steepest-descent, etc.).

The following analysis is focused on the number of required flops at each grid point. The devised algorithms are based on the structure of the covariance matrix and therefore their complexity is derived from its size. There are 4 variables that affect the complexity:

- L - the number of receiving BS. Since the covariance matrix is block-diagonal, the cost function may be derived as a sum of L distinct cost functions.
- K - the number of snapshots. This variable affects only the estimation of the sample-covariance matrix. The sample covariance is free of the parameters of interest and therefore may be estimated outside the grid-search loop. Thus, K has a negligible effect on the overall complexity.
- M - the number of antennas per BS. This variable affects the size of the covariance matrix.
- N_s - the time-bandwidth product of the emitter signal. This variable affects the size of the covariance matrix.

The cost functions involve computations such as matrix determinant (MLE and AMLE), matrix trace (MLE/AMLE/WLS/LSE), and projection (time-delay MLE). These computations may be efficiently implemented using the well-known, Singular Value Decomposition (SVD) algorithm. The number of FLOPS required for calculating the (complex) matrix SVD of a matrix $\mathbf{A} \in \mathbb{C}^{m \times n}$, $\mathbf{A} = \mathbf{U}\mathbf{\Sigma}\mathbf{V}^H$ using the R-SVD algorithm, when only $\mathbf{\Sigma}$ containing the eigenvalues of \mathbf{A} is required, equals $2mn^2 + 2n^3$ (see e.g., [113, p. 254]).

The computation of the projection matrix, which is the main calculation in (5.44), may be accomplished using the SVD as follows: $\mathbf{A}(\mathbf{A}^H\mathbf{A})^{-1}\mathbf{A}^H = \mathbf{U}\mathbf{U}^H$. For this case where the sub-matrix, \mathbf{U} , is required, the number of flops consumed by the R-SVD algorithm is $4m^2n + 13n^3$. Other operations such as $n \times n$ matrix multiplication or inversion are estimated as $O(n^3)$.

Table 5.1 provides a breakdown for the number of FLOPS consumed on every grid point, by each of the algorithms discussed in section 5.3, (assuming non-parallel implementation).

Under the quasi-static channel assumption, the size of the ℓ th array covariance matrix is $MN_s \times MN_s$. The complexity of the respective angle-only algorithms may be obtained by setting $N_s = 1$. As shown, the complexity of the angle-only algorithms is reduced by a factor of $O(N_s^3)$ compared to the complexity of the algorithms utilizing both time-delay and angle information. However, as demonstrated by the numerical examples, the lower complexity comes at the price of lower estimation accuracy performance.

Similar to other single-step emitter geolocation algorithms, the implementation of the devised algorithms assumes the position estimation is done at a mobile location center (MLC), which is a centric facility within the network (or the “cloud”). The MLC collects the raw samples of signals received by the various base-stations, jointly processes them and estimates the emitter position according to one of the proposed algorithms. The base-stations may transfer the samples to the MLC either over a wired “backbone” connection or via a wireless “sideband” channel. Clearly, an algorithm utilizing the embedded time-delay information for the emitter localization entails an underlying assumption that all the base stations are time-synchronized. However, as demonstrated in sec. 5.3.2, provided that the signal is constant-modulus, (an assumption which holds for synchronization sequences in many communication systems), and the localization is done solely using the embedded angular information, then tight time-synchronization between the base-stations is not required. This makes the angular-based algorithms more robust to timing errors.

Table 5.1: Computational Complexity of DPD under Local Scattering

Algorithm	Main Computations	# FLOPS
MLE	<ol style="list-style-type: none"> 1. \mathbf{R}_ℓ^{-1} 2. $\tilde{\mathbf{X}} = \mathbf{R}_\ell^{-1} \hat{\mathbf{R}}_\ell$ 3. $\text{Tr}\{\tilde{\mathbf{X}}\}$ 4. \mathbf{R} 	<ol style="list-style-type: none"> 1. $O(L[N_s M]^3)$ 2. $O(L[N_s M]^3)$ 3. $O(4L[N_s M]^3)$ 4. $O(4L[N_s M]^3)$ Total: $O(10L[N_s M]^3)$
AMLE	<ol style="list-style-type: none"> 1. $\tilde{\mathbf{X}} = \hat{\mathbf{R}}_\ell^{-1} \mathbf{R}_\ell$ 2. $\text{Tr}\{\tilde{\mathbf{X}}\}$ 3. \mathbf{R} 	<ol style="list-style-type: none"> 1. $O(L[N_s M]^3)$ 2. $O(4L[N_s M]^3)$ 3. $O(4L[N_s M]^3)$ Total: $O(9L[N_s M]^3)$
LS (time-delay & angle)	$\mathbf{X} \triangleq (\mathbf{R}_\ell - \hat{\mathbf{R}}_\ell)$ <ol style="list-style-type: none"> 1. $\tilde{\mathbf{X}} = \mathbf{X}\mathbf{X}^H$ 2. $\text{Tr}\{\tilde{\mathbf{X}}\}$ 	<ol style="list-style-type: none"> 1. $O(L[N_s M]^3)$ 2. $O(4L[N_s M]^3)$ Total: $O(5L[N_s M]^3)$
WLS (time-delay & angle)	<ol style="list-style-type: none"> 1. $\mathbf{X} = \mathbf{W}_\ell(\mathbf{R}_\ell - \hat{\mathbf{R}}_\ell)$ 2. $\tilde{\mathbf{X}} = \mathbf{X}\mathbf{X}^H$ 3. $\text{Tr}\{\tilde{\mathbf{X}}\}$ 	<ol style="list-style-type: none"> 1. $O(L[N_s M]^3)$ 2. $O(L[N_s M]^3)$ 3. $O(4L[N_s M]^3)$ Total: $O(6L[N_s M]^3)$
LS (time-delay only)	<ol style="list-style-type: none"> 1. $\hat{\mathbf{\Pi}}_G, \mathbf{G}_\ell[(MN_s) \times M]$ 2. $\tilde{\mathbf{X}} = \hat{\mathbf{\Pi}}_G \hat{\mathbf{R}}$ 3. $\text{Tr}\{\tilde{\mathbf{X}}\}$ 	<ol style="list-style-type: none"> 1. $O(4L[N_s M^2]^3)$ 2. $O(L[N_s M]^3)$ 3. $O(L[N_s M]^3)$ Total: $O(4L[N_s M^2]^3)$

5.6 Summary

In this chapter, we presented and analyzed optimal and sub-optimal algorithms for direct (single-step) geolocation of a stationary radio emitter subjected to local scattering in its vicinity. The local scattering was analytically modeled using the Gaussian Angle of Arrival assumption, which forms a time-varying Rayleigh fading channel.

The proposed algorithms estimate the emitter position directly from the received signal samples, by extracting the position information from both fading channel statistics, as well as temporal channel correlations that exist when the Rayleigh fading channel is quasi-static. It is shown that the suboptimal LSE achieves the same error performance as the 1-step MLE and attains the CRLB. In addition, it outperforms the 2-step estimators formerly suggested for geolocating the distributed source. The proposed method enables the joint estimate of the emitter position as well as the observed angular spread at the receiving sites. This makes it also a useful technique for channel modeling and characterization.

A numerical analysis of the CRLB has revealed that under quasi-static

5.6. Summary

channels, for which the temporal channel coherence may be exploited, the position estimation error is nearly independent of the scattering environment parameters. In contrast, under fast-fading channels, the lack of temporal channel coherence eliminates the time-delay information and therefore dependence of the estimation error in the scattering environment parameters is prominent.

Chapter 6

Conclusions

In this dissertation, we analyzed 3 novel emitter and target geolocation problems, and proposed direct geolocation algorithms, which enable localization of emitters or passive targets directly from the raw samples of the received signals. Direct position determination is an optimal geolocation method, which consistently exhibits superior performance compared to the classical, two-step geolocation approach. Its strength stems from the fact that the two-step method estimates the location-dependent parameters while overlooking the constraint that all these different parameters correspond to the same position. This performance superiority is manifested mainly under low-SNR regime.

This advantage of the DPD approach comes at the expense of higher computational complexity and higher bandwidth that is required for transferring the raw signal samples from all the receive sites to the central processing facility. However, we have shown that the bandwidth consumption may be significantly reduced when the SPG method is employed. In such case, the amount of data to be transferred is reduced by a factor of L compared to a classical geolocation system utilizing L receive sites.

In chapter 3, we explored the effect of transmit signal diversity on the position estimation accuracy. It was shown that this diversity improves the accuracy by effectively converting the Rayleigh channel fading in simple AWGN channel. We have also demonstrated the supremacy of the DPD approach over the two-step approach for the application of passive radar.

In chapter 4, we presented maximum likelihood algorithms for direct positioning of a stationary radio transmitter in a single-platform geolocation (SPG) system. Contrary to classic HF single-site location (HF-SSL) systems, which rely on ionospheric refractions in order to determine the position of the HF transmitter, the proposed SPG system uses a single receiver equipped with an antenna array and multiple, passive signal transponders in order to locate an RF emitter within a pre-defined search area. In addition, we provided theoretical performance analysis for SPG using a compact (concentrated) CRLB. The bound also revealed some fundamental limitations resulting from the deployment of signal transponders.

In chapter 5, we formulated the mathematical model for geolocation in the presence of local scattering. Using this model, the direct geolocation approach has shown prominent advantage over two-step methods. In this case, the centralized direct method enabled the extraction of position-dependent information embedded in the angular spread measure to localize the emitter - information that could not be utilized by the alternative two-step methods.

6.1 Directions for Future Work

Some works that have been realized in the framework of the dissertation have not been described in this document. For example, the application of direct positioning to state-of-the-art OFDM communication systems. This idea was initially explored in [21], [23]. To date, many OFDM systems use multiple antennas on the transmit and receive sides, which exploit signal diversity to achieve higher data throughput. It would be of great interest to explore the application of direct geolocation methods to MIMO-OFDM communication systems. Further on, the work presented in chapter 5 could be extended to handle Ricean channels, including both LoS and NLoS paths, which often characterize indoor scenarios. In this framework, the emitting sources could also be modeled as OFDM or MIMO-OFDM.

The MIMO radar model could be extended for high-speed moving targets, exploiting the embedded position-dependent information expressed by the Doppler frequency shifts. In addition, the reception model could be ex-

tended to account for ground clutter and multipath effects, resulting in non-diagonal noise matrix. In this context, the identifiability of targets in clutter may be of interest. Additionally, the concept of SPG could be applied to MIMO radar as well. Furthermore, the extension of multipath effects may be considered also for the model of SPG systems, including effects of local scattering in the vicinity of the emitting source and/or the transponders. In the aspect of performance analysis, the work presented here could be extended for Bayesian performance analysis (e.g., Bayesian CRLB, Ziv-Zakai or Weiss-Weinstein bounds). Some preliminary work in the context of underwater acoustic signal propagation models and matched-field processing has been published by Xu *et al.* [108]. This work could be extended to common RF signals DPD, and more specifically, to the models discussed in this dissertation.

APPENDICES

Appendix A

Appendix Related to Chapter 3

A.1 Derivation of Cramér Rao Lower Bound

In this appendix, we derive the Cramér Rao lower bound (CRLB) for the MIMO Radar signal model defined in chapter 3. The CRLB provides a lower bound on the covariance matrix of any unbiased estimator. In other words, the difference between the covariance and the CRLB is a positive semi-definite matrix. The CRLB is expected to be a good predictor of estimation performance for a large number of data samples. In fact, under mild regularity conditions, the maximum likelihood estimator achieves the CRLB asymptotically, as the number of data samples tends to infinity. We can obtain a lower bound the performance by evaluating the CRLB for *known* signals that is conditioned on the vector of channel attenuation $\boldsymbol{\alpha} \triangleq [\boldsymbol{\alpha}_1^H, \dots, \boldsymbol{\alpha}_L^H]^H$. Once we derive the conditioned CRLB, we can obtain a lower bound by calculating the average CRLB. The average CRLB is the average of the “snapshot-CRLB” over the received signal energy statistics (or equivalently, over the fading channel statistics) [83].

A.1.1 Known Signals

Recall that the frequency-domain representation of the received signal model is given by,

$$\bar{\mathbf{r}}_{\ell,k} = \tilde{\mathbf{a}}_{\ell,k} \boldsymbol{\alpha}_\ell^T \bar{\mathbf{s}}_k + \bar{\mathbf{n}}_{\ell,k} \quad (\text{A.1})$$

For complex Gaussian data vectors, $\bar{\mathbf{r}} \sim \mathcal{CN}(\mathbf{m}, \mathbf{R})$, the elements of the Fisher information matrix (FIM) are given by [119],

$$\mathbf{J}_{ij} = \text{tr} \left\{ \mathbf{R}^{-1} \frac{\partial \mathbf{R}}{\partial \psi_i} \mathbf{R}^{-1} \frac{\partial \mathbf{R}}{\partial \psi_j} \right\} + 2\Re \left\{ \frac{\partial \mathbf{m}^H}{\partial \psi_i} \mathbf{R}^{-1} \frac{\partial \mathbf{m}}{\partial \psi_j} \right\} \quad (\text{A.2})$$

where ψ_i is the i th element of the unknown parameter vector. If we regard the signal samples as non-random variables, the data covariance is equal to the noise covariance, which is independent of the unknown parameters under the assumption that the noise covariance is known. For simplicity, we assume that the noise power σ_n^2 is given and the signal waveforms are known and, therefore the vector of unknown parameters is $\boldsymbol{\psi} = [x_t, y_t, \bar{\boldsymbol{\alpha}}_1, \dots, \bar{\boldsymbol{\alpha}}_L, \tilde{\boldsymbol{\alpha}}_1, \dots, \tilde{\boldsymbol{\alpha}}_L]^T$, where $\bar{\boldsymbol{\alpha}}_\ell$ and $\tilde{\boldsymbol{\alpha}}_\ell$ correspond to the real and imaginary parts of $\boldsymbol{\alpha}_\ell$, respectively. Under these assumptions the (i, j) element of the conditioned FIM is given by,

$$[\bar{\mathbf{J}}]_{ij} = 2\Re \left\{ \frac{\partial \mathbf{m}^H}{\partial \psi_i} \mathbf{R}^{-1} \frac{\partial \mathbf{m}}{\partial \psi_j} \right\} \quad (\text{A.3})$$

while the complete conditioned FIM is defined as,

$$\bar{\mathbf{J}} \triangleq \begin{bmatrix} \bar{\mathbf{J}}_{\bar{\boldsymbol{\alpha}}\bar{\boldsymbol{\alpha}}} & \bar{\mathbf{J}}_{\bar{\boldsymbol{\alpha}}\tilde{\boldsymbol{\alpha}}} & \bar{\mathbf{J}}_{\bar{\boldsymbol{\alpha}}\mathbf{p}} \\ \bar{\mathbf{J}}_{\tilde{\boldsymbol{\alpha}}\bar{\boldsymbol{\alpha}}}^T & \bar{\mathbf{J}}_{\tilde{\boldsymbol{\alpha}}\tilde{\boldsymbol{\alpha}}} & \bar{\mathbf{J}}_{\tilde{\boldsymbol{\alpha}}\mathbf{p}} \\ \bar{\mathbf{J}}_{\mathbf{p}\bar{\boldsymbol{\alpha}}}^T & \bar{\mathbf{J}}_{\mathbf{p}\tilde{\boldsymbol{\alpha}}}^T & \bar{\mathbf{J}}_{\mathbf{p}\mathbf{p}} \end{bmatrix} \quad (\text{A.4})$$

From (A.1) the mean of the data is given by

$$\mathbf{m}_{\ell,k} \triangleq \tilde{\mathbf{a}}_{\ell,k} \boldsymbol{\alpha}_\ell^T \bar{\mathbf{s}}_k = \tilde{\mathbf{a}}_{\ell,k} \bar{\mathbf{s}}_k^T \boldsymbol{\alpha}_\ell \quad (\text{A.5})$$

with,

$$\mathbf{m}_k \triangleq [\mathbf{m}_{1,k}^H, \mathbf{m}_{2,k}^H, \dots, \mathbf{m}_{L,k}^H]^H \quad (\text{A.6})$$

$$\mathbf{m} \triangleq [\mathbf{m}_0^H, \mathbf{m}_1^H, \dots, \mathbf{m}_{K-1}^H]^H \quad (\text{A.7})$$

The Block $\bar{\mathbf{J}}_{\text{pp}}$

Differentiating with respect to the unknown target coordinates we have,

$$\frac{\partial \mathbf{m}_k}{\partial x} = \left[\frac{\partial \mathbf{m}_{1,k}^H}{\partial x}, \dots, \frac{\partial \mathbf{m}_{L,k}^H}{\partial x} \right]^H \quad (\text{A.8})$$

$$\frac{\partial \mathbf{m}_k}{\partial y} = \left[\frac{\partial \mathbf{m}_{1,k}^H}{\partial y}, \dots, \frac{\partial \mathbf{m}_{L,k}^H}{\partial y} \right]^H \quad (\text{A.9})$$

$$\frac{\partial \mathbf{m}_{\ell,k}}{\partial x} = \frac{\partial \tilde{\mathbf{a}}_{\ell,k}}{\partial x} \boldsymbol{\alpha}_{\ell}^T \bar{\mathbf{s}}_k + \tilde{\mathbf{a}}_{\ell,k} \boldsymbol{\alpha}_{\ell}^T \frac{\partial \bar{\mathbf{s}}_k}{\partial x} \quad (\text{A.10})$$

$$\frac{\partial \mathbf{m}_{\ell,k}}{\partial y} = \frac{\partial \tilde{\mathbf{a}}_{\ell,k}}{\partial y} \boldsymbol{\alpha}_{\ell}^T \bar{\mathbf{s}}_k + \tilde{\mathbf{a}}_{\ell,k} \boldsymbol{\alpha}_{\ell}^T \frac{\partial \bar{\mathbf{s}}_k}{\partial y} \quad (\text{A.11})$$

In order to obtain explicit expressions for the partial derivatives with respect to the position coordinates, we denote the location of the m th transmitter by, $\mathbf{q}_m = (\bar{x}_m, \bar{y}_m)$. Further, recall that $\tau_{\ell,m} = \frac{1}{c}(\tilde{d}_{\ell} + d_m)$ where c is the speed of light and,

$$\begin{aligned} \tilde{d}_{\ell} &= \|\mathbf{p} - \tilde{\mathbf{q}}_{\ell}\| = \sqrt{(x - \tilde{x}_{\ell})^2 + (y - \tilde{y}_{\ell})^2} \\ d_m &= \|\mathbf{p} - \mathbf{q}_m\| = \sqrt{(x - \bar{x}_m)^2 + (y - \bar{y}_m)^2} \end{aligned} \quad (\text{A.12})$$

Thus,

$$\begin{aligned} \frac{\partial \tilde{\tau}_{\ell}}{\partial x} &= \frac{1}{c} \cdot \frac{x - \tilde{x}_{\ell}}{\tilde{d}_{\ell}} = \frac{1}{c} \cdot \cos \tilde{\theta}_{\ell} \\ \frac{\partial \tilde{\tau}_{\ell}}{\partial y} &= \frac{1}{c} \cdot \sin \tilde{\theta}_{\ell} \\ \frac{\partial \tau_m}{\partial x} &= \frac{1}{c} \cdot \cos \theta_m \\ \frac{\partial \tau_m}{\partial y} &= \frac{1}{c} \cdot \sin \theta_m \end{aligned} \quad (\text{A.13})$$

Now we obtain,

$$\frac{\partial \tilde{\mathbf{a}}_{\ell,k}}{\partial x} = -\imath \left[\frac{2\pi}{\lambda} + \frac{\omega_k}{c} \right] \cos \tilde{\theta}_\ell \tilde{\mathbf{a}}_{\ell,k} \quad (\text{A.14})$$

Recall that $\lambda = c/f_c$ and $\omega_k = 2\pi f_s k/K$ where f_c and f_s are the RF carrier and the baseband sampling frequencies, respectively. Typically, $f_c \gg f_s$ and therefore we may write,

$$\frac{\partial \tilde{\mathbf{a}}_{\ell,k}}{\partial x} = -\imath \frac{2\pi}{\lambda} \cos \tilde{\theta}_\ell \tilde{\mathbf{a}}_{\ell,k} \quad (\text{A.15})$$

$$\frac{\partial \tilde{\mathbf{a}}_{\ell,k}}{\partial y} = -\imath \frac{2\pi}{\lambda} \sin \tilde{\theta}_\ell \tilde{\mathbf{a}}_{\ell,k} \quad (\text{A.16})$$

We notice as well that,

$$\frac{\partial \bar{\mathbf{s}}_k}{\partial x} = -\imath \frac{\omega_k}{c} \Xi_c \bar{\mathbf{s}}_k \quad (\text{A.17})$$

$$\frac{\partial \bar{\mathbf{s}}_k}{\partial y} = -\imath \frac{\omega_k}{c} \Xi_s \bar{\mathbf{s}}_k \quad (\text{A.18})$$

where,

$$\Xi_c \triangleq \text{diag} \{ \cos \theta_1, \dots, \cos \theta_{M_t} \} \quad (\text{A.19})$$

$$\Xi_s \triangleq \text{diag} \{ \sin \theta_1, \dots, \sin \theta_{M_t} \} \quad (\text{A.20})$$

A more compact notation can be obtained by using the following definitions. Let,

$$\mathbf{S}_k \triangleq \mathbf{I}_L \otimes \bar{\mathbf{s}}_k \quad (\text{A.21})$$

$$\dot{\mathbf{S}}_{kx} \triangleq \mathbf{I}_L \otimes \frac{\partial \bar{\mathbf{s}}_k}{\partial x}, \quad \dot{\mathbf{S}}_{ky} \triangleq \mathbf{I}_L \otimes \frac{\partial \bar{\mathbf{s}}_k}{\partial y} \quad (\text{A.22})$$

$$\boldsymbol{\alpha} \triangleq [\boldsymbol{\alpha}_1^H, \dots, \boldsymbol{\alpha}_L^H]^H \quad (\text{A.23})$$

Further define,

$$\dot{\mathbf{A}}_{kx} \triangleq \text{diag} \left\{ \frac{\partial \tilde{\mathbf{a}}_{1,k}}{\partial x}, \dots, \frac{\partial \tilde{\mathbf{a}}_{L,k}}{\partial x} \right\} \quad (\text{A.24})$$

where $\dot{\mathbf{A}}_{ky}$ is similarly defined and $\text{diag}\{\mathbf{X}_1, \dots, \mathbf{X}_R\}$, is defined as $HR \times TR$ block-diagonal matrix where \mathbf{X}_n is a $H \times T$ matrix. Now the partial derivatives with respect to the coordinates can be compactly written as,

$$\dot{\mathbf{d}}_{kx} \triangleq \dot{\mathbf{A}}_{kx} \mathbf{S}_k^T \boldsymbol{\alpha} + \mathbf{A}_k \dot{\mathbf{S}}_{kx}^T \boldsymbol{\alpha} \quad (\text{A.25})$$

$$\dot{\mathbf{d}}_{ky} \triangleq \dot{\mathbf{A}}_{ky} \mathbf{S}_k^T \boldsymbol{\alpha} + \mathbf{A}_k \dot{\mathbf{S}}_{ky}^T \boldsymbol{\alpha} \quad (\text{A.26})$$

$$\dot{\mathbf{d}}_x \triangleq [\dot{\mathbf{d}}_{0x}^H, \dots, \dot{\mathbf{d}}_{K-1x}^H]^H \quad (\text{A.27})$$

$$\dot{\mathbf{d}}_y \triangleq [\dot{\mathbf{d}}_{0y}^H, \dots, \dot{\mathbf{d}}_{K-1y}^H]^H \quad (\text{A.28})$$

where \mathbf{A}_k is defined in (3.32). Using (A.25)-(A.28) the $\bar{\mathbf{J}}_{\mathbf{pp}}$ elements can be obtained as,

$$\bar{J}_{xx} = \frac{2}{\sigma_n^2} \Re \left\{ \dot{\mathbf{d}}_x^H \dot{\mathbf{d}}_x \right\} \quad (\text{A.29})$$

$$\bar{J}_{yy} = \frac{2}{\sigma_n^2} \Re \left\{ \dot{\mathbf{d}}_y^H \dot{\mathbf{d}}_y \right\} \quad (\text{A.30})$$

$$\bar{J}_{xy} = \frac{2}{\sigma_n^2} \Re \left\{ \dot{\mathbf{d}}_x^H \dot{\mathbf{d}}_y \right\} \quad (\text{A.31})$$

Arranging in matrix form,

$$\bar{\mathbf{J}}_{\mathbf{pp}} \triangleq \begin{bmatrix} \bar{J}_{xx} & \bar{J}_{xy} \\ \bar{J}_{xy} & \bar{J}_{yy} \end{bmatrix} \quad (\text{A.32})$$

The Blocks $\bar{\mathbf{J}}_{\tilde{\alpha}\mathbf{p}}$ and $\bar{\mathbf{J}}_{\tilde{\alpha}\mathbf{p}}$

The derivatives with respect to the gain and phase components of the channel attenuation coefficients vector are given by,

$$\frac{\partial \mathbf{m}_k}{\partial \tilde{\alpha}_{\ell,m}} = \mathbf{e}_\ell \otimes \tilde{\mathbf{a}}_{\ell,k} \tilde{\mathbf{s}}_k^T \mathbf{e}_m \quad (\text{A.33})$$

$$\frac{\partial \mathbf{m}_k}{\partial \tilde{\alpha}_{\ell,m}} = \iota \mathbf{e}_\ell \otimes \tilde{\mathbf{a}}_{\ell,k} \tilde{\mathbf{s}}_k^T \mathbf{e}_m \quad (\text{A.34})$$

where \mathbf{e}_d denotes the d th column vector of an $D \times D$ identity matrix. In a matrix form this can be compactly written as,

$$\frac{\partial \mathbf{m}_k}{\partial \bar{\alpha}} = \bar{\mathbf{s}}_k^T \otimes \mathbf{A}_k \quad (\text{A.35})$$

$$\frac{\partial \mathbf{m}_k}{\partial \tilde{\alpha}} = i \bar{\mathbf{s}}_k^T \otimes \mathbf{A}_k \quad (\text{A.36})$$

Define,

$$\mathbf{W}_k \triangleq \bar{\mathbf{s}}_k^T \otimes \mathbf{A}_k \quad (\text{A.37})$$

$$\mathbf{W} \triangleq [\mathbf{W}_0^H, \dots, \mathbf{W}_{K-1}^H]^H \quad (\text{A.38})$$

The elements constructing the $\bar{\mathbf{J}}_{\bar{\alpha}\mathbf{p}}$ and $\bar{\mathbf{J}}_{\tilde{\alpha}\mathbf{p}}$ FIM blocks are given by,

$$\bar{\mathbf{J}}_{\bar{\alpha}x} = \frac{2}{\sigma_n^2} \Re \left\{ \mathbf{W}^H \dot{\mathbf{d}}_x \right\} \quad (\text{A.39})$$

$$\bar{\mathbf{J}}_{\bar{\alpha}y} = \frac{2}{\sigma_n^2} \Re \left\{ \mathbf{W}^H \dot{\mathbf{d}}_y \right\} \quad (\text{A.40})$$

$$\bar{\mathbf{J}}_{\tilde{\alpha}x} = -\frac{2}{\sigma_n^2} \Im \left\{ \mathbf{W}^H \dot{\mathbf{d}}_x \right\} \quad (\text{A.41})$$

$$\bar{\mathbf{J}}_{\tilde{\alpha}y} = -\frac{2}{\sigma_n^2} \Im \left\{ \mathbf{W}^H \dot{\mathbf{d}}_y \right\} \quad (\text{A.42})$$

In matrix form, the block $\bar{\mathbf{J}}_{\bar{\alpha}\mathbf{p}}$ is arranged as,

$$\begin{aligned} \bar{\mathbf{J}}_{\bar{\alpha}\mathbf{p}} &\triangleq \begin{bmatrix} \bar{\mathbf{J}}_{\bar{\alpha}x} & \bar{\mathbf{J}}_{\bar{\alpha}y} \end{bmatrix} \\ \bar{\mathbf{J}}_{\tilde{\alpha}\mathbf{p}} &\triangleq \begin{bmatrix} \bar{\mathbf{J}}_{\tilde{\alpha}x} & \bar{\mathbf{J}}_{\tilde{\alpha}y} \end{bmatrix} \end{aligned} \quad (\text{A.43})$$

The Blocks $\bar{\mathbf{J}}_{\bar{\alpha}\bar{\alpha}}$, $\bar{\mathbf{J}}_{\tilde{\alpha}\tilde{\alpha}}$ and $\bar{\mathbf{J}}_{\bar{\alpha}\tilde{\alpha}}$

We have,

$$\bar{\mathbf{J}}_{\bar{\alpha}\bar{\alpha}} = \bar{\mathbf{J}}_{\tilde{\alpha}\tilde{\alpha}} = \frac{2}{\sigma_n^2} \Re \left\{ \mathbf{W}^H \mathbf{W} \right\} \quad (\text{A.44})$$

$$\bar{\mathbf{J}}_{\bar{\alpha}\tilde{\alpha}} = -\bar{\mathbf{J}}_{\tilde{\alpha}\bar{\alpha}} = -\frac{2}{\sigma_n^2} \Im \left\{ \mathbf{W}^H \mathbf{W} \right\} \quad (\text{A.45})$$

The CRLB conditioned on $\boldsymbol{\alpha}$ is obtained by inverting the conditioned FIM defined in (A.4). The average CRLB can now be found by using,

$$\overline{\text{CRLB}} = \int_{-\infty}^{\infty} \text{CRLB}|_{\boldsymbol{\alpha}} p_{\boldsymbol{\alpha}}(\boldsymbol{\alpha}) d\boldsymbol{\alpha} \quad (\text{A.46})$$

This concludes the derivation of the CRLB for known signals.

A.1.2 Random Gaussian Signals

We now derive the CRLB under the assumption that the transmitted signals are samples of a zero-mean, Complex Gaussian random process. In this case, $\mathbf{r} \sim \mathcal{CN}(0, \mathbf{R})$ and therefore the elements of the FIM are given by

$$\mathbf{J}_{ij} = \text{tr} \left\{ \mathbf{R}^{-1} \frac{\partial \mathbf{R}}{\partial \psi_i} \mathbf{R}^{-1} \frac{\partial \mathbf{R}}{\partial \psi_j} \right\} \quad (\text{A.47})$$

The covariance matrix of the data snapshot is calculated for a given set of fading coefficients vectors. The average CRLB is obtained numerically by averaging over a large number of fading vectors realizations. Under the above assumptions, the vector of unknown parameters is simply reduced to the target coordinates $\boldsymbol{\psi} = [x_t, y_t]^T$.

Recall that,

$$\mathbf{R}_{\ell,i,k,j} |_{\alpha_\ell, \alpha_i} = \frac{1}{M_t} \boldsymbol{\alpha}_\ell^H \boldsymbol{\alpha}_i \tilde{\mathbf{a}}_{\ell,k} \tilde{\mathbf{a}}_{i,j}^H \delta_{k,j} + \sigma_n^2 \mathbf{I}_{M_r} \delta_{\ell,i} \delta_{k,j} \quad (\text{A.48})$$

Define,

$$\tilde{\mathbf{a}}_k \triangleq [\tilde{\mathbf{a}}_{1k}^H, \dots, \tilde{\mathbf{a}}_{Lk}^H]^H \quad (\text{A.49})$$

$$\bar{\mathbf{A}}_k \triangleq \tilde{\mathbf{a}}_k \tilde{\mathbf{a}}_k^H \quad (\text{A.50})$$

$$\boldsymbol{\Omega} \triangleq [\boldsymbol{\alpha}_1, \dots, \boldsymbol{\alpha}_L] \quad (\text{A.51})$$

$$\boldsymbol{\Pi} \triangleq \boldsymbol{\Omega}^H \boldsymbol{\Omega} \quad (\text{A.52})$$

$$\mathbf{H} \triangleq \mathbf{1}_{M_r \times M_r} \quad (\text{A.53})$$

$$\tilde{\mathbf{B}} \triangleq \boldsymbol{\Pi} \otimes \mathbf{H} \quad (\text{A.54})$$

where $\mathbf{1}_{N \times M}$ denotes an $N \times M$ matrix of ones.

In matrix form, the covariance matrix \mathbf{R}_k can now be written as,

$$\mathbf{R}_k = \frac{1}{M_t} \tilde{\mathbf{B}} \odot \bar{\mathbf{A}}_k + \sigma_n^2 \mathbf{I}_{M_r L} \quad (\text{A.55})$$

The matrix \mathbf{R} is block diagonal with K blocks and, therefore,

$$\bar{\mathbf{J}}_{ij} = \sum_{k=0}^{K-1} \text{tr} \left\{ \mathbf{R}_k^{-1} \frac{\partial \mathbf{R}_k}{\partial \psi_i} \mathbf{R}_k^{-1} \frac{\partial \mathbf{R}_k}{\partial \psi_j} \right\} \quad (\text{A.56})$$

The derivatives with respect to the target coordinates are given by,

$$\frac{\partial \mathbf{R}_k}{\partial x} = \frac{1}{M_t} \tilde{\mathbf{B}} \odot (\dot{\tilde{\mathbf{a}}}_{kx} \tilde{\mathbf{a}}_k^H + \tilde{\mathbf{a}}_k \dot{\tilde{\mathbf{a}}}_{kx}^H) \quad (\text{A.57})$$

$$\frac{\partial \mathbf{R}_k}{\partial y} = \frac{1}{M_t} \tilde{\mathbf{B}} \odot (\dot{\tilde{\mathbf{a}}}_{ky} \tilde{\mathbf{a}}_k^H + \tilde{\mathbf{a}}_k \dot{\tilde{\mathbf{a}}}_{ky}^H) \quad (\text{A.58})$$

For compact notation define,

$$\dot{\mathbf{D}}_{kx} \triangleq \tilde{\mathbf{B}} \odot (\dot{\tilde{\mathbf{a}}}_{kx} \tilde{\mathbf{a}}_k^H), \quad \dot{\mathbf{D}}_{ky} \triangleq \tilde{\mathbf{B}} \odot (\dot{\tilde{\mathbf{a}}}_{ky} \tilde{\mathbf{a}}_k^H) \quad (\text{A.59})$$

Recall that $\text{Tr}\{\mathbf{X}^H\} = \{\text{Tr}(\mathbf{X})\}^* \Rightarrow \text{Tr}\{\mathbf{X} + \mathbf{X}^H\} = 2\Re\{\text{Tr}(\mathbf{X})\}$. Thus, by plugging (A.57) into (A.56), and noticing that $\tilde{\mathbf{B}}^H = \tilde{\mathbf{B}}$, we may write,

$$\begin{aligned} \bar{J}_{xx} &= \\ & \frac{2}{M_t^2} \Re \sum_{k=0}^{K-1} \text{Tr} \left\{ (\dot{\mathbf{D}}_{kx} + \dot{\mathbf{D}}_{kx}^H) \mathbf{R}_k^{-1} \dot{\mathbf{D}}_{kx} \mathbf{R}_k^{-1} \right\} \end{aligned} \quad (\text{A.60})$$

Similarly, we have

$$\begin{aligned} \bar{J}_{yy} &= \\ & \frac{2}{M_t^2} \Re \sum_{k=0}^{K-1} \text{Tr} \left\{ (\dot{\mathbf{D}}_{ky} + \dot{\mathbf{D}}_{ky}^H) \mathbf{R}_k^{-1} \dot{\mathbf{D}}_{ky} \mathbf{R}_k^{-1} \right\} \end{aligned} \quad (\text{A.61})$$

$$\begin{aligned} \bar{J}_{xy} &= \\ & \frac{2}{M_t^2} \Re \sum_{k=0}^{K-1} \text{Tr} \left\{ (\dot{\mathbf{D}}_{kx} + \dot{\mathbf{D}}_{kx}^H) \mathbf{R}_k^{-1} \dot{\mathbf{D}}_{ky} \mathbf{R}_k^{-1} \right\} \end{aligned} \quad (\text{A.62})$$

The average CRLB is obtained by inverting the FIM defined in (C.35) and evaluating (B.33). This concludes the CRLB derivation for the MIMO Radar signal models.

Appendix B

Appendix Related to Chapter 4

B.1 Derivation of Cramér Rao Lower Bound for Wideband SPG

In this appendix, we derive the (concentrated) CRLB for the wideband signal case of the SPG system model. While the problem involves many nuisance parameters, we are interested only in the bound on the position estimation accuracy. In order to avoid a tedious derivation and inversion of the complete FIM that includes all the parameters in the problem, we provide a compact derivation of the so-called “concentrated” CRLB. This bound is based on the “concentrated” log-likelihood function, in which the nuisance parameters are replaced with their maximum likelihood estimates. This “concentrated” log-likelihood function is differentiated twice and averaged over many independent observations. The average has been shown to approach the inverse CRLB of the parameters of interest in the large sample limit [37]. For simplicity, the bound is derived under the assumption of planar problem geometry (i.e., $z = 0$).

Recall from (4.14) that the received signal model is given by,

$$\bar{\mathbf{r}} = \sum_{k=1}^K \mathbf{D}_k \boldsymbol{\alpha}_k + \bar{\mathbf{n}}_k \quad (\text{B.1})$$

Define,

$$\begin{aligned}
\tilde{\mathbf{r}} &\triangleq [\tilde{\mathbf{r}}_1^T, \dots, \tilde{\mathbf{r}}_K^T]^T \\
\tilde{\mathbf{D}} &\triangleq \begin{bmatrix} \mathbf{D}_1 & 0 & \cdots & 0 \\ 0 & \mathbf{D}_2 & \cdots & 0 \\ \vdots & \vdots & \ddots & \vdots \\ 0 & \cdots & 0 & \mathbf{D}_K \end{bmatrix} \\
\tilde{\boldsymbol{\alpha}} &\triangleq [\boldsymbol{\alpha}_1^T, \dots, \boldsymbol{\alpha}_K^T]^T \\
\tilde{\mathbf{n}} &\triangleq [\tilde{\mathbf{n}}_1^T, \dots, \tilde{\mathbf{n}}_K^T]^T
\end{aligned} \tag{B.2}$$

Using these definitions we obtain the vectorized signal model as,

$$\tilde{\mathbf{r}} = \tilde{\mathbf{D}}\tilde{\boldsymbol{\alpha}} + \tilde{\mathbf{n}} \tag{B.3}$$

Now, the probability density function of a deterministic signal with length of $K \cdot N \cdot M$ samples, can be stated as (see e.g., [117]),

$$p(\tilde{\mathbf{r}}|\mathbf{p}, t_0, \tilde{\boldsymbol{\alpha}}, \sigma^2) = \frac{1}{|\pi\sigma^2\mathbf{I}|} \exp \left\{ -\sigma^{-2} \|\tilde{\mathbf{r}} - \tilde{\mathbf{D}}\tilde{\boldsymbol{\alpha}}\|^2 \right\} \tag{B.4}$$

Hence the negative log-likelihood function may be recast as,

$$\begin{aligned}
&-\log[p(\tilde{\mathbf{r}}|\mathbf{p}, t_0, \tilde{\boldsymbol{\alpha}}, \sigma^2)] \\
&= MNK \log(\pi\sigma^2) + \frac{1}{\sigma^2} \|\tilde{\mathbf{r}} - \tilde{\mathbf{D}}\tilde{\boldsymbol{\alpha}}\|^2
\end{aligned} \tag{B.5}$$

The vector of complex attenuations $\tilde{\boldsymbol{\alpha}}$ is considered a set of nuisance parameters. To reduce the CRLB evaluation complexity we replace $\tilde{\boldsymbol{\alpha}}$ with its maximum likelihood estimate, $\hat{\boldsymbol{\alpha}}$, that is given by:

$$\hat{\boldsymbol{\alpha}} = \left(\tilde{\mathbf{D}}^H \tilde{\mathbf{D}} \right)^{-1} \tilde{\mathbf{D}}^H \tilde{\mathbf{r}} \tag{B.6}$$

After substituting $\hat{\boldsymbol{\alpha}}$ back into (B.5), we obtain the 'concentrated-log-likelihood'

function as,

$$\begin{aligned}
 \mathcal{L} &= MNK \log(\pi\sigma^2) + \frac{1}{\sigma^2} \|\tilde{\mathbf{r}} - \tilde{\mathbf{D}} \left(\tilde{\mathbf{D}}^H \tilde{\mathbf{D}} \right)^{-1} \tilde{\mathbf{D}}^H \tilde{\mathbf{r}}\|^2 \\
 &= MNK \log(\pi\sigma^2) + \frac{1}{\sigma^2} \text{Tr}\{\tilde{\mathbf{r}}\tilde{\mathbf{r}}^H - \mathbf{\Pi}\tilde{\mathbf{r}}\tilde{\mathbf{r}}^H\} \\
 &= MNK \log(\pi\sigma^2) + \frac{1}{\sigma^2} \text{Tr}\{(\mathbf{I} - \mathbf{\Pi})\tilde{\mathbf{r}}\tilde{\mathbf{r}}^H\} \\
 &= MNK \log(\pi\sigma^2) + \frac{1}{\sigma^2} \text{Tr}\{\mathbf{\Pi}^\perp \tilde{\mathbf{r}}\tilde{\mathbf{r}}^H\}
 \end{aligned} \tag{B.7}$$

where $\mathbf{\Pi} \triangleq \tilde{\mathbf{D}}(\tilde{\mathbf{D}}^H \tilde{\mathbf{D}})^{-1} \tilde{\mathbf{D}}^H$ is the projection matrix to the column space of $\tilde{\mathbf{D}}$, and $\mathbf{\Pi}^\perp \triangleq \mathbf{I} - \mathbf{\Pi}$ denotes the projection matrix onto the subspace orthogonal to the column space of $\tilde{\mathbf{D}}$. To evaluate the concentrated CRLB for the parameters' vector of interest, $\mathbf{p} = [x, y]^T$, the theorem proved in [37] states that,

$$\mathbf{J}_{\mathbf{p}\mathbf{p}} = \lim_{J \rightarrow \infty} \frac{\partial^2 \bar{\mathcal{L}}_J}{\partial \mathbf{p} \partial \mathbf{p}^T} \tag{B.8}$$

where $\bar{\mathcal{L}}_J$ is the average log-likelihood function when there are J independent realizations of the observation vector $\tilde{\mathbf{r}}$, (i.e., there are J independent realizations of the noise vector $\tilde{\mathbf{n}}$).

Let us begin by evaluating the FIM element J_{xx} . Applying (B.8) on (B.7) we obtain,

$$J_{xx} = \lim_{J \rightarrow \infty} \frac{1}{\sigma^2} \cdot \text{Tr} \left\{ \frac{\partial^2 \mathbf{\Pi}^\perp}{\partial x^2} \cdot \frac{1}{J} \sum_{j=1}^J \tilde{\mathbf{r}}_j \tilde{\mathbf{r}}_j^H \right\} \tag{B.9}$$

When we have infinite number of realizations of the observation vector then,

$$\lim_{J \rightarrow \infty} \frac{1}{J} \sum_{j=1}^J \tilde{\mathbf{r}}_j \tilde{\mathbf{r}}_j^H = E\{\tilde{\mathbf{r}}_j \tilde{\mathbf{r}}_j^H\} = \tilde{\mathbf{D}} \tilde{\boldsymbol{\alpha}} \tilde{\boldsymbol{\alpha}}^H \tilde{\mathbf{D}}^H + \sigma^2 \mathbf{I} \tag{B.10}$$

Now the \mathbf{J}_{pp} FIM elements may be derived as follows,

$$J_{xx} = \frac{1}{\sigma^2} \cdot \text{Tr} \left[\frac{\partial^2 \Pi^\perp}{\partial x^2} \left(\tilde{\mathbf{D}} \tilde{\alpha} \tilde{\alpha}^H \tilde{\mathbf{D}}^H + \sigma^2 \mathbf{I} \right) \right] \quad (\text{B.11})$$

$$J_{xy} = \frac{1}{\sigma^2} \cdot \text{Tr} \left[\frac{\partial^2 \Pi^\perp}{\partial x \partial y} \left(\tilde{\mathbf{D}} \tilde{\alpha} \tilde{\alpha}^H \tilde{\mathbf{D}}^H + \sigma^2 \mathbf{I} \right) \right] \quad (\text{B.12})$$

$$J_{yy} = \frac{1}{\sigma^2} \cdot \text{Tr} \left[\frac{\partial^2 \Pi^\perp}{\partial y^2} \left(\tilde{\mathbf{D}} \tilde{\alpha} \tilde{\alpha}^H \tilde{\mathbf{D}}^H + \sigma^2 \mathbf{I} \right) \right] \quad (\text{B.13})$$

$$J_{t_0 t_0} = \frac{1}{\sigma^2} \cdot \text{Tr} \left[\frac{\partial^2 \Pi^\perp}{\partial t_0^2} \left(\tilde{\mathbf{D}} \tilde{\alpha} \tilde{\alpha}^H \tilde{\mathbf{D}}^H + \sigma^2 \mathbf{I} \right) \right] \quad (\text{B.14})$$

$$J_{t_0 x} = \frac{1}{\sigma^2} \cdot \text{Tr} \left[\frac{\partial^2 \Pi^\perp}{\partial t_0 \partial x} \left(\tilde{\mathbf{D}} \tilde{\alpha} \tilde{\alpha}^H \tilde{\mathbf{D}}^H + \sigma^2 \mathbf{I} \right) \right] \quad (\text{B.15})$$

$$J_{t_0 y} = \frac{1}{\sigma^2} \cdot \text{Tr} \left[\frac{\partial^2 \Pi^\perp}{\partial t_0 \partial y} \left(\tilde{\mathbf{D}} \tilde{\alpha} \tilde{\alpha}^H \tilde{\mathbf{D}}^H + \sigma^2 \mathbf{I} \right) \right] \quad (\text{B.16})$$

We shall now obtain compact expressions for the FIM elements. Define $\tilde{\mathbf{B}} = (\tilde{\mathbf{D}}^H \tilde{\mathbf{D}})^{-1}$, $\dot{\mathcal{D}}_x \triangleq \frac{\partial \tilde{\mathbf{D}}}{\partial x}$, $\dot{\mathcal{B}}_x \triangleq \frac{\partial \tilde{\mathbf{B}}}{\partial x}$ then (see [119, eqn. (A.392)]):

$$\begin{aligned} \frac{\partial \Pi^\perp}{\partial x} &= -\frac{\partial \tilde{\mathbf{D}} \tilde{\mathbf{B}} \tilde{\mathbf{D}}^H}{\partial x} \\ &= -\dot{\mathcal{D}}_x \tilde{\mathbf{B}} \tilde{\mathbf{D}}^H - \tilde{\mathbf{D}} \dot{\mathcal{B}}_x \tilde{\mathbf{D}}^H - \tilde{\mathbf{D}} \tilde{\mathbf{B}} \dot{\mathcal{D}}_x^H \\ &= -\dot{\mathcal{D}}_x \tilde{\mathbf{B}} \tilde{\mathbf{D}}^H - \tilde{\mathbf{D}} \tilde{\mathbf{B}} \dot{\mathcal{D}}_x^H \\ &\quad + \tilde{\mathbf{D}} \left\{ \tilde{\mathbf{B}} \left[\dot{\mathcal{D}}_x^H \tilde{\mathbf{D}} + \tilde{\mathbf{D}}^H \dot{\mathcal{D}}_x \right] \tilde{\mathbf{B}} \right\} \tilde{\mathbf{D}}^H \\ &= -\Pi^\perp \dot{\mathcal{D}}_x \tilde{\mathbf{B}} \tilde{\mathbf{D}}^H - \tilde{\mathbf{D}} \tilde{\mathbf{B}} \dot{\mathcal{D}}_x^H \Pi^\perp \end{aligned} \quad (\text{B.17})$$

Further notice that $\tilde{\mathbf{B}} = \tilde{\mathbf{B}}^H$, $(\Pi^\perp)^H = \Pi^\perp$ and let $\mathbf{G}_x \triangleq \Pi^\perp \dot{\mathcal{D}}_x \tilde{\mathbf{B}} \tilde{\mathbf{D}}^H$, then (B.17) may be recast as,

$$\frac{\partial \Pi^\perp}{\partial x} \triangleq \dot{\Pi}_x^\perp = -\mathbf{G}_x - \mathbf{G}_x^H \quad (\text{B.18})$$

Now the second derivative may be obtained as,

$$\frac{\partial^2 \Pi^\perp}{\partial x^2} = -\mathbf{G}_{xx} - \mathbf{G}_{xx}^H \quad (\text{B.19})$$

Denote $\frac{\partial \dot{\mathbf{D}}_x}{\partial x} \triangleq \ddot{\mathbf{D}}_{xx}$ then,

$$\begin{aligned}
 \mathbf{G}_{xx} &\triangleq \frac{\partial \mathbf{G}_x}{\partial x} = \frac{\partial \left(\Pi^\perp \dot{\mathbf{D}}_x \tilde{\mathbf{B}} \tilde{\mathbf{D}}^H \right)}{\partial x} \\
 &= \dot{\Pi}_x^\perp \dot{\mathbf{D}}_x \tilde{\mathbf{B}} \tilde{\mathbf{D}}^H + \Pi^\perp \ddot{\mathbf{D}}_{xx} \tilde{\mathbf{B}} \tilde{\mathbf{D}}^H \\
 &\quad + \Pi^\perp \dot{\mathbf{D}}_x \dot{\mathbf{B}}_x \tilde{\mathbf{D}}^H + \Pi^\perp \dot{\mathbf{D}}_x \tilde{\mathbf{B}} \dot{\mathbf{D}}_x^H \\
 &= -(\mathbf{G}_x + \mathbf{G}_x^H) \dot{\mathbf{D}}_x \tilde{\mathbf{B}} \tilde{\mathbf{D}}^H + \Pi^\perp \ddot{\mathbf{D}}_{xx} \tilde{\mathbf{B}} \tilde{\mathbf{D}}^H \\
 &\quad - \Pi^\perp \dot{\mathbf{D}}_x \left\{ \tilde{\mathbf{B}} \left[\dot{\mathbf{D}}_x^H \tilde{\mathbf{D}} + \tilde{\mathbf{D}}^H \dot{\mathbf{D}}_x \right] \tilde{\mathbf{B}} \right\} \tilde{\mathbf{D}}^H \\
 &\quad + \Pi^\perp \dot{\mathbf{D}}_x \tilde{\mathbf{B}} \dot{\mathbf{D}}_x^H \\
 &= -(\mathbf{G}_x + \mathbf{G}_x^H) \dot{\mathbf{D}}_x \tilde{\mathbf{B}} \tilde{\mathbf{D}}^H + \Pi^\perp \ddot{\mathbf{D}}_{xx} \tilde{\mathbf{B}} \tilde{\mathbf{D}}^H \\
 &\quad - \Pi^\perp \dot{\mathbf{D}}_x \tilde{\mathbf{B}} \dot{\mathbf{D}}_x^H \Pi - \Pi^\perp \dot{\mathbf{D}}_x \tilde{\mathbf{B}} \tilde{\mathbf{D}}^H \dot{\mathbf{D}}_x \tilde{\mathbf{B}} \tilde{\mathbf{D}}^H \\
 &\quad + \Pi^\perp \dot{\mathbf{D}}_x \tilde{\mathbf{B}} \dot{\mathbf{D}}_x^H \\
 &= -(\mathbf{G}_x + \mathbf{G}_x^H) \dot{\mathbf{D}}_x \tilde{\mathbf{B}} \tilde{\mathbf{D}}^H + \Pi^\perp \ddot{\mathbf{D}}_{xx} \tilde{\mathbf{B}} \tilde{\mathbf{D}}^H \\
 &\quad - \mathbf{G}_x \dot{\mathbf{D}}_x \tilde{\mathbf{B}} \tilde{\mathbf{D}}^H + \Pi^\perp \dot{\mathbf{D}}_x \tilde{\mathbf{B}} \dot{\mathbf{D}}_x^H (\mathbf{I} - \Pi) \\
 &= -(2\mathbf{G}_x + \mathbf{G}_x^H) \dot{\mathbf{D}}_x \tilde{\mathbf{B}} \tilde{\mathbf{D}}^H + \Pi^\perp \ddot{\mathbf{D}}_{xx} \tilde{\mathbf{B}} \tilde{\mathbf{D}}^H \\
 &\quad + \Pi^\perp \dot{\mathbf{D}}_x \tilde{\mathbf{B}} \dot{\mathbf{D}}_x^H \Pi^\perp \\
 &= -(2\mathbf{G}_x + \mathbf{G}_x^H) \dot{\mathbf{D}}_x \tilde{\mathbf{B}} \tilde{\mathbf{D}}^H + \Pi^\perp \ddot{\mathbf{D}}_{xx} \tilde{\mathbf{B}} \tilde{\mathbf{D}}^H \\
 &\quad + \mathbf{G}_x \mathbf{G}_x^H
 \end{aligned} \tag{B.20}$$

Defining $\mathbf{\Omega} \triangleq \tilde{\mathbf{\alpha}} \tilde{\mathbf{\alpha}}^H$ and plugging (B.20) back into (B.11), we have,

$$\begin{aligned}
 J_{xx} &= -\sigma^{-2} \cdot \text{Tr} \left[\tilde{\mathbf{D}}^H (\mathbf{G}_{xx} + \mathbf{G}_{xx}^H) \tilde{\mathbf{D}} \mathbf{\Omega} \right] \\
 &\quad - \text{Tr} \left[\mathbf{G}_{xx} + \mathbf{G}_{xx}^H \right] \\
 &= -\sigma^{-2} \cdot \text{Tr} \left[\tilde{\mathbf{D}}^H \mathbf{G}_{xx} \tilde{\mathbf{D}} \mathbf{\Omega} \right] - \sigma^{-2} \cdot \text{Tr} \left[\tilde{\mathbf{D}}^H \mathbf{G}_{xx}^H \tilde{\mathbf{D}} \mathbf{\Omega} \right] \\
 &\quad - \text{Tr} \left[\mathbf{G}_{xx} \right] - \text{Tr} \left[\mathbf{G}_{xx}^H \right]
 \end{aligned} \tag{B.21}$$

Noticing that: $\tilde{\mathbf{D}}^H \Pi^\perp, \Pi^\perp \tilde{\mathbf{D}} = \mathbf{0}$, $\tilde{\mathbf{B}} \tilde{\mathbf{D}}^H \tilde{\mathbf{D}} = \mathbf{I}$ and using the cyclic-shift

property of the trace operator we have:

$$\begin{aligned}
 \text{Tr} \left[\tilde{\mathbf{D}}^H \mathbf{G}_{xx} \tilde{\mathbf{D}} \Omega \right] &= \text{Tr} \left[\tilde{\mathbf{D}}^H \left\{ - (2\mathbf{G}_x + \mathbf{G}_x^H) \dot{\mathcal{D}}_x \tilde{\mathbf{B}} \tilde{\mathbf{D}}^H \right. \right. \\
 &\quad \left. \left. + \mathbf{\Pi}^\perp \ddot{\mathcal{D}}_{xx} \tilde{\mathbf{B}} \tilde{\mathbf{D}}^H + \mathbf{G}_x \mathbf{G}_x^H \right\} \tilde{\mathbf{D}} \Omega \right] \\
 &= -\text{Tr} \left[\tilde{\mathbf{D}}^H \mathbf{G}_x^H \dot{\mathcal{D}}_x \Omega \right] \\
 &= -\text{Tr} \left[\dot{\mathcal{D}}_x^H \mathbf{\Pi}^\perp \dot{\mathcal{D}}_x \Omega \right] \\
 &= -\tilde{\alpha}^H \dot{\mathcal{D}}_x^H \mathbf{\Pi}^\perp \dot{\mathcal{D}}_x \tilde{\alpha} \tag{B.22}
 \end{aligned}$$

$$\begin{aligned}
 \text{Tr} [\mathbf{G}_{xx}] &= \text{Tr} \left[-\tilde{\mathbf{D}}^H (2\mathbf{G}_x + \mathbf{G}_x^H) \dot{\mathcal{D}}_x \tilde{\mathbf{B}} \right. \\
 &\quad \left. + \mathbf{\Pi}^\perp \ddot{\mathcal{D}}_{xx} \tilde{\mathbf{B}} \tilde{\mathbf{D}}^H + \mathbf{G}_x \mathbf{G}_x^H \right] \\
 &= -\text{Tr} \left[\dot{\mathcal{D}}_x^H \mathbf{\Pi}^\perp \dot{\mathcal{D}}_x \tilde{\mathbf{B}} - \mathbf{G}_x \mathbf{G}_x^H \right] \\
 &= 0 \tag{B.23}
 \end{aligned}$$

Substituting (B.22)-(B.23) back in (B.21), we have,

$$J_{xx} = \frac{2}{\sigma^2} \cdot \tilde{\alpha}^H \dot{\mathcal{D}}_x^H \mathbf{\Pi}^\perp \dot{\mathcal{D}}_x \tilde{\alpha} \tag{B.24}$$

Using $\dot{\mathcal{D}}_y \triangleq \frac{\partial \tilde{\mathbf{D}}}{\partial y}$, then by symmetry we have,

$$J_{yy} = \frac{2}{\sigma^2} \cdot \tilde{\alpha}^H \dot{\mathcal{D}}_y^H \mathbf{\Pi}^\perp \dot{\mathcal{D}}_y \tilde{\alpha} \tag{B.25}$$

The cross-terms are obtained using,

$$\frac{\partial^2 \mathbf{\Pi}^\perp}{\partial x \partial y} = -\mathbf{G}_{xy} - \mathbf{G}_{xy}^H \tag{B.26}$$

with,

$$\begin{aligned}
 \mathbf{G}_{xy} &\triangleq \frac{\partial \mathbf{G}_x}{\partial y} = \frac{\partial \left(\Pi^\perp \dot{\mathcal{D}}_x \tilde{\mathbf{B}} \tilde{\mathbf{D}}^H \right)}{\partial y} \\
 &= -(\mathbf{G}_y + \mathbf{G}_y^H) \dot{\mathcal{D}}_x \tilde{\mathbf{B}} \tilde{\mathbf{D}}^H + \Pi^\perp \ddot{\mathcal{D}}_{xy} \tilde{\mathbf{B}} \tilde{\mathbf{D}}^H \\
 &\quad - \Pi^\perp \dot{\mathcal{D}}_x \left\{ \tilde{\mathbf{B}} \left[\dot{\mathcal{D}}_y^H \tilde{\mathbf{D}} + \tilde{\mathbf{D}}^H \dot{\mathcal{D}}_y \right] \tilde{\mathbf{B}} \right\} \tilde{\mathbf{D}}^H \\
 &\quad + \Pi^\perp \dot{\mathcal{D}}_x \tilde{\mathbf{B}} \dot{\mathcal{D}}_y^H \\
 &= -(\mathbf{G}_y + \mathbf{G}_y^H) \dot{\mathcal{D}}_x \tilde{\mathbf{B}} \tilde{\mathbf{D}}^H + \Pi^\perp \ddot{\mathcal{D}}_{xy} \tilde{\mathbf{B}} \tilde{\mathbf{D}}^H \\
 &\quad - \Pi^\perp \dot{\mathcal{D}}_x \tilde{\mathbf{B}} \dot{\mathcal{D}}_y^H \Pi - \Pi^\perp \dot{\mathcal{D}}_x \tilde{\mathbf{B}} \tilde{\mathbf{D}}^H \dot{\mathcal{D}}_y \tilde{\mathbf{B}} \tilde{\mathbf{D}}^H \\
 &\quad + \Pi^\perp \dot{\mathcal{D}}_x \tilde{\mathbf{B}} \dot{\mathcal{D}}_y^H \\
 &= -(\mathbf{G}_y + \mathbf{G}_y^H) \dot{\mathcal{D}}_x \tilde{\mathbf{B}} \tilde{\mathbf{D}}^H + \Pi^\perp \ddot{\mathcal{D}}_{xy} \tilde{\mathbf{B}} \tilde{\mathbf{D}}^H \\
 &\quad + \Pi^\perp \dot{\mathcal{D}}_x \tilde{\mathbf{B}} \dot{\mathcal{D}}_y^H (\mathbf{I} - \Pi) - \Pi^\perp \dot{\mathcal{D}}_x \tilde{\mathbf{B}} \tilde{\mathbf{D}}^H \dot{\mathcal{D}}_y \tilde{\mathbf{B}} \tilde{\mathbf{D}}^H \\
 &= -(\mathbf{G}_y + \mathbf{G}_y^H) \dot{\mathcal{D}}_x \tilde{\mathbf{B}} \tilde{\mathbf{D}}^H + \Pi^\perp \ddot{\mathcal{D}}_{xy} \tilde{\mathbf{B}} \tilde{\mathbf{D}}^H \\
 &\quad + \Pi^\perp \dot{\mathcal{D}}_x \tilde{\mathbf{B}} \dot{\mathcal{D}}_y^H \Pi^\perp - \Pi^\perp \dot{\mathcal{D}}_x \tilde{\mathbf{B}} \tilde{\mathbf{D}}^H \dot{\mathcal{D}}_y \tilde{\mathbf{B}} \tilde{\mathbf{D}}^H \\
 &= -(\mathbf{G}_y + \mathbf{G}_y^H) \dot{\mathcal{D}}_x \tilde{\mathbf{B}} \tilde{\mathbf{D}}^H + \Pi^\perp \ddot{\mathcal{D}}_{xy} \tilde{\mathbf{B}} \tilde{\mathbf{D}}^H \\
 &\quad + \mathbf{G}_x \mathbf{G}_y^H - \Pi^\perp \dot{\mathcal{D}}_x \tilde{\mathbf{B}} \tilde{\mathbf{D}}^H \dot{\mathcal{D}}_y \tilde{\mathbf{B}} \tilde{\mathbf{D}}^H
 \end{aligned} \tag{B.27}$$

Plugging (B.26)-(B.27) back into (B.12) we get,

$$J_{xy} = \frac{2}{\sigma^2} \cdot \tilde{\boldsymbol{\alpha}}^H \dot{\mathcal{D}}_x^H \Pi^\perp \dot{\mathcal{D}}_y \tilde{\boldsymbol{\alpha}} \tag{B.28}$$

Finally, using $\dot{\mathcal{D}}_{t_0} \triangleq \frac{\partial \tilde{\mathbf{D}}}{\partial t_0}$, the remaining t_0 -dependent FIM elements can be obtained as,

$$J_{t_0 t_0} = \frac{2}{\sigma^2} \cdot \tilde{\boldsymbol{\alpha}}^H \dot{\mathcal{D}}_{t_0}^H \Pi^\perp \dot{\mathcal{D}}_{t_0} \tilde{\boldsymbol{\alpha}} \tag{B.29}$$

$$J_{t_0 x} = \frac{2}{\sigma^2} \cdot \tilde{\boldsymbol{\alpha}}^H \dot{\mathcal{D}}_{t_0}^H \Pi^\perp \dot{\mathcal{D}}_x \tilde{\boldsymbol{\alpha}} \tag{B.30}$$

$$J_{t_0 y} = \frac{2}{\sigma^2} \cdot \tilde{\boldsymbol{\alpha}}^H \dot{\mathcal{D}}_{t_0}^H \Pi^\perp \dot{\mathcal{D}}_y \tilde{\boldsymbol{\alpha}} \tag{B.31}$$

Arranging in matrix form,

$$\mathbf{J} \triangleq \begin{bmatrix} J_{xx} & J_{xy} & J_{xt_0} \\ J_{yx} & J_{yy} & J_{yt_0} \\ J_{t_0x} & J_{t_0y} & J_{t_0t_0} \end{bmatrix} \quad (\text{B.32})$$

The CRLB is obtained by inverting the FIM defined in (C.35). Notice that this CRLB is conditioned on a specific realization of $\tilde{\boldsymbol{\alpha}}$. To remove this conditioning, we need to average the CRLB expression over the entire range of possible $\tilde{\boldsymbol{\alpha}}$ values and obtain ‘‘average concentrated CRLB’’. This is accomplished by evaluating the integral,

$$\overline{\text{CRLB}} = \int_{-\infty}^{\infty} \text{CRLB} \big|_{\tilde{\boldsymbol{\alpha}} p_{\tilde{\boldsymbol{\alpha}}}(\tilde{\boldsymbol{\alpha}})} d\tilde{\boldsymbol{\alpha}} \quad (\text{B.33})$$

We will now obtain explicit expressions for the partial derivatives with respect to the unknown concentrated CRLB parameters. Recall that,

$$\begin{aligned} \tilde{\mathbf{D}}_k(\mathbf{p}, t_0) &\triangleq [\tilde{\mathbf{d}}_{0,k}, \tilde{\mathbf{d}}_{1,k}, \dots, \tilde{\mathbf{d}}_{L,k}] \\ \tilde{\mathbf{d}}_{\ell,k} &\triangleq (\tilde{\mathbf{E}}_{\ell,k} \tilde{\mathbf{Z}} \tilde{\mathbf{s}}_k) \otimes \mathbf{a}_{\ell,k} \\ \tilde{\mathbf{s}}_k &\triangleq [\bar{s}_k(f_{-N} - f_{\ell,k}), \dots, \bar{s}_k(f_N - f_{\ell,k})]^T \end{aligned} \quad (\text{B.34})$$

The partial derivative w.r.t parameters of interest are given by

$$\begin{aligned} \dot{\mathcal{D}}_{kx} &= [\dot{\tilde{\mathbf{d}}}_{0,k}^x \mathbf{0}, \dots, \mathbf{0}] \\ \dot{\mathcal{D}}_{ky} &= [\dot{\tilde{\mathbf{d}}}_{0,k}^y \mathbf{0}, \dots, \mathbf{0}] \\ \dot{\mathcal{D}}_{kt_0} &= [\dot{\tilde{\mathbf{d}}}_{0,k}^{t_0} \dot{\tilde{\mathbf{d}}}_{1,k}^{t_0}, \dots, \dot{\tilde{\mathbf{d}}}_{L,k}^{t_0}] \end{aligned} \quad (\text{B.35})$$

The derivatives w.r.t to the position coordinate x is obtained using the chain-rule,

$$\begin{aligned} \dot{\tilde{\mathbf{d}}}_{0,k}^x &= (\dot{\tilde{\mathbf{E}}}_{\ell,k}^x \tilde{\mathbf{Z}} \tilde{\mathbf{s}}_k) \otimes \mathbf{a}_{\ell,k} + (\tilde{\mathbf{E}}_{\ell,k} \dot{\tilde{\mathbf{Z}} \tilde{\mathbf{s}}_k}^x) \otimes \mathbf{a}_{\ell,k} \\ &\quad + (\tilde{\mathbf{E}}_{\ell,k} \tilde{\mathbf{Z}} \dot{\tilde{\mathbf{s}}_k}^x) \otimes \dot{\mathbf{a}}_{\ell,k}^x \end{aligned} \quad (\text{B.36})$$

The derivative w.r.t. y is obtained similarly.

The partial derivatives of $\mathbf{a}_{\ell,k}$ are obtained as follows. Let the m th element in the array be located during the k th observation interval at $\mathbf{q}_k^m = [x_{q,k}^m, y_{q,k}^m]^T$ while the array center is located at $\mathbf{q}_k = [x_{q,k}, y_{q,k}]^T$. The response of the m th element to a signal arriving from position $\mathbf{p}_\ell = [x_\ell, y_\ell]^T$ is given by,

$$\begin{aligned} [\mathbf{a}_{\ell,k}]_m &= \frac{1}{\sqrt{M}} e^{-i2\pi \frac{d_{\ell,k}^m}{\lambda}} \\ d_{\ell,k}^m &\triangleq \|\mathbf{p}_\ell - \mathbf{q}_k^m\| \\ &= \sqrt{(x_\ell - x_{q,k}^m)^2 + (y_\ell - y_{q,k}^m)^2} \end{aligned} \quad (\text{B.37})$$

where λ is the carrier signal wavelength.

Now, we have,

$$\begin{aligned} \dot{\mathbf{a}}_{\ell,k}^x &\triangleq \frac{\partial \dot{\mathbf{a}}_{\ell,k}^x}{\partial x} = -i \frac{2\pi}{\lambda} \cdot \frac{x_\ell - x_{q,k}^m}{d_{\ell,k}^m} \cdot \mathbf{a}_{\ell,k} \\ &= -i \frac{2\pi}{\lambda} \cos \theta_{\ell,k} \cdot \mathbf{a}_{\ell,k} \end{aligned} \quad (\text{B.38})$$

$$\dot{\mathbf{a}}_{\ell,k}^y \triangleq \frac{\partial \dot{\mathbf{a}}_{\ell,k}^y}{\partial y} = -i \frac{2\pi}{\lambda} \sin \theta_{\ell,k} \cdot \mathbf{a}_{\ell,k} \quad (\text{B.39})$$

where $\theta_{\ell,k}$ is the angle between the line connecting the receiver and the emitter/transponder and the x -axis. Next, we obtain the partial derivatives of $\tilde{\mathbf{E}}_{\ell,k}$. Recall that $\tau_{\ell,k} = \bar{\tau}_{\ell,k} + \tilde{\tau}_{\ell,k}$, where c is the propagation speed. Notice that only $\bar{\tau}_{\ell,k}$ depends on the emitter coordinates:

$$\begin{aligned} \bar{\tau}_{\ell,k} &\triangleq \bar{\tau}_\ell \triangleq \frac{1}{c} \|\mathbf{p}_0 - \mathbf{p}_\ell\|^2, \quad \forall \ell \neq 0 \\ &= \frac{1}{c} \sqrt{(x - x_\ell)^2 + (y - y_\ell)^2} \triangleq \frac{\bar{d}_\ell}{c} \end{aligned} \quad (\text{B.40})$$

$$\begin{aligned} \bar{\tau}_{0,k} &\triangleq \frac{1}{c} \|\mathbf{p}_0 - \mathbf{q}_k\|^2 \\ &= \frac{1}{c} \sqrt{(x - x_{q,k})^2 + (y - y_{q,k})^2} \triangleq \frac{\bar{d}_{0,k}}{c} \end{aligned} \quad (\text{B.41})$$

Using (B.40) we have,

$$\begin{aligned}
 \frac{\partial \bar{\tau}_\ell}{\partial x} &= \frac{1}{c} \cdot \frac{x - x_\ell}{\bar{d}_\ell} \triangleq \frac{1}{c} \cdot \cos \theta_\ell \\
 \frac{\partial \bar{\tau}_\ell}{\partial y} &= \frac{1}{c} \cdot \frac{y - y_\ell}{\bar{d}_\ell} \triangleq \frac{1}{c} \cdot \sin \theta_\ell \\
 \frac{\partial \bar{\tau}_{0,k}}{\partial x} &= \frac{1}{c} \cdot \frac{x - x_{q,k}}{\bar{d}_{0,k}} \triangleq \frac{1}{c} \cdot \cos \theta_{0,k} \\
 \frac{\partial \bar{\tau}_{0,k}}{\partial y} &= \frac{1}{c} \cdot \frac{y - y_{q,k}}{\bar{d}_{0,k}} \triangleq \frac{1}{c} \cdot \sin \theta_{0,k}
 \end{aligned} \tag{B.42}$$

Thus,

$$\begin{aligned}
 \dot{\mathbf{E}}_{0,k}^x &\triangleq \frac{\partial \tilde{\mathbf{E}}_{0,k}}{\partial x} = -\iota \frac{\cos \theta_{0,k}}{c} \mathbf{\Omega} \tilde{\mathbf{E}}_{0,k} \\
 \dot{\mathbf{E}}_{0,k}^y &\triangleq \frac{\partial \tilde{\mathbf{E}}_{0,k}}{\partial y} = -\iota \frac{\sin \theta_{0,k}}{c} \mathbf{\Omega} \tilde{\mathbf{E}}_{0,k} \\
 \dot{\mathbf{E}}_{\ell,k}^x &\triangleq \frac{\partial \tilde{\mathbf{E}}_{\ell,k}}{\partial x} = -\iota \frac{\cos \theta_\ell}{c} \mathbf{\Omega} \tilde{\mathbf{E}}_{\ell,k} \\
 \dot{\mathbf{E}}_{\ell,k}^y &\triangleq \frac{\partial \tilde{\mathbf{E}}_{\ell,k}}{\partial y} = -\iota \frac{\sin \theta_\ell}{c} \mathbf{\Omega} \tilde{\mathbf{E}}_{\ell,k}
 \end{aligned} \tag{B.43}$$

where,

$$\begin{aligned}
 \boldsymbol{\omega} &\triangleq [2\pi f_{-N}, 2\pi f_{-N+1}, \dots, 2\pi f_N]^T \\
 \mathbf{\Omega} &\triangleq \text{diag}\{\boldsymbol{\omega}\}
 \end{aligned} \tag{B.44}$$

The derivatives w.r.t. frequency shift $f_{\ell,k}$ is given by,

$$\begin{aligned}
 \dot{\mathbf{s}}_k^x &\triangleq \\
 &-\frac{\partial f_{\ell,k}}{\partial x} \cdot [\dot{\mathbf{s}}_k(f_{-N} - f_{\ell,k}), \dots, \dot{\mathbf{s}}_k(f_N - f_{\ell,k})]^T
 \end{aligned} \tag{B.45}$$

Notice that,

$$\begin{aligned}
 \frac{c}{f_c} f_{\ell,k} &= \bar{\mathbf{v}}_{\ell,k}^T \frac{\mathbf{p}^\ell - \mathbf{q}_k}{\|\mathbf{p}^\ell - \mathbf{q}_k\|}, \quad \ell = 0 \dots L \\
 \frac{c}{f_c} \dot{f}_{\ell,k}^x &= \frac{c}{f_c} \frac{\partial f_{\ell,k}}{\partial x} = \frac{v_{\ell,k}^x}{d_{\ell,k}} - \frac{\bar{\mathbf{v}}_{\ell,k}}{d_{\ell,k}} \cos \theta_{\ell,k} \cos \phi_{\ell,k} \\
 \frac{c}{f_c} \dot{f}_{\ell,k}^y &= \frac{c}{f_c} \frac{\partial f_{\ell,k}}{\partial y} = \frac{v_{\ell,k}^y}{d_{\ell,k}} - \frac{\bar{\mathbf{v}}_{\ell,k}}{d_{\ell,k}} \sin \theta_{\ell,k} \sin \phi_{\ell,k}
 \end{aligned} \tag{B.46}$$

where, $\phi_{\ell,k}$ is the angle between the receiver velocity vector and the line connecting the receiver and the emitter. Finally, the derivative of $\tilde{\mathbf{Z}}$ w.r.t. t_0 is given by,

$$\dot{\mathbf{d}}_{0,k}^{t_0} = (\tilde{\mathbf{E}}_{\ell,k} \dot{\tilde{\mathbf{Z}}} \check{\mathbf{s}}_k) \otimes \mathbf{a}_{\ell,k} \tag{B.47}$$

where,

$$\dot{\tilde{\mathbf{Z}}} = -\imath \tilde{\mathbf{Z}} \boldsymbol{\omega} \tag{B.48}$$

This concludes the concentrated CRLB derivation.

B.2 Derivation of Multiple-Receiver DPD

The SPG system analyzed in chapter 4, estimates the emitter position using both angular and time-delay information. The multi-antenna receiving platform can extract both angular and time-delay information, while the transponders provide additional time-delay information via induced multipath. Considering the amount of position-dependent information that may be utilized by the system, the SPG system may be considered as equivalent to a system that consists of a single, multi-antenna receiver (equipped with an M -antenna array), and L single-antenna receivers.

In this section, we derive an algorithm for direct position determination (DPD) using the equivalent, multiple-receivers system configuration. This algorithm serves as a benchmark in section 4.4, for comparing SPG system performance. The following DPD algorithm is derived under similar signal

and channel model assumptions, as outlined in section 4.2. The additive noise power of the receivers in the equivalent system, is assumed to be normalized to enable fair comparison with the SPG system.

Following [14], the algorithm aims to maximize a sum of distinct cost functions: a cost function for the multi-antenna moving receiver and a cost function for the single antenna receivers. The received signal models are given by,

$$r_{\ell,k}(t) = s(t - \tau_{\ell,k}(\mathbf{p}) - t_0)\alpha_{\ell,k} + n_{\ell,k}, \quad \ell = 1 \dots L \quad (\text{B.49})$$

$$\begin{aligned} \mathbf{r}_{0,k}(t) &= \mathbf{a}_k(\mathbf{p})s_k(t - \tau_{0,k}(\mathbf{p}) - t_0)e^{j2\pi t f_k(\mathbf{p})}\alpha_{0,k} + \mathbf{n}_{0,k}(t), \\ &\quad -T/2 \leq t \leq T/2 \end{aligned} \quad (\text{B.50})$$

For the single-antenna receivers the cost function can be constructed as follows. Define the following vectors:

$$\begin{aligned} \bar{\mathbf{r}}_{\ell,k} &\triangleq [r_{\ell,k}(f_{-N}), \dots, r_{\ell,k}(f_N)]^T \\ \tilde{\mathbf{s}}_k &\triangleq [\bar{s}_k(f_{-N})e^{-j2\pi f_{-N}t_0}, \dots, \bar{s}_k(f_N)e^{-j2\pi f_N t_0}]^T \\ \bar{\mathbf{n}}_{\ell,k} &\triangleq [n_{\ell,k}(f_{-N}), \dots, n_{\ell,k}(f_N)]^T \end{aligned} \quad (\text{B.51})$$

Then in vectorized form (B.49) is recast as,

$$\bar{\mathbf{r}}_{\ell,k} = \tilde{\mathbf{E}}_{\ell,k}\tilde{\mathbf{s}}_k\alpha_{\ell,k} + \bar{\mathbf{n}}_{\ell,k} \quad (\text{B.52})$$

The cost function that should be minimized for the single antenna, static receivers is given by,

$$Q_\ell = \sum_{k=1}^K \|\bar{\mathbf{r}}_{\ell,k} - \tilde{\mathbf{E}}_{\ell,k}\tilde{\mathbf{s}}_k\alpha_{\ell,k}\|^2 \quad (\text{B.53})$$

and the LS estimate for the complex channel attenuation that minimizes this cost function is given by:

$$\hat{\alpha}_{\ell,k} = \tilde{\mathbf{s}}_k^H \tilde{\mathbf{E}}_{\ell,k}^H \bar{\mathbf{r}}_{\ell,k} \quad (\text{B.54})$$

B.2.1 Unknown Signals

After plugging (B.54) back into (B.53), the position-dependent cost function to be maximized for the single-antenna receivers can be recast as,

$$\begin{aligned}
 \tilde{Q} &= \sum_{k=1}^K \sum_{\ell=1}^L \tilde{\mathbf{s}}_k^H \tilde{\mathbf{E}}_{\ell,k}^H \bar{\mathbf{r}}_{\ell,k} \bar{\mathbf{r}}_{\ell,k}^H \tilde{\mathbf{E}}_{\ell,k} \tilde{\mathbf{s}}_k \\
 &= \sum_{k=1}^K \tilde{\mathbf{s}}_k^H \left\{ \sum_{\ell=1}^L \tilde{\mathbf{E}}_{\ell,k}^H \bar{\mathbf{r}}_{\ell,k} \bar{\mathbf{r}}_{\ell,k}^H \tilde{\mathbf{E}}_{\ell,k} \right\} \tilde{\mathbf{s}}_k
 \end{aligned} \tag{B.55}$$

Define,

$$\begin{aligned}
 \mathbf{u}_{\ell,k} &\triangleq \tilde{\mathbf{E}}_{\ell,k}^H \bar{\mathbf{r}}_{\ell,k} \\
 \mathbf{U}_k &\triangleq [\mathbf{u}_{1,k}, \dots, \mathbf{u}_{L,k}] \\
 \mathbf{H}_k &\triangleq \mathbf{U}_k^H \mathbf{U}_k
 \end{aligned} \tag{B.56}$$

Then,

$$\tilde{Q} = \sum_{k=1}^K \lambda_{\max} \{ \mathbf{H}_k \} \tag{B.57}$$

For multi-antenna moving receiver we use the definition,

$$\tilde{\mathbf{d}}_{0,k} \triangleq \underbrace{(\tilde{\mathbf{F}}_{0,k} \tilde{\mathbf{E}}_{0,k} \tilde{\mathbf{s}}_k)}_{\tilde{\mathbf{w}}_{0,k}} \otimes \mathbf{a}_k$$

and obtain the cost function as,

$$Q_0 = \sum_{k=1}^K \|\bar{\mathbf{r}}_{0,k} - \tilde{\mathbf{d}}_{0,k} \alpha_{0,k}\|^2 \tag{B.58}$$

The LS estimate for the complex (LoS) path gain is given by,

$$\begin{aligned}
\hat{\alpha}_{0,k} &= \left(\tilde{\mathbf{d}}_{0,k}^H \tilde{\mathbf{d}}_{0,k} \right)^{-1} \tilde{\mathbf{d}}_{0,k}^H \bar{\mathbf{r}}_{0,k} \\
&= \left(\left[\tilde{\mathbf{s}}_k^H \tilde{\mathbf{W}}_{0,k}^H \otimes \mathbf{a}_k^H \right] \left[\tilde{\mathbf{W}}_{0,k} \tilde{\mathbf{s}}_k \otimes \mathbf{a}_k \right] \right)^{-1} \cdot \\
&\quad \tilde{\mathbf{s}}_k^H \tilde{\mathbf{W}}_{0,k}^H \otimes \mathbf{a}_k^H \bar{\mathbf{r}}_{0,k} \\
&= \left(\left[\tilde{\mathbf{s}}_k^H \tilde{\mathbf{W}}_{0,k}^H \tilde{\mathbf{W}}_{0,k} \tilde{\mathbf{s}}_k \otimes \mathbf{a}_k^H \mathbf{a}_k \right] \right)^{-1} \tilde{\mathbf{s}}_k^H \tilde{\mathbf{W}}_{0,k}^H \otimes \mathbf{a}_k^H \bar{\mathbf{r}}_{0,k} \\
&= \tilde{\mathbf{s}}_k^H \underbrace{\tilde{\mathbf{W}}_{0,k}^H \otimes \mathbf{a}_k^H}_{\tilde{\mathbf{Y}}_k^H} \bar{\mathbf{r}}_{0,k}
\end{aligned}$$

The cost function for the multi-antenna moving receiver is given by,

$$\begin{aligned}
\tilde{Q}_0 &= \sum_{k=1}^K \tilde{\mathbf{s}}_k^H \tilde{\mathbf{Y}}_k^H \bar{\mathbf{r}}_{0,k} \bar{\mathbf{r}}_{0,k}^H \tilde{\mathbf{Y}}_k \tilde{\mathbf{s}}_k \\
&= \sum_{k=1}^K \lambda_{\max} \left\{ \tilde{\mathbf{Y}}_k^H \bar{\mathbf{r}}_{0,k} \bar{\mathbf{r}}_{0,k}^H \tilde{\mathbf{Y}}_k \right\} \\
&= \sum_{k=1}^K \bar{\mathbf{r}}_{0,k}^H \tilde{\mathbf{Y}}_k \tilde{\mathbf{Y}}_k^H \bar{\mathbf{r}}_{0,k}
\end{aligned} \tag{B.59}$$

Finally, the position estimate is given by maximizing the sum of the two cost functions,

$$\hat{\mathbf{p}} = \underset{\mathbf{p}}{\operatorname{argmax}} \left\{ \sum_{k=1}^K \bar{\mathbf{r}}_{0,k}^H \tilde{\mathbf{Y}}_k \tilde{\mathbf{Y}}_k^H \bar{\mathbf{r}}_{0,k} + \lambda_{\max} \{ \mathbf{H}_k \} \right\} \tag{B.60}$$

B.2.2 Known Signals

In the case of known signals the position is obtained via maximizing the following expression over the range space of \mathbf{p} and the clock offset, t_0 .

$$\hat{\mathbf{p}} = \operatorname{argmax}_{\mathbf{p}, t_0} \left\{ \sum_{k=1}^K \tilde{\mathbf{s}}_k^H \left[\tilde{\mathbf{Y}}_k^H \bar{\mathbf{r}}_{0,k} \bar{\mathbf{r}}_{0,k}^H \tilde{\mathbf{Y}}_k + \sum_{\ell=1}^L \tilde{\mathbf{E}}_{\ell,k}^H \bar{\mathbf{r}}_{\ell,k} \bar{\mathbf{r}}_{\ell,k}^H \tilde{\mathbf{E}}_{\ell,k} \right] \tilde{\mathbf{s}}_k \right\} \quad (\text{B.61})$$

B.3 SPG for Deterministic, Unknown Signal Waveform

In this section, we derive an algorithm for direct SPG under the assumption that the transmitted signal waveform is unknown under the assumptions outlined in [25]. The algorithm first minimizes over the unknown signal samples, thereby eliminating the unknown signal waveform from the cost function. The k th signal frequency coefficient that minimizes (4.15) is given by,

$$\hat{s}_k = \left(\boldsymbol{\alpha}^H \tilde{\mathbf{A}}_k^H \tilde{\mathbf{A}}_k \boldsymbol{\alpha} \right)^{-1} \boldsymbol{\alpha}^H \tilde{\mathbf{A}}_k^H \bar{\mathbf{r}}_k \quad (\text{B.62})$$

Substituting (B.62) back in (4.15) we get,

$$Q(\boldsymbol{\alpha}, \mathbf{p}) = \sum_{k=0}^{K-1} \left\| \bar{\mathbf{r}}_k - \tilde{\mathbf{A}}_k \boldsymbol{\alpha} \left(\boldsymbol{\alpha}^H \tilde{\mathbf{A}}_k^H \tilde{\mathbf{A}}_k \boldsymbol{\alpha} \right)^{-1} \boldsymbol{\alpha}^H \tilde{\mathbf{A}}_k^H \bar{\mathbf{r}}_k \right\|^2 \quad (\text{B.63})$$

The minimization of $Q(\boldsymbol{\alpha}, \mathbf{p})$ is equivalent to maximizing $\tilde{Q}(\boldsymbol{\alpha}, \mathbf{p})$, which is given by

$$\begin{aligned} \tilde{Q}(\boldsymbol{\alpha}, \mathbf{p}) &= \sum_{k=0}^{K-1} \bar{\mathbf{r}}_k^H \tilde{\mathbf{A}}_k \boldsymbol{\alpha} \left(\boldsymbol{\alpha}^H \tilde{\mathbf{A}}_k^H \tilde{\mathbf{A}}_k \boldsymbol{\alpha} \right)^{-1} \boldsymbol{\alpha}^H \tilde{\mathbf{A}}_k^H \bar{\mathbf{r}}_k \\ &= \sum_{k=0}^{K-1} \frac{\boldsymbol{\alpha}^H \mathbf{f}_k \mathbf{f}_k^H \boldsymbol{\alpha}}{\boldsymbol{\alpha}^H \mathbf{C}_k \boldsymbol{\alpha}} \end{aligned} \quad (\text{B.64})$$

where $\mathbf{f}_k \triangleq \tilde{\mathbf{A}}_k^H \bar{\mathbf{r}}_k$, $\mathbf{C}_k \triangleq \tilde{\mathbf{A}}_k^H \tilde{\mathbf{A}}_k$. Unfortunately, there is no simple solution for maximizing the cost function in the form of (B.64). An iterative solution to a similar optimization problem has been proposed by Kiers in [30], (though the problem addressed in [30] involves real rather than complex data).

We seek a maximum for $\tilde{Q}(\boldsymbol{\alpha}, \mathbf{p})$, which is equivalent to minimizing $-\tilde{Q}(\boldsymbol{\alpha}, \mathbf{p})$. Denote a specific value of $\boldsymbol{\alpha}$ by $\boldsymbol{\alpha}_0$, and consider the inequality,

$$\left| (\boldsymbol{\alpha}^H \mathbf{C}_k \boldsymbol{\alpha})^{-1/2} \boldsymbol{\alpha}^H \mathbf{f}_k - (\boldsymbol{\alpha}^H \mathbf{C}_k \boldsymbol{\alpha})^{1/2} (\boldsymbol{\alpha}_0^H \mathbf{C}_k \boldsymbol{\alpha}_0)^{-1} \boldsymbol{\alpha}_0^H \mathbf{f}_k \right|^2 \geq 0 \quad (\text{B.65})$$

After expanding the expression in (B.65) and rearranging the terms we get,

$$\begin{aligned} & (\boldsymbol{\alpha}^H \mathbf{C}_k \boldsymbol{\alpha})^{-1} |\boldsymbol{\alpha}^H \mathbf{f}_k|^2 \geq \\ & 2\Re \{ (\boldsymbol{\alpha}_0^H \mathbf{C}_k \boldsymbol{\alpha}_0)^{-1} \mathbf{f}_k^H \boldsymbol{\alpha}_0 \boldsymbol{\alpha}^H \mathbf{f}_k \} \\ & - (\boldsymbol{\alpha}^H \mathbf{C}_k \boldsymbol{\alpha}) (\boldsymbol{\alpha}_0^H \mathbf{C}_k \boldsymbol{\alpha}_0)^{-2} |\boldsymbol{\alpha}_0^H \mathbf{f}_k|^2 \end{aligned} \quad (\text{B.66})$$

By defining $w_k \triangleq \mathbf{f}_k^H \boldsymbol{\alpha}_0 (\boldsymbol{\alpha}_0^H \mathbf{C}_k \boldsymbol{\alpha}_0)^{-1}$ and summing over k we obtain,

$$\begin{aligned} -\tilde{Q}(\boldsymbol{\alpha}, \mathbf{p}) & \triangleq H(\boldsymbol{\alpha}, \mathbf{p}) \\ & = - \sum_{k=0}^{K-1} (\boldsymbol{\alpha}^H \mathbf{C}_k \boldsymbol{\alpha})^{-1} |\boldsymbol{\alpha}^H \mathbf{f}_k|^2 \leq \\ & \quad -2 \sum_{k=0}^{K-1} \Re \{ w_k \boldsymbol{\alpha}^H \mathbf{f}_k \} + \sum_{k=0}^{K-1} (\boldsymbol{\alpha}^H \mathbf{C}_k \boldsymbol{\alpha}) |w_k|^2 \\ & \triangleq G(\boldsymbol{\alpha}, \boldsymbol{\alpha}_0, \mathbf{p}) \end{aligned} \quad (\text{B.67})$$

Next,

$$\begin{aligned}
 G(\boldsymbol{\alpha}, \boldsymbol{\alpha}_0, \mathbf{p}) &= -\boldsymbol{\alpha}^H \underbrace{\left(\sum_{k=0}^{K-1} w_k \mathbf{f}_k \right)}_{\boldsymbol{\beta}} - \left(\sum_{k=0}^{K-1} w_k^* \mathbf{f}_k^H \right) \boldsymbol{\alpha} \\
 &+ \boldsymbol{\alpha}^H \underbrace{\left(\sum_{k=0}^{K-1} |w_k|^2 \mathbf{C}_k \right)}_{\mathbf{C}} \boldsymbol{\alpha} \\
 &= -\boldsymbol{\alpha}^H \boldsymbol{\beta} - \boldsymbol{\beta}^H \boldsymbol{\alpha} + \boldsymbol{\alpha}^H \mathbf{C} \boldsymbol{\alpha}
 \end{aligned} \tag{B.68}$$

Equation (B.68) may be recast as,

$$G(\boldsymbol{\alpha}, \boldsymbol{\alpha}_0, \mathbf{p}) = \|\mathbf{C}^{-1/2} \boldsymbol{\beta} - \mathbf{C}^{1/2} \boldsymbol{\alpha}\|^2 - \boldsymbol{\beta}^H \mathbf{C}^{-1} \boldsymbol{\beta} \tag{B.69}$$

$G(\boldsymbol{\alpha}, \boldsymbol{\alpha}_0, \mathbf{p})$ is minimized by choosing $\hat{\boldsymbol{\alpha}} = \mathbf{C}^{-1} \boldsymbol{\beta}$.

To summarize this result, we have derived a function $G(\boldsymbol{\alpha}, \boldsymbol{\alpha}_0, \mathbf{p})$ that upper-bounds the function of interest, $-\tilde{Q}(\boldsymbol{\alpha}, \mathbf{p})$. For the bounding function we can easily obtain a minimum over $\boldsymbol{\alpha}$. Thus, we can iteratively decrease the function of interest in order to find a (local) minimum point.

To prove that this iterative procedure converges to a minimum point notice that (suppressing the dependence on \mathbf{p}): $H(\boldsymbol{\alpha}) \leq G(\boldsymbol{\alpha}, \boldsymbol{\alpha}_0)$ and $H(\boldsymbol{\alpha}_0) = G(\boldsymbol{\alpha}_0, \boldsymbol{\alpha}_0)$. Suppose $\boldsymbol{\alpha}_1$ minimizes $G(\boldsymbol{\alpha}, \boldsymbol{\alpha}_0)$ w.r.t. $\boldsymbol{\alpha}$ so that $G(\boldsymbol{\alpha}_1, \boldsymbol{\alpha}_0) \leq G(\boldsymbol{\alpha}_0, \boldsymbol{\alpha}_0)$. Then we get $H(\boldsymbol{\alpha}_1) \leq G(\boldsymbol{\alpha}_1, \boldsymbol{\alpha}_0) \leq G(\boldsymbol{\alpha}_0, \boldsymbol{\alpha}_0) = H(\boldsymbol{\alpha}_0)$. Thus, $H(\boldsymbol{\alpha}_1) \leq H(\boldsymbol{\alpha}_0)$. Further, $G(\boldsymbol{\alpha}_1, \boldsymbol{\alpha}_1) = H(\boldsymbol{\alpha}_1)$ and by minimizing $G(\boldsymbol{\alpha}, \boldsymbol{\alpha}_1)$ w.r.t. $\boldsymbol{\alpha}$ we get $\boldsymbol{\alpha}_2$ so that $H(\boldsymbol{\alpha}_2) \leq G(\boldsymbol{\alpha}_2, \boldsymbol{\alpha}_1) \leq G(\boldsymbol{\alpha}_1, \boldsymbol{\alpha}_1) = H(\boldsymbol{\alpha}_1)$. Thus, $H(\boldsymbol{\alpha}_2) \leq H(\boldsymbol{\alpha}_1) \leq H(\boldsymbol{\alpha}_0)$. We have just described an iterative procedure in which the cost function does not increase.

The point of convergence of any iterative process depends on the selection of the initial value of the changing variables. We propose selecting the initial value of $\boldsymbol{\alpha}_0$ as the eigenvector that corresponds to the largest eigenvalue of a matrix $\boldsymbol{\Omega}$, whose K column vectors are given by $\boldsymbol{\alpha}_k$ that maximizes,

$$\tilde{Q}_k = \frac{\boldsymbol{\alpha}^H \tilde{\mathbf{A}}_k^H \tilde{\boldsymbol{\Gamma}}_k \tilde{\boldsymbol{\Gamma}}_k^H \tilde{\mathbf{A}}_k \boldsymbol{\alpha}}{\boldsymbol{\alpha}^H \tilde{\mathbf{A}}_k^H \tilde{\mathbf{A}}_k \boldsymbol{\alpha}}$$

and is given by $\boldsymbol{\alpha}_k = (\tilde{\mathbf{A}}_k^H \tilde{\mathbf{A}}_k)^{-1} \tilde{\mathbf{A}}_k^H \tilde{\mathbf{r}}_k$.

The iterative process for maximizing $\tilde{Q}(\boldsymbol{\alpha}, \mathbf{p})$ and estimating the emitter position may be implemented as described in Algorithm 8.

<p>Define the area of interest and determine a suitable grid of locations</p> <p>$\mathbf{p}_1, \mathbf{p}_2 \dots \mathbf{p}_g$</p> <p>for $j = 1$ to g do</p> <div style="margin-left: 20px;"> <p>1. Set $\mathbf{f}_k = \tilde{\mathbf{A}}_k^H \tilde{\mathbf{r}}_k$; $\mathbf{C}_k = \tilde{\mathbf{A}}_k^H \tilde{\mathbf{A}}_k$</p> <p>2. Choose $\boldsymbol{\alpha}_0$</p> <p>while $\tilde{Q}^i(\boldsymbol{\alpha}, \mathbf{p}_j) - \tilde{Q}^{i-1}(\boldsymbol{\alpha}, \mathbf{p}_j) > \epsilon \cdot \tilde{Q}^{i-1}(\boldsymbol{\alpha}, \mathbf{p}_j)$ do</p> <div style="margin-left: 20px;"> <p>1. Evaluate: $w_k \triangleq \mathbf{f}_k^H \boldsymbol{\alpha}_0 (\boldsymbol{\alpha}_0^H \mathbf{C}_k^H \boldsymbol{\alpha}_0)$.</p> <p>2. Evaluate: $\mathbf{C} = \sum_k w_k ^2 \mathbf{C}_k$; $\boldsymbol{\beta} = \sum_k w_k \mathbf{f}_k$</p> <p>3. Find: $\hat{\boldsymbol{\alpha}} = \mathbf{C}^{-1} \boldsymbol{\beta}$</p> <p>4. Set: $\boldsymbol{\alpha}_0 = \hat{\boldsymbol{\alpha}}$</p> <p>5. Evaluate: $\tilde{Q}^i(\boldsymbol{\alpha}, \mathbf{p}_j) = \sum_k \frac{\boldsymbol{\alpha}_0^H \mathbf{f}_k \mathbf{f}_k^H \boldsymbol{\alpha}_0}{\boldsymbol{\alpha}_0^H \mathbf{C}_k \boldsymbol{\alpha}_0}$</p> </div> <p>end</p> </div> <p>end</p> <p>Find the grid point for which \tilde{Q} is the biggest. This grid point is the estimated position.</p>

Algorithm 8: Direct SPG Algorithm for Unknown, Arbitrary Emitter Signal

Appendix C

Appendix Related to Chapter 5

C.1 Derivation of Cramér Rao Lower Bound for Geolocation in Rayleigh Fading Channels

In this section, we derive the CRLB for emitter geolocation in Rayleigh fading channel model introduced in chapter 5. Given K independent samples of zero mean complex Gaussian process $\tilde{\mathbf{y}}_{\ell,k}$ whose statistics depend on the vector of parameters $\boldsymbol{\eta}$, the elements of the FIM are given by,

$$\mathbf{J}_{mn} = K \cdot \sum_{\ell=1}^L \text{Tr} \left\{ \tilde{\mathbf{R}}_{\ell}^{-1} \frac{\partial \tilde{\mathbf{R}}_{\ell}}{\partial \eta_m} \tilde{\mathbf{R}}_{\ell}^{-1} \frac{\partial \tilde{\mathbf{R}}_{\ell}}{\partial \eta_n} \right\} \quad (\text{C.1})$$

For simplicity, the bound is derived under the assumption of planar problem geometry (i.e., $z = 0$). In such case, the vector of parameters is defined as $\boldsymbol{\eta} = [x, y, \sigma_{\mathbf{p}}, t_0]^T$.

Recall that,

$$\tilde{\mathbf{R}}_{\ell} = \mathbf{G}_{\ell} \mathbf{R}_{b,\ell} \mathbf{G}_{\ell}^H + \sigma_n^2 \mathbf{I}_{NM} \quad (\text{C.2})$$

An explicit expression for the inverse of $\tilde{\mathbf{R}}_{\ell}$ may be obtained using the matrix-

inversion lemma [116],

$$\begin{aligned}\tilde{\mathbf{R}}_\ell^{-1} &= \sigma_n^{-2}(\mathbf{I}_{MN} - \mathbf{G}_\ell[\sigma_n^2\mathbf{R}_{b,\ell}^{-1} + \mathbf{G}_\ell^H\mathbf{G}_\ell]^{-1}\mathbf{G}_\ell^H) \\ &= \sigma_n^{-2}(\mathbf{I}_{MN} - \mathbf{G}_\ell[\sigma_n^2\mathbf{R}_{b,\ell}^{-1} + N \cdot \mathbf{I}_M]^{-1}\mathbf{G}_\ell^H)\end{aligned}\quad (\text{C.3})$$

Next, we will obtain expressions for the partial derivatives of the covariance matrix $\tilde{\mathbf{R}}_\ell$ w.r.t. the parameters of interest.

C.1.1 Derivatives w.r.t. Emitter Coordinates

Using the chain-rule we have,

$$\frac{\partial \tilde{\mathbf{R}}_\ell}{\partial x} = \dot{\mathbf{G}}_{\ell,x} \mathbf{R}_{b,\ell} \mathbf{G}_\ell^H + \mathbf{G}_\ell \dot{\mathbf{R}}_{b,\ell}^x \mathbf{G}_\ell^H + \mathbf{G}_\ell \mathbf{R}_{b,\ell} \dot{\mathbf{G}}_{\ell,x}^H \quad (\text{C.4})$$

$$\frac{\partial \tilde{\mathbf{R}}_\ell}{\partial y} = \dot{\mathbf{G}}_{\ell,y} \mathbf{R}_{b,\ell} \mathbf{G}_\ell^H + \mathbf{G}_\ell \dot{\mathbf{R}}_{b,\ell}^y \mathbf{G}_\ell^H + \mathbf{G}_\ell \mathbf{R}_{b,\ell} \dot{\mathbf{G}}_{\ell,y}^H \quad (\text{C.5})$$

where,

$$\begin{aligned}\dot{\mathbf{G}}_{\ell,x} &\triangleq \frac{\partial \mathbf{G}_\ell}{\partial x} = (\dot{\mathbf{D}}_{\ell,x} \bar{\mathbf{s}}) \otimes \mathbf{I}_M \\ &= (\mathcal{D}_{\ell,x} \mathbf{D}_\ell \bar{\mathbf{s}}) \otimes \mathbf{I}_M \\ \dot{\mathbf{G}}_{\ell,y} &\triangleq \frac{\partial \mathbf{G}_\ell}{\partial y} = (\mathcal{D}_{\ell,y} \mathbf{D}_\ell \bar{\mathbf{s}}) \otimes \mathbf{I}_M\end{aligned}\quad (\text{C.6})$$

with,

$$\begin{aligned}\mathcal{D}_{\ell,x} &\triangleq \text{diag} \left\{ -\omega_0 \frac{\partial \tau_\ell}{\partial x}, -\omega_1 \frac{\partial \tau_\ell}{\partial x}, \dots, -\omega_{N-1} \frac{\partial \tau_\ell}{\partial x} \right\} \\ \mathcal{D}_{\ell,y} &\triangleq \text{diag} \left\{ -\omega_0 \frac{\partial \tau_\ell}{\partial y}, -\omega_1 \frac{\partial \tau_\ell}{\partial y}, \dots, -\omega_{N-1} \frac{\partial \tau_\ell}{\partial y} \right\}\end{aligned}\quad (\text{C.7})$$

and $\omega_n \triangleq 2\pi f_n$. The derivative of the time delay are defined in (B.40)-(B.42).

Notice that (5.15) may also be recast as [116]:

$$\mathbf{R}_{b,\ell} = \mathbf{A}_\ell \mathbf{B}_\ell \mathbf{A}_\ell^H \quad (\text{C.8})$$

where $\mathbf{A}_\ell \triangleq \text{diag}\{\mathbf{a}_\ell\}$. Using (C.8) the expressions of $\dot{\mathbf{R}}_{b,\ell}^x$, $\dot{\mathbf{R}}_{b,\ell}^y$ are given by,

$$\begin{aligned}\dot{\mathbf{R}}_{b,\ell}^x &\triangleq \frac{\partial \mathbf{R}_{b,\ell}}{\partial x} = \frac{\partial \mathbf{A}_\ell \mathbf{B}_\ell \mathbf{A}_\ell^H}{\partial x} \\ &= \dot{\mathbf{A}}_{\ell,x} \mathbf{B}_\ell \mathbf{A}_\ell^H + \mathbf{A}_\ell \dot{\mathbf{B}}_{\ell,x} \mathbf{A}_\ell^H + \mathbf{A}_\ell \mathbf{B}_\ell \dot{\mathbf{A}}_{\ell,x}^H\end{aligned}\quad (\text{C.9})$$

$$\begin{aligned}\dot{\mathbf{R}}_{b,\ell}^y &\triangleq \frac{\partial \mathbf{R}_{b,\ell}}{\partial y} = \frac{\partial \mathbf{A}_\ell \mathbf{B}_\ell \mathbf{A}_\ell^H}{\partial y} \\ &= \dot{\mathbf{A}}_{\ell,y} \mathbf{B}_\ell \mathbf{A}_\ell^H + \mathbf{A}_\ell \dot{\mathbf{B}}_{\ell,y} \mathbf{A}_\ell^H + \mathbf{A}_\ell \mathbf{B}_\ell \dot{\mathbf{A}}_{\ell,y}^H\end{aligned}\quad (\text{C.10})$$

The partial derivatives of \mathbf{A}_ℓ w.r.t. emitter coordinates are obtained as follows. From (B.37) the derivatives of the m th diagonal element are given by,

$$\begin{aligned}[\dot{\mathbf{A}}_\ell^x]_m &\triangleq \frac{\partial [\mathbf{A}_\ell]_m}{\partial x} \\ &= \frac{i2\pi}{\lambda} [\bar{x}_{\ell,m} \cos \dot{\theta}_{\ell,x} + \bar{y}_{\ell,m} \sin \dot{\theta}_{\ell,x}] \cdot [\mathbf{A}_\ell]_m\end{aligned}\quad (\text{C.11})$$

$$\begin{aligned}[\dot{\mathbf{A}}_\ell^y]_m &\triangleq \frac{\partial [\mathbf{A}_\ell]_m}{\partial y} \\ &= \frac{i2\pi}{\lambda} [\bar{x}_{\ell,m} \cos \dot{\theta}_{\ell,y} + \bar{y}_{\ell,m} \sin \dot{\theta}_{\ell,y}] \cdot [\mathbf{A}_\ell]_m\end{aligned}\quad (\text{C.12})$$

where the partial derivatives of the angle terms may be obtained by applying the chain-rule:

$$\sin \dot{\theta}_{\ell,x} \triangleq \frac{\partial \sin \theta_\ell}{\partial x} = -\frac{(y - \bar{y}_\ell)(x - \bar{x}_\ell)}{d_\ell^3}\quad (\text{C.13})$$

$$\sin \dot{\theta}_{\ell,y} \triangleq \frac{\partial \sin \theta_\ell}{\partial y} = \frac{(x - \bar{x}_\ell)^2}{d_\ell^3}\quad (\text{C.14})$$

$$\cos \dot{\theta}_{\ell,x} \triangleq \frac{\partial \cos \theta_\ell}{\partial x} = \frac{(y - \bar{y}_\ell)^2}{d_\ell^3}\quad (\text{C.15})$$

$$\cos \dot{\theta}_{\ell,y} \triangleq \frac{\partial \cos \theta_\ell}{\partial y} = -\frac{(x - \bar{x}_\ell)(y - \bar{y}_\ell)}{d_\ell^3}\quad (\text{C.16})$$

Let $\dot{\mathcal{A}}_{\ell,x}$ and $\dot{\mathcal{A}}_{\ell,y}$ be $M \times M$ diagonal matrices with the m th diagonal entry in each matrix equal to:

$$[\dot{\mathcal{A}}_{\ell,x}]_m \triangleq \frac{i2\pi}{\lambda} [\bar{x}_{\ell,m} \cos \dot{\theta}_{\ell,x} + \bar{y}_{\ell,m} \sin \dot{\theta}_{\ell,x}]\quad (\text{C.17})$$

$$[\dot{\mathbf{A}}_{\ell,y}]_m \triangleq \frac{i2\pi}{\lambda} [\bar{x}_{\ell,m} \cos \dot{\theta}_{\ell,y} + \bar{y}_{\ell,m} \sin \dot{\theta}_{\ell,y}] \quad (\text{C.18})$$

Hence,

$$\dot{\mathbf{A}}_{\ell}^x = \dot{\mathbf{A}}_{\ell,x} \mathbf{A}_{\ell} \quad (\text{C.19})$$

$$\dot{\mathbf{A}}_{\ell}^y = \dot{\mathbf{A}}_{\ell,y} \mathbf{A}_{\ell} \quad (\text{C.20})$$

The derivative of the spatial-spreading matrix \mathbf{B}_{ℓ} may be obtained as follows. From (5.7) and (5.16), we have:

$$[\mathbf{B}_{\ell}]_{m,l} = e^{-\frac{2\pi^2\sigma_{\mathbf{p}}^2}{\lambda^2 d_{\ell}^2} [\Delta_{\ell,x}^{m,l} \sin \theta_{\ell} - \Delta_{\ell,y}^{m,l} \cos \theta_{\ell}]^2} \quad (\text{C.21})$$

Again, the dependence in the emitter coordinates is embedded in θ_{ℓ} . Thus,

$$\begin{aligned} \frac{\partial[\mathbf{B}_{\ell}]_{m,l}}{\partial x} &= -\frac{2\pi^2}{\lambda^2} \left(\frac{2\sigma_{\mathbf{p}}^2}{d_{\ell}^2} [\Delta_{\ell,x}^{m,l} \sin \theta_{\ell} - \Delta_{\ell,y}^{m,l} \cos \theta_{\ell}] \right. \\ &\quad \cdot [\Delta_{\ell,x}^{m,l} \sin \dot{\theta}_{\ell,x} - \Delta_{\ell,y}^{m,l} \cos \dot{\theta}_{\ell,x}] \\ &\quad \left. - \frac{\sigma_{\mathbf{p}}^2(x - \bar{x}_{\ell})}{d_{\ell}^3} [\Delta_{\ell,x}^{m,l} \sin \theta_{\ell} - \Delta_{\ell,y}^{m,l} \cos \theta_{\ell}]^2 \right) \cdot [\mathbf{B}_{\ell}]_{m,l} \end{aligned} \quad (\text{C.22})$$

$$\begin{aligned} \frac{\partial[\mathbf{B}_{\ell}]_{m,l}}{\partial y} &= -\frac{2\pi^2}{\lambda^2} \left(\frac{2\sigma_{\mathbf{p}}^2}{d_{\ell}^2} [\Delta_{\ell,x}^{m,l} \sin \theta_{\ell} - \Delta_{\ell,y}^{m,l} \cos \theta_{\ell}] \right. \\ &\quad \cdot [\Delta_{\ell,x}^{m,l} \sin \dot{\theta}_{\ell,y} - \Delta_{\ell,y}^{m,l} \cos \dot{\theta}_{\ell,y}] \\ &\quad \left. - \frac{\sigma_{\mathbf{p}}^2(y - \bar{y}_{\ell})}{d_{\ell}^3} [\Delta_{\ell,x}^{m,l} \sin \theta_{\ell} - \Delta_{\ell,y}^{m,l} \cos \theta_{\ell}]^2 \right) \cdot [\mathbf{B}_{\ell}]_{m,l} \end{aligned} \quad (\text{C.23})$$

Define, $\dot{\mathbf{B}}_{\ell,x}$ and $\dot{\mathbf{B}}_{\ell,y}$ as $M \times M$ matrices with entries:

$$\begin{aligned} [\dot{\mathbf{B}}_{\ell,x}]_{m,l} \triangleq & -\frac{2\pi^2}{\lambda^2} \left(\frac{2\sigma_{\mathbf{p}}^2}{d_\ell^2} [\Delta_{\ell,x}^{m,l} \sin \theta_\ell - \Delta_{\ell,y}^{m,l} \cos \theta_\ell] \right. \\ & \cdot [\Delta_{\ell,x}^{m,l} \sin \dot{\theta}_{\ell,x} - \Delta_{\ell,y}^{m,l} \cos \dot{\theta}_{\ell,x}] \\ & \left. - \frac{\sigma_{\mathbf{p}}^2(x - \bar{x}_\ell)}{d_\ell^3} [\Delta_{\ell,x}^{m,l} \sin \theta_\ell - \Delta_{\ell,y}^{m,l} \cos \theta_\ell]^2 \right) \end{aligned} \quad (\text{C.24})$$

$$\begin{aligned} [\dot{\mathbf{B}}_{\ell,y}]_{m,l} \triangleq & -\frac{2\pi^2}{\lambda^2} \left(\frac{2\sigma_{\mathbf{p}}^2}{d_\ell^2} [\Delta_{\ell,x}^{m,l} \sin \theta_\ell - \Delta_{\ell,y}^{m,l} \cos \theta_\ell] \right. \\ & \cdot [\Delta_{\ell,x}^{m,l} \sin \dot{\theta}_{\ell,y} - \Delta_{\ell,y}^{m,l} \cos \dot{\theta}_{\ell,y}] \\ & \left. - \frac{\sigma_{\mathbf{p}}^2(y - \bar{y}_\ell)}{d_\ell^3} [\Delta_{\ell,x}^{m,l} \sin \theta_\ell - \Delta_{\ell,y}^{m,l} \cos \theta_\ell]^2 \right) \end{aligned} \quad (\text{C.25})$$

Using (C.24)-(C.25),

$$\dot{\mathbf{B}}_{\ell,x} = \dot{\mathbf{B}}_{\ell,x} \odot \mathbf{B}_\ell \quad (\text{C.26})$$

$$\dot{\mathbf{B}}_{\ell,y} = \dot{\mathbf{B}}_{\ell,y} \odot \mathbf{B}_\ell \quad (\text{C.27})$$

C.1.2 Derivatives w.r.t. Position Spread $\sigma_{\mathbf{p}}$

The derivative of $\mathbf{R}_{b,\ell}$ w.r.t. the position-spread is given by,

$$\frac{\partial \mathbf{R}_{b,\ell}}{\partial \sigma_{\mathbf{p}}} = \frac{\partial \mathbf{A}_\ell \mathbf{B}_\ell \mathbf{A}_\ell^H}{\partial \sigma_{\mathbf{p}}} = \mathbf{A}_\ell \dot{\mathbf{B}}_{\ell,\sigma_{\mathbf{p}}} \mathbf{A}_\ell^H \quad (\text{C.28})$$

The expression for $\dot{\mathbf{B}}_{\ell,\sigma_{\mathbf{p}}}$ may be obtained as follows. Recall from (5.16),

$$\frac{\partial [\mathbf{B}_\ell]_{m,l}}{\partial \sigma_{\mathbf{p}}} = -\frac{4\pi^2 \sigma_{\mathbf{p}}}{\lambda^2 d_\ell^2} [\Delta_{\ell,x}^{m,l} \sin \theta_\ell - \Delta_{\ell,y}^{m,l} \cos \theta_\ell]^2 \cdot [\mathbf{B}_\ell]_{m,l} \quad (\text{C.29})$$

Define,

$$[\dot{\mathbf{B}}_{\ell,\sigma_{\mathbf{p}}}]_{m,l} \triangleq -\frac{4\pi^2 \sigma_{\mathbf{p}}}{\lambda^2 d_\ell^2} [\Delta_{\ell,x}^{m,l} \sin \theta_\ell - \Delta_{\ell,y}^{m,l} \cos \theta_\ell]^2 \quad (\text{C.30})$$

Using (C.30) we obtain,

$$\dot{\mathbf{B}}_{\ell, \sigma_{\mathbf{p}}} = \dot{\mathbf{B}}_{\ell, \sigma_{\mathbf{p}}} \odot \mathbf{B}_{\ell} \quad (\text{C.31})$$

C.1.3 Derivatives w.r.t. Transmit Time t_0

The dependence in the transmit time t_0 is embedded in \mathbf{G}_{ℓ} . Therefore:

$$\frac{\partial \tilde{\mathbf{R}}_{\ell}}{\partial t_0} = \dot{\mathbf{G}}_{\ell, t_0} \mathbf{R}_{b, \ell} \mathbf{G}_{\ell}^H + \mathbf{G}_{\ell} \mathbf{R}_{b, \ell} \dot{\mathbf{G}}_{\ell, t_0}^H \quad (\text{C.32})$$

where,

$$\dot{\mathbf{G}}_{\ell, t_0} \triangleq \frac{\partial \mathbf{G}_{\ell}}{\partial t_0} = (\dot{\mathbf{D}}_{\ell, t_0} \bar{\mathbf{s}}) \otimes \mathbf{I}_M (\mathcal{D}_{\ell, t_0} \mathbf{D}_{\ell} \bar{\mathbf{s}}) \otimes \mathbf{I}_M \quad (\text{C.33})$$

with,

$$\mathcal{D}_{\ell, t_0} \triangleq \text{diag} \{-\omega_0, -\omega_1, \dots, -\omega_{N-1}\} \quad (\text{C.34})$$

The FIM is given by,

$$\mathbf{J} \triangleq \begin{bmatrix} J_{xx} & J_{xy} & J_{x\sigma_{\mathbf{p}}} & J_{xt_0} \\ J_{yx} & J_{yy} & J_{y\sigma_{\mathbf{p}}} & J_{yt_0} \\ J_{\sigma_{\mathbf{p}}x} & J_{\sigma_{\mathbf{p}}y} & J_{\sigma_{\mathbf{p}}\sigma_{\mathbf{p}}} & J_{\sigma_{\mathbf{p}}t_0} \\ J_{t_0x} & J_{t_0y} & J_{t_0\sigma_{\mathbf{p}}} & J_{t_0t_0} \end{bmatrix} \quad (\text{C.35})$$

The CRLB is obtained by inverting the FIM defined in (C.35). This concludes the CRLB derivation and concludes the appendix.

BIBLIOGRAPHY

List of Publications

Journal Papers by the Author

- Paper 1** O. Bar-Shalom and A. J. Weiss, “Efficient Direct Position Determination of OFDM Signals,” *IET Radar, Sonar & Navigation*, vol. 3, no. 2, pp. 101–111, Apr. 2009.
- Paper 2** O. Bar-Shalom and A. J. Weiss, “Direct positioning of stationary targets using MIMO radar,” *Signal Processing*, vol. 91, pp. 2345 – 2358, October 2011.
- Paper 3** O. Bar-Shalom and A. J. Weiss, “Transponder-Aided Single Platform Geolocation,” *IEEE Trans. on Signal Processing*, vol. 61, no. 5, pp. 1239–1248, Mar. 2013.
- Paper 4** O. Bar-Shalom and A. J. Weiss, “Emitter Geolocation Using Single Moving Receiver,” *Signal Processing*, vol. 105, pp. 70-83, Dec. 2014.
- Paper 5** O. Bar-Shalom and A. J. Weiss, “Direct Emitter Geolocation Under Local Scattering,” *Signal Processing*, vol. 117, pp. 102-114, Dec. 2015.

Conference Papers by the Author

Paper 6 O. Bar-Shalom and A. J. Weiss, “Direct Position Determination of OFDM Signals,” in *Proc. of 8th IEEE Workshop on Signal Processing Advances in Wireless Communications (SPAWC)*, Helsinki, Finland, June 2007.

Paper 7 O. Bar-Shalom and A. J. Weiss, “Direct Position Determination Using MIMO Radar,” in *Proc. of the 25th Convention of Electrical and Electronics Engineers in Israel, IEEEI-2008*, pp. 575–579, Eilat, Israel, 3-5 Dec. 2008.

References

- [1] R. G. Stansfield, "Statistical theory of DF fixing," *Journal IEE*, vol. 94, Part 3A, no. 15, pp. 762-770, 1947.
- [2] M. Wax, "Model-based processing in sensor arrays," *Advances in Spectrum Analysis and Array Processing*, Vol. III, S. Haykin, Ed., Prentice-Hall, Englewood Cliffs, NJ, USA, 1995.
- [3] H. Krim, and M. Viberg, "Two decades of array signal processing research: the parametric approach," *IEEE Signal Processing Magazine*, vol. 13, no. 4, pp. 67-94, 1996.
- [4] J. J. Bussgang, J.M. Zagami, S.A. Parl and K.D. Melillo, "Providing universal location services using a wireless E911 location network," *IEEE Communications Magazine*, 1998.
- [5] M. Wax, and T. Kailath, "Decentralized processing in sensor arrays," *IEEE Trans. Acoustics, Speech, and Signal Processing*, vol. 33, no. 5, pp. 1123-1129, 1985.
- [6] R. J. Kozick, and B. M. Sadler, "Source localization with distributed sensor arrays and partial spatial coherence," *IEEE Trans. Signal Processing*, vol. 52, no. 3, pp. 601-616, 2004.
- [7] M. Wax, and T. Kailath, "Optimum localization of multiple sources by passive arrays," *IEEE Trans. Acoustics, Speech, and Signal Processing*, vol. 31, no. 5, pp. 1210-1217, 1983.
- [8] A. Ward, A. Jones, and A. Hopper, "A new location technique for the active office," *IEEE Personal Communications*, vol. 4, no. 5, pp. 4247, Oct. 1997.
- [9] L. F. McNamara, "Ionospheric modelling in support of single station location of long range transmitters," *Journal of Atmospheric and Terrestrial Physics*, vol. 50, no. 9, pp. 781 – 795, Sept. 1988.

- [10] H. C. Horing, "Comparison of the fixing accuracy of single-station locators and triangulation systems assuming ideal shortwave propagation in the ionosphere," *IEE Proceedings F: Radar and Signal Processing*, vol. 137, no. 3, pp. 173–176, June 1990.
- [11] R. L. Johnson, Q. R. Black, and A. G. Sonsteby, "HF multipath passive single site radio location," *IEEE Trans. on Aerospace and Electronic Systems*, vol. 30, no. 2, pp. 462–470, Apr. 1994.
- [12] J. E. Giesbrecht, R. Clarke, and D. Abbott, "Improved techniques for monitoring the HF spectrum," in *SPIE Conference Series*, D. Abbott, K. Eshraghian, C. A. Musca, D. Pavlidis, & N. Weste, Ed., Mar. 2004, vol. 5274, pp. 112–122.
- [13] G. A. Fabrizio and A. Heitmann, "Single site geolocation method for a linear array," in *Radar Conference (RADAR), 2012 IEEE*, pp. 885–890, 7–11 May 2012.
- [14] A. J. Weiss, "Direct Position Determination of Narrowband Radio Frequency Transmitters," *IEEE Signal Processing Lett.*, vol. 11, no. 5, pp. 513–516, May 2004.
- [15] A. J. Weiss and A. Amar, "Direct Position Determination Of Multiple Radio Signals," *EURASIP Journal on Advances in Signal Processing*, vol. JASP-2005, no. 1, pp. 37–49, Jan. 2005.
- [16] A. Amar and A. J. Weiss, "Direct Position Determination in the Presence of Model Errors - Known Waveforms," *Elsevier jour. on Digital Signal Processing*, no. 16, pp. 52–83, 2006.
- [17] A. Amar and A. J. Weiss, "Fundamental limitations on the number of resolvable emitters using a geolocation system," *IEEE Trans. on Signal Processing*, vol. 55, no. 5, pp. 2193–2202, May 2007.
- [18] A. Amar and A. J. Weiss, "Localization of narrowband radio emitters based on doppler frequency shifts," *IEEE Trans. on Signal Processing*, vol. 56, no. 11, pp. 5500–5508, Nov. 2008.
- [19] A. J. Weiss and A. Amar, "Direct Geolocation of Stationary Wideband Radio Signal Based on Time Delays and Doppler Shifts," in *IEEE/SP 15th Workshop on Statistical Signal Processing (SSP)*, pp. 101–104, Aug. 31–Sept. 3, 2009.

- [20] A. J. Weiss, "Direct Geolocation of Wideband Emitters Based on Delay and Doppler," *IEEE Trans. on Signal Processing*, vol. 59, no. 6, pp. 2513–2521, June 2011.
- [21] O. Bar-Shalom and A. J. Weiss, "Direct Position Determination of OFDM Signals," in *Proc. of 8'th IEEE Workshop on Signal Processing Advances in Wireless Communications (SPAWC)*, Helsinki, Finland, June 2007.
- [22] O. Bar-Shalom and A. J. Weiss, "Direct position determination using MIMO radar," in *Proc. of 25th Convention of Electrical and Electronics Engineers in Israel, IEEEI-2008*, Eilat, Israel, pp.575–579, 3-5 Dec. 2008.
- [23] O. Bar-Shalom and A. J. Weiss, "Efficient Direct Position Determination of OFDM Signals," *IET Radar, Sonar & Navigation*, vol. 3, no. 2, pp. 101–111, Apr. 2009.
- [24] O. Bar-Shalom and A. J. Weiss, "Direct positioning of stationary targets using MIMO RADAR," *Signal Processing*, vol. 91, pp. 2345–2358, Oct. 2011.
- [25] O. Bar-Shalom and A. J. Weiss, "Transponder-Aided Single Platform Geolocation," *IEEE Trans. on Signal Processing*, vol. 61, no. 5, pp. 1239–1248, Mar. 2013.
- [26] O. Bar-Shalom and A. J. Weiss, "Emitter Geolocation Using Single Moving Receiver," *Signal Processing*, vol. 105, pp. 70-83, Dec. 2014.
- [27] O. Bar-Shalom and A. J. Weiss, "Direct Emitter Geolocation Under Local Scattering," *Signal Processing*, vol. 117, pp. 102-114, Dec. 2015.
- [28] P. Closas, C. Fernandez-Prades, and J.A. Fernandez-Rubio, "Maximum Likelihood Estimation of Position in GNSS," *IEEE Signal Processing Lett.*, vol. 14, no. 5, pp. 359 –362, May 2007.
- [29] A. B. Baggeroer, W. A. Kuperman, and P. N. Mikhalevsky, "An Overview of Matched Field Methods in Ocean Acoustics," *IEEE Jour. of Oceanic Eng.*, vol. 18, no. 4, pp. 401–424, Oct. 1993.
- [30] H. A. L. Kiers, "Maximization of sums of quotients of quadratic forms and some generalizations," *Psychometrika*, vol. 60, pp. 221–245, June 1995.
- [31] M. Oispuu and U. Nickel, "Direct detection and position determination of multiple sources with intermittent emission," *Signal Processing*, vol. 90, no. 12, pp. 3056 – 3064, 2010.

- [32] Yunye Jin, Wee-Seng Soh, and Wai-Choong Wong, "Indoor localization with channel impulse response based fingerprint and nonparametric regression," *IEEE Trans. on Wireless Communications*, vol. 9, no. 3, pp. 1120–1127, Mar. 2010.
- [33] K. Becker, "An Efficient Method of Passive Emitter Location," *IEEE Trans. on Aerospace and Electronic Systems*, vol. 28, no. 4, pp. 1091–1104, Oct. 1992.
- [34] P. C. Chestnut, "Emitter Location Accuracy Using TDOA and Differential Doppler," *IEEE Trans. on Aerospace and Electronic Systems*, vol. AES-18, no. 2, pp. 214–218, Mar. 1982.
- [35] D. J. Torrieri, "Statistical Theory of Passive Location Systems," *IEEE Trans. on Aerospace and Electronic Systems*, vol. AES-20, no. 2, pp. 183–198, Mar. 1984.
- [36] S. Stein, "Differential Delay/Doppler ML Estimation with Unknown Signals," *IEEE Trans. on Signal Processing*, vol. 41, no. 8, pp. 2717–2719, Aug. 1993.
- [37] B. Hochwald and A. Nehorai, "Concentrated Cramer-Rao bound expressions," *IEEE Trans. on Information Theory*, vol. 40, no. 2, pp. 363–371, Mar. 1994.
- [38] A. Coluccia, F. Ricciato and G. Ricci, "Positioning Based on Signals of Opportunity," *IEEE Comm. Letters*, vol. 18, no. 2, pp. 356–359, Feb. 2014
- [39] C. Yan and H. H. Fan, "Asynchronous Differential TDOA for non-GPS Navigation Using Signals of Opportunity," in *ICASSP 2008*, pp. 5312–5315, Mar. 31-Apr. 4, 2008.
- [40] Y. Wang, X. Ma and G. Leus, "Robust Time-Based Localization for Asynchronous Networks," *IEEE Trans. on Signal Processing*, vol. 59, no. 9, pp. 4397–4410, Sept. 2011
- [41] W. S. Hodgkiss and L. W. Nolte, "Covariance between fourier coefficients representing the time waveforms observed from an array of sensors," *The Journal of the Acoustical Society of America*, vol. 59, no. 3, 1976.
- [42] R. B. Ertel, P. Cardieri, K. W. Sowerby, T. S. Rappaport, and J. H. Reed, "Overview of spatial channel models for antenna array communication systems," *IEEE Personal Communications*, vol. 5, no. 1, pp. 10–22, Feb. 1998.

- [43] P. Zetterberg, "The spectrum efficiency of a base-station antenna array system for spatially selective transmission, report version," Tech. Rep., Royal Institute of Technology (KTH), 1994.
- [44] P. Zetterberg and B. Ottersten, "The spectrum efficiency of a base station antenna array system for spatially selective transmission," in *IEEE 44th Vehicular Technology Conference*, vol.3, pp. 1517–1521, June 1994.
- [45] P. Zetterberg, *Mobile Cellular Communications with Base Station Antenna Arrays: Spectrum Efficiency, Algorithms and Propagation Models*, Ph.d. dissertation, Royal Institute of Technology, Stockholm, Sweden, June 1997.
- [46] P. Zetterberg and B. Ottersten, "The spectrum efficiency of a base station antenna array system for spatially selective transmission," *IEEE Trans. on Vehicular Technology*, vol. 44, no. 3, pp. 651–660, Aug. 1995.
- [47] T. Trump and B. Ottersten, "Estimation of nominal direction of arrival and angular spread using an array of sensors," *Signal Processing*, vol. 50, no. 1-2, pp. 57 – 69, 1996, Special Issue on Subspace Methods, Part I: Array Signal Processing and Subspace Computations.
- [48] B. Ottersten, "Spatial Division Multiple Access (SDMA) in Wireless Communications," in *Nordic Radio Symposium*, 1995.
- [49] B. Ottersten, "Array processing for wireless communications," in *Proc. of 8th IEEE Signal Processing Workshop on Statistical Signal and Array Processing*, pp. 466–473, June 1996.
- [50] K. V. S. Hari and B. Ottersten, "Parameter estimation using a sensor array in a rician fading channel," *Sadhana*, vol. 23, pp. 5–15, 1998.
- [51] D. Astély and B. Ottersten, "The Effects of Local Scattering on Direction of Arrival Estimation with MUSIC," *IEEE Trans. on Signal Processing*, vol. 47, no. 12, pp. 3220 –3234, Dec. 1999.
- [52] D. Astély, B. Ottersten, and A. L. Swindlehurst, "Generalised Array Manifold model for Wireless Communication Channels with Local Scattering," *IEE Proc. Radar, Sonar and Navigation*, vol. 145, no. 1, pp. 51–57, Feb. 1998.
- [53] S. Valaee, B. Champagne, and P. Kabal, "Parametric localization of distributed sources," *Signal Processing, IEEE Transactions on*, vol. 43, no. 9, pp. 2144–2153, Sep. 1995.

- [54] Y. Meng, P. Stoica, and K. M. Wong, "Estimation of the directions of arrival of spatially dispersed signals in array processing," *IEE Proc. - Radar, Sonar and Navigation*, vol. 143, no. 1, pp. 1–9, Feb. 1996.
- [55] G. Fuks, J. Goldberg, and H. Messer, "Bearing Estimation in a Ricean Channel – part I: Inherent Accuracy Limitations," *IEEE Trans. on Signal Processing*, vol. 49, no. 5, pp. 925–937, May 2001.
- [56] R. Raich, J. Goldberg, and H. Messer, "Bearing estimation for a distributed source: modeling, inherent accuracy limitations and algorithms," *IEEE Trans. on Signal Processing*, vol. 48, no. 2, pp. 429–441, Feb. 2000.
- [57] J. Friedmann, R. Raich, J. Goldberg, and H. Messer, "Bearing Estimation for a Distributed Source of Nonconstant Modulus - Bounds and Analysis," *IEEE Trans. on Signal Processing*, vol. 51, no. 12, pp. 3027–3035, Dec. 2003.
- [58] E. Biglieri and S. Shamai J. Proakis, "Fading Channels: Information-Theoretic And Communications Aspects," *IEEE Trans. on Information Theory*, vol. 44, no. 6, pp. 2619–2692, Oct 1998.
- [59] G. J. Foschini and M. J. Gans, "On limits of wireless communications in a fading environment when using multiple antennas," *Wireless Personal Communications*, vol. 6, pp. 311–335, 1998.
- [60] M. Viberg and B. Ottersten, "Sensor array processing based on subspace fitting," *IEEE Trans. on Signal Processing*, vol. 39, no. 5, pp. 1110–1121, May 1991.
- [61] B. Ottersten, M. Viberg, P. Stoica, and A. Nehorai, "Exact and Large Sample ML Techniques for Parameter Estimation and Detection in Array Processing," in *Radar Array Processing*, S. Haykin, J. Litva, and T. J. Shepherd, Eds., pp. 99–151. Springer-Verlag, New-York, USA, 1993.
- [62] E. Fishler, A. M. Haimovich, R. S. Blum, D. Chizhik, L. J. Cimini, and R. A. Valenzuela, "MIMO radar: an idea whose time has come," in *Proc. of IEEE Radar Conference*, pp. 71 – 78, New Jersey Inst. of Technol., Newark, NJ, USA, 26-29 Apr. 2004.
- [63] Jian Li and Peter Stoica, *MIMO Radar Signal Processing*, John Wiley & Sons, Inc., Hoboken, New Jersey, 2009.
- [64] N. H. Lehmann, E. Fishler, A. M. Haimovich, R. S. Blum, D. Chizhik, L. J. Cimini, and R. A. Valenzuela, "Evaluation of Transmit Diversity

- in MIMO-Radar Direction Finding,” *IEEE Trans. on Signal Processing*, vol. 55, no. 2.2, pp. 2215 – 2225, May 2007.
- [65] E. Fishler, A. M. Haimovich, R. S. Blum, D. Chizhik, L. J. Cimini, and R. A. Valenzuela, “Spatial Diversity In Radars-Models and Detection Performance,” *IEEE Trans. on Signal Processing*, vol. 54, no. 3, pp. 823 – 838, Mar. 2006.
- [66] P. Stoica, J. Li, and Y. Xie, “On Probing Signal Design For MIMO Radar,” *IEEE Trans. on Signal Processing*, vol. 55, no. 8, pp. 4151–4161, Aug. 2007.
- [67] J. Li and P. Stoica, “MIMO Radar with Colocated Antennas,” *IEEE Signal Processing Magazine*, vol. 24, no. 5, pp. 106–114, 2007.
- [68] P. E. Howland, “Editorial: Passive radar systems,” *IEE Proceedings on Radar, Sonar and Navigation*, vol. 152, no. 3, pp. 105–106, 2005.
- [69] P. E. Howland, D. Maksimiuk, and G. Reitsma, “FM radio based bistatic radar,” *IEE Proceedings on Radar, Sonar and Navigation*, vol. 152, no. 3, pp. 107–115, 2005.
- [70] “Multi-Static Primary Surveillance Radar (MSPSR) - An examination of Alternative Frequency Bands,” Tech. Rep., Roke Manor Research Limited, july 2008, [available online: <http://www.roke.co.uk/sectors/atm/>].
- [71] I. Bekkerman and J. Tabrikian, “Target Detection and Localization Using MIMO Radars and Sonars,” *IEEE Trans. Signal Processing*, vol. 54, no. 10, pp. 3873–3883, Oct. 2006.
- [72] H. Godrich, A. M. Haimovich, and R. S. Blum, “Target localization techniques and tools for MIMO radar,” in *Proc. of the IEEE Radar Conference RADAR '08*, pp. 1–6, 26-30 May 2008.
- [73] H. Godrich, A. M. Haimovich, and R. S. Blum, “Cramer Rao bound on target localization estimation in MIMO radar systems,” in *Proc. of the 42nd Annual Conference on Information Sciences and Systems, CISS 2008*, pp. 134–139, 19-21 Mar. 2008.
- [74] C. M. Hoyuela, A. J. Terzuoli Jr., and R. P. Wasky, “Determining possible receiver locations for passive radar,” *IEE Proceedings on Radar, Sonar and Navigation*, vol. 152, no. 3, pp. 206–214, 2005.

- [75] D. Poullin, “Passive detection using digital broadcasters (DAB, DVB) with COFDM modulation,” *IEEE Proceedings on Radar, Sonar and Navigation*, vol. 152, no. 3, pp. 143–152, 2005.
- [76] W.-C. Li, P. Wei, and X.-C. Xiao, “TDOA and T2/R radar based target location method and performance analysis,” *IEEE Proceedings on Radar, Sonar and Navigation*, vol. 152, no. 3, pp. 219–223, 2005.
- [77] N. H. Lehmann, A. M. Haimovich, R.S. Blum, and L. Cimini, “High resolution capabilities of MIMO radar,” in *Signals, Systems and Computers, 2006. ACSSC '06. Fortieth Asilomar Conference on*, pp. 25–30, Oct. 2006.
- [78] H. Godrich, A. M. Haimovich, and R. S. Blum, “Target localisation techniques and tools for multiple-input multiple-output radar,” *Radar, Sonar Navigation, IET*, vol. 3, no. 4, pp. 314–327, august 2009.
- [79] H. Godrich, A. M. Haimovich, and R. S. Blum, “Target Localization Accuracy Gain in MIMO Radar-Based Systems,” *IEEE Trans. on Information Theory*, vol. 56, no. 6, pp. 2783–2803, June 2010.
- [80] F. Daum and J. Huang, “MIMO radar: Snake oil or good idea?,” in *Proc. of the International Waveform Diversity and Design Conference 2009*, pp. 113–117, 8-13 Feb. 2009.
- [81] S. Buzzi, M. Lops, and S. Sardellitti, “Further Results on Cramér-Rao Bounds for Parameter Estimation in Long-Code DS/CDMA Systems,” *IEEE Trans. on Signal Processing*, vol. 53, no. 3, pp. 1216–1221, Mar. 2005.
- [82] A. B. Baggeroer, W. A. Kuperman, and P. N. Mikhalevsky, “An Overview of Matched Field Methods in Ocean Acoustics,” *IEEE Jour. of Oceanic Eng.*, vol. 18, no. 4, pp. 401–424, Oct. 1993.
- [83] H. Minn, X. Fu, and V. K. Bhargava, “Optimal Periodic Training Signal for Frequency Offset Estimation in Frequency-Selective Fading Channels,” *IEEE Trans. on Communications*, vol. 54, no. 6, pp. 1081–1096, June 2006.
- [84] J. J. Caffery: *Wireless Location in CDMA Cellular Radio Systems*, Kluwer Academic Publishers, Boston, 1999.
- [85] S. Al-Jazzar and J. J. Caffery, “ESPRIT-based Joint AOA/Delay Estimation for CDMA Systems,” in *Proc. of IEEE Wireless Communications and Networking Conference (WCNC)*, vol. 4, pp. 2244–2249, Mar. 2004.

- [86] F. Gustafsson, and F. Gunnarsson, "Mobile positioning using wireless networks: possibilities and fundamental limitations based on available wireless network measurements," *IEEE Signal Proc. Mag.*, vol. 22, no. 4, pp. 41–53, July 2005.
- [87] A. H. Sayed, A. Tarighat, and N. Khajehnouri, "Network-based wireless location: challenges faced in developing techniques for accurate wireless location information," *IEEE Signal Proc. Mag.*, vol. 22, no. 4, pp. 24–40, July 2005.
- [88] N. Patwari, J. N. Ash, S. Kyperountas, A. O. Hero III, R. L. Moses, and N. S. Correal, "Locating the nodes: cooperative localization in wireless sensor networks," *IEEE Signal Proc. Mag.*, vol. 22, no. 4, pp. 54–69, July 2005.
- [89] S. Gezici, Z. Tian, G. B. Giannakis, H. Kobayashi, A. F. Molisch, H. V. Poor and Z. Sahinoglu, "Localization via ultra-wideband radios: a look at positioning aspects for future sensor networks," *IEEE Signal Proc. Mag.*, vol. 22, no. 4, pp. 70–84, July 2005.
- [90] H. Bölcskei and A. J. Paulraj, "Space-frequency coded broadband OFDM systems," *Proc. of IEEE Wireless Communications and Networking Conference (WCNC) 2000*, vol. 1, pp. 1-6, 23-28 Sept. 2000.
- [91] A. J. Paulraj, D. A. Gore, R. U. Nabar and H. Bölcskei, "An overview of MIMO communications - a key to gigabit wireless," *Proc. of the IEEE*, vol. 92, no. 2, pp. 198–218, Feb. 2004.
- [92] H. Bölcskei, M. Borgmann and A. J. Paulraj, "Impact of the Propagation Environment on the Performance of Space-Frequency Coded MIMO-OFDM," *IEEE Jour. on Selected Areas in Comm.*, vol. 21, no. 3, pp. 427–439, Sept. 2003.
- [93] H. Bölcskei, D. Gesbert, and A. J. Paulraj, "On the capacity of OFDM-based spatial multiplexing systems," *IEEE Trans. on Comm.*, vol. 50, no. 2, pp. 225-234, Feb. 2002.
- [94] G. Sun, J. W. Chen Guo, and K. J. R. Liu, "Signal processing techniques in network-aided positioning: a survey of state-of-the-art positioning designs," *IEEE Signal Processing Magazine*, vol.22, no.4, pp. 12-23, July 2005.
- [95] Y.-H. Jo, J.-Y. Lee, D.-H. Ha, and S.-H. Kang, "Accuracy Enhancement for UWB Indoor Positioning Using Ray Tracing," *Position, Location, And*

- Navigation Symposium, 2006 IEEE/ION*, vol., no., pp. 565-568, April 25-27, 2006.
- [96] L. Cong and W. Zhuang, "Hybrid TDOA/AOA Mobile User Location for Wideband CDMA Cellular Systems," *IEEE Trans. on Wireless Communications*, vol. 1, no. 3, pp. 439-447, July 2002.
- [97] J. Rinne and M. Renfors, "Pilot spacing in orthogonal frequency division multiplexing systems on practical channels," *IEEE Trans. on Consumer Elect.*, vol. 42, no. 4, pp. 959-962, Nov. 1996.
- [98] S.-G. Kang, Y.-M. Ha, and E.-K. Joo, "A comparative investigation on channel estimation algorithms for OFDM in mobile communications," *IEEE Trans. on Broadcasting*, vol. 49, no. 2, pp. 142-149, June 2003.
- [99] P. J. Voltz and D. Hernandez, "Maximum likelihood time of arrival estimation for real-time physical location tracking of 802.11a/g mobile stations in indoor environments," Position Location and Navigation Symposium (PLANS), 2004, pp. 585-591, 26-29 April 2004.
- [100] S. Kaiser, S. Plass, A. Dammann, and K. Fazel, *Multi-Carrier Spread Spectrum 2007*, vol. 1 of *Lecture Notes Electrical Engineering*, chapter Positioning with Generalized Multi-Carrier Communications Signals, pp. 287-296, Springer Netherlands, June 2007.
- [101] W. J. MacLean and J. K. Tsotsos, "Fast pattern recognition using gradient-descent search in an image pyramid," in *Proc. of the 15'th International Conference on Pattern Recognition (ICPR)*, Barcelona, Spain, vol. 2, pp. 877-881, 3-7 Sept. 2000.
- [102] S. Gleason, M. Hunt, and W. Jatko, "Subpixel measurement of image features based on paraboloid surface fit," in *Proc. of the SPIE*, 1990, vol. 1386.
- [103] R. Moddemeijer, "On the determination of the position of extrema of sampled correlators," *IEEE Trans. Signal Processing*, vol. 39, no. 1, pp. 216-219, Jan. 1991.
- [104] A. Forenza, D. J. Love and R. W. Heath, "Simplified Spatial Correlation Models for Clustered MIMO Channels With Different Array Configurations," *IEEE Trans. Vehicular Technology*, vol. 56, no. 4, pp. 1924-1934, July 2007.

- [105] G. Giunta, “Fine Estimators of Two-Dimensional Parameters and Application to Spatial Shift Estimation,” *IEEE Trans. on Signal Processing*, vol. 47, no. 12, pp. 3201–3207, Dec. 1999.
- [106] G. Jacovitti and G. Scarano, “Discrete Time Techniques for Time Delay Estimation,” *IEEE Trans. Signal Processing*, vol. 41, no. 2, pp. 525–533, Feb. 1993.
- [107] Z. Chen, C. Du, J. Wang, and Y. He, “PPFS - a paraboloid prediction based fractional pixel search strategy for H.26L,” in *Proc. of IEEE International Symposium on Circuits and Systems (ISCAS)*. IEEE, Mar. 2002, vol. 3, pp. III–9– III–12.
- [108] Wen Xu, A. B. Baggeroer, and C. D. Richmond, “Bayesian bounds for matched-field parameter estimation,” *IEEE Trans. on Signal Processing*, vol. 52, no. 12, pp. 3293–3305, Dec 2004.
- [109] WiMAX Forum: *Mobile WiMAX Part II: A Comparative Analysis*, May 2006.
- [110] Wireless LAN Medium Access Control (MAC) and Physical Layer (PHY) specifications Amendment 4: Further Higher Data Rate Extension in the 2.4 GHz Band: IEEE std 802.11g.-2003
- [111] A. Papoulis, *Probability, Random Variables and Stochastic Processes*, McGraw Hill, Inc., 3rd edition, 1991.
- [112] C. D. Meyer, *Matrix Analysis and Applied Linear Algebra*, SIAM, 2000.
- [113] G. H. Golub and C. F. Van Loan, *Matrix Computations*, Johns Hopkins University Press, Baltimore and London, 3rd edition, 1996.
- [114] T. H. Cormen, C. E. Leiserson, R. L. Rivest, and C. Stein, *Introduction to Algorithms*, The MIT Press, Cambridge, Massachusetts, 2nd edition, 2001.
- [115] M. R. Spiegel, *Mathematical Handbook of Formulas and Tables*, Schaum’s Outline Series. McGraw-Hill, New York, 32nd edition, 1994.
- [116] M. Brookes, *The Matrix Reference Manual*, 2011, [online] <http://www.ee.ic.ac.uk/hp/staff/dmb/matrix/intro.html>.
- [117] B. Ottersten, M. Viberg, P. Stoica, and A. Nehorai, “Exact and Large Sample ML Techniques for Parameter Estimation and Detection in Array Processing,” in *Radar Array Processing*, S. Haykin, J. Litva, and T.J. Shepherd, Eds., pp. 99–151. Springer-Verlag, New-York, USA, 1993.

-
- [118] H. L. Van Trees, *Detection, Estimation, and Modulation Theory, Part III: Radar & Sonar Signal Processing and Gaussian Signals in Noise.*, John Wiley & Sons, Inc., New York, 2001.
- [119] H. L. Van Trees, *Detection, Estimation and Modulation Theory - Part IV: Optimum array processing*, Wiley-Interscience, New York, 1st edition, 2002.
- [120] J. C. Liberti Jr. and T. S. Rappaport, *Smart Antennas for Wireless Communications: IS-95 and Third Generation CDMA Applications*, Prentice Hall PTR, Upper Saddle River, NJ 07458, 1999.
- [121] G. L. Stüber, *Principles of Mobile Communication*, Kluwer Academic Publishers, 2nd edition, 2002.
- [122] L. F. McNamara, *The Ionosphere: Communications, Surveillance, and Direction Finding*, Krieger Publishing Company, Malbar Florida, 1991.